SIMULATION OF REFRIGERATED SPACE WITH RADIATION

A THESIS SUBMITTED TO
THE GRADUATE SCHOOL OF NATURAL AND APPLIED SCIENCES
OF
MIDDLE EAST TECHNICAL UNIVERSITY

BY

ÖZGÜR BAYER

IN PARTIAL FULLFILLMENT OF THE REQUIREMENTS
FOR
THE DEGREE OF DOCTOR OF PHILOSOPHY
IN
MECHANICAL ENGINEERING

FEBRUARY 2009

Approval of the thesis:

SIMULATION OF REFRIGERATED SPACE WITH RADIATION

submitted by **ÖZGÜR BAYER** in partial fulfillment of requirements for the degree of **Doctor of Philosophy in Mechanical Engineering Department, Middle East Technical University** by,

Prof. Dr. Canan Özgen
Dean, Graduate School of **Natural and Applied Sciences**   _____

Prof. Dr. Suha Oral
Head of Department, **Mechanical Engineering**   _____

Prof. Dr. Rüknettin Oskay
Supervisor, **Mechanical Engineering Dept., METU**   _____

Assist. Prof. Dr. İlker Tarı
Co-Supervisor, **Mechanical Engineering Dept., METU**   _____

Examining Committee Members

Prof. Dr. Ediz Paykoç
Mechanical Engineering Dept., METU   _____

Prof. Dr. Rüknettin Oskay
Mechanical Engineering Dept., METU   _____

Prof. Dr. Faruk Arınç
Mechanical Engineering Dept., METU   _____

Prof. Dr. Nevin Selçuk
Chemical Engineering Dept., METU   _____

Assist. Prof. Dr. İlker Tarı
Mechanical Engineering Dept., METU   _____

Prof. Dr. Ali Durmaz
Mechanical Engineering Dept., Gazi University   _____

                                        Date   _____

I hereby declare that all information in this document has been obtained and presented in accordance with academic rules and ethical conduct. I also declare that, as required by these rules and conduct, I have fully cited and referenced all material and results that are not original to this work.

Name, Last name: Özgür BAYER

Signature:

ABSTRACT

SIMULATION OF REFRIGERATED SPACE WITH RADIATION

Bayer, Özgür

Ph.D., Department of Mechanical Engineering

Supervisor   : Prof. Dr. Rüknettin Oskay

Co-Supervisor : Assist. Prof. Dr. İlker Tarı

February 2009, 156 pages

Performance of a refrigerator can be characterized with its ability to maintain a preset low temperature by spending the least amount of electricity. It is important to understand natural convection inside a refrigerator for optimizing its design for performance. Computational Fluid Dynamics (CFD) together with experiments is a very powerful tool for visualizing flow and temperature fields that are essential for understanding a phenomenon that involves both fluid and heat flow. In this aspect, simulations are performed for compartment and total refrigerator models using the package program Fluent which is based on finite volume method. An experimental study is performed to determine the constant wall temperature boundary conditions for the numerical models. Effect of radiation is also investigated by comparing the numerical study of a different full refrigerator model with a similar one in literature. While evaluating the radiation effect, convection boundary condition is selected by defining overall heat transfer coefficient between the ambient room air at a constant temperature

and the inner surfaces of the walls. Based on assumptions, related heat transfer analyses are done using compartment and total refrigerator model analyses. Performing CFD simulations of a refrigerator cabinet for visualizing the flow and temperature fields which is the aim of the study is achieved and some observations that can be useful in design optimization are made.

ÖZ

SOĞUTULMUŞ HACMİN IŞIMALI BENZETİMİ

Bayer, Özgür

Doktora, Makina Mühendisliği Bölümü

Tez Töneticisi   : Prof. Dr. Rüknettin Oskay

Ortak Tez Töneticisi : Y. Doç. Dr. İlker Tarı

Şubat 2009, 156 sayfa

Bir buzdolabının performansı önceden ayarlanmış düşük sıcaklığı en az miktarda elektik harcayarak koruyabilmesi yeteneği ile karakterize edilebilir. Buzdolabının içerisindeki doğal taşınımı anlamak performans için tasarımını optimize etmek açısından önemlidir. Hesaplamalı akışkanlar dinamiği, deneylerle birlikte, akışkan ve ısı akışını içeren bir fenomeni anlamak için gerekli olan akış ve sıcaklık alanlarının görüntülenmesi için çok güçlü bir araçtır. Bu çerçevede, sonlu hacim metodu temelli Fluent paket programı kullanılarak kompartman ve tüm buzdolabı modelleri için simülasyonlar gerçekleştirilmiştir. Sayısal modeller için sabit duvar sıcaklığı sınır koşulları elde etmek üzere deneysel çalışma yürütülmüştür. Radyasyon etkisi farklı bir bütün buzdolabı modelinin sayısal analizi ile literatürdeki benzerinin karşılaştırılması yoluyla incelenmiştir. Radyasyon etkisi değerlendirilirken çevre odanın sabit sıcaklıktaki havası ile duvarların iç yüzeyleri arasında genel ısı transferi katsayısı tanımlayarak taşınım sınır koşulu seçilmiştir. Kabullere dayanarak kompartman ve tüm buzdolabı model analizleri kullanılıp ilgili ısı

transferi analizleri yapılmıştır. Hesaplamalı akışkanlar dinamiği analizleri yürütülerek çalışmanın amacı olan buzdolabı kabininin simülasyonu, akış ve sıcaklık alanlarının görüntülenmesi yoluyla başarılmış ve tasarım optimizasyonu için yararlı olabilecek bazı gözlemler yapılmıştır.

Anahtar Kelimeler: Doğal taşınım, hesaplamalı akışkanlar dinamiği, sayısal analiz, radyasyon, buzdolabı, ısı transferi.

Sevgili Helime Halam'a, Emek ve Özlemle...

ACKNOWLEDGEMENTS

TABLE OF CONTENTS

LIST OF TABLES

TABLES

LIST OF FIGURES

FIGURES

LIST OF SYMBOLS

A : Area (m^2), Aspect ratio

a,b,c,

d,e,f : Dimensions (m)

c_p : Constant pressure specific heat (J/kgK)

F : Function, View factor

g : Gravitational acceleration (9.81 m/s^2)

h : Heat transfer coefficient (W/m^2K)

k : Turbulent kinetic energy (m^2/s^2)

L : Length (m)

Nu : Nusselt number

P' : Change in hydrostatic pressure (Pa)

P_o : Hydrostatic pressure (Pa)

Pr : Prandtl number

$q^{"}$: Heat flux (W/m^2)

Ra : Rayleigh number

t : Time (s)

T : Temperature (K)

u : Velocity component in x direction (m/s)

U : Overall heat transfer coefficient (W/m^2K)

v : Velocity component in y direction (m/s)

Vel : Velocity (m/s)

w : Velocity component in z direction (m/s)

x, y, z : Spatial coordinates

Greek Letters:

α : Thermal diffusivity (m^2/s)

β : Volumetric thermal expansion coefficient (K^{-1})

μ : Dynamic viscosity (Ns/m^2)

ρ : Density (kg/m^3)

ν : Kinematic viscosity (m^2/s)

ε : Turbulent energy dissipation (m^2/s^3), emissivity

σ : Stefan-Boltzman constant (W/m^2K^4)

Φ : Scalar quantity

Subscripts:

amb   : Ambient

conv   : Convection

eff   : Effective

evap   : Evaporator

H   : Height

i   : Initial

o   : Operating

rad   : Radiation

ref   : Reference

t   : Turbulent

T   : Thermal

W   : Width

CHAPTER 1

INTRODUCTION

In recent years, users are paying more attention to the refrigerator's performance of keeping food fresh. Therefore, the problem of keeping food fresh in the refrigerator cabinet is one of research areas of engineers. The optimum design of the refrigerated space which also leads to energy savings for the whole system is investigated for this purpose. Since the fresh quality of food as well as the power consumption of the refrigerator directly depend on temperature and airflow distributions inside the cooling chamber, simulation, analysis and design optimization of the refrigerated space are necessities.
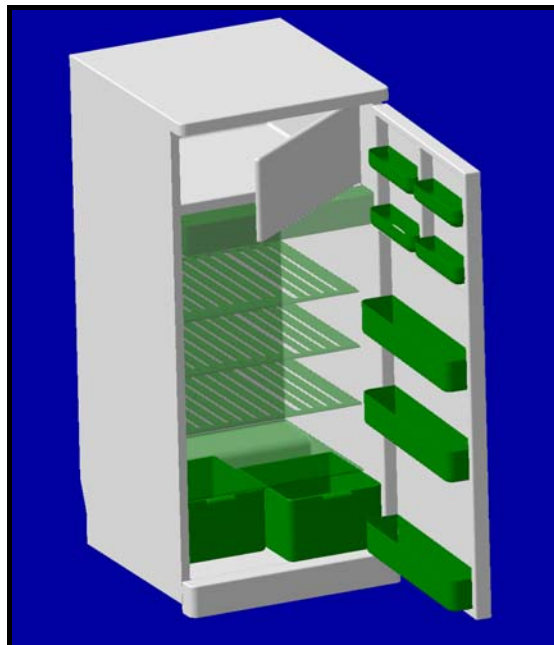
Figure 1.1. Domestic household refrigerator

From this point of view, the engineering problem in this field is modeling the refrigerated space to simulate fluid flow and temperature distribution, and using the results of these numerical simulations for optimizing the design of the refrigerated space. The refrigerated space is taken as a 3-D cabinet divided into compartments with grills.

The detailed literature survey covering the experimental work also shows that the surface temperatures of the compartments are different with circulation loops and the problem is unsteady. CFD codes can be used in the analysis of the problem.

1.1. Literature Survey

Natural convection in enclosures has been extensively studied both experimentally and numerically. The size of the research effort dedicated to this topic during the past three decades reflects the fact that natural convection in enclosures is a challenging subject; and it is one of the simplest multiple-scale, coupled non-linear flow problems and provides a convenient tool for the development of new numerical algorithms. First general reviews were focused on the importance of scaling analysis and experiments to determine flow details. Essentials of scaling techniques were outlined, implication of these for numerical methods was revealed and inadequacies of purely numerical solutions were pointed out [1-3]. Among various enclosures, square and rectangular cavities are the most extensively studied structures since many engineering applications including air flow in solar collector cavities, rooms, cavity walls, double pane windows, electronic equipment and refrigerated spaces can be simplified to these geometries.

Enclosures in which the natural convection phenomena investigated are selected as 2-D or 3-D, air filled, partitioned or unpartitioned cavities with different

boundary conditions (specified sidewall temperatures or heating from sides with uniform heat flux) and flow regimes.

1.1.1. 2-D Studies

One of the detailed studies, performed by Corcione [4], is steady laminar natural convection in air-filled, 2-D rectangular enclosures heated from below and cooled from above for a wide variety of thermal boundary conditions at the sidewalls. The simulations were performed for several values of both the width-to-height aspect ratio of the enclosure in the range between 0.66 and 8, and the Rayleigh number based on the cavity height in the range between 10^3 and 10^6, whose influence upon the flow patterns, temperature distributions and heat transfer rates were analyzed and compared with the benchmark numerical solution [5].

Markatos and Pericleous presented a computational method to study the free convection laminar and turbulent flow and heat transfer in a square cavity with differentially heated side walls, ranging the Rayleigh numbers from 10^3 to 10^{16} [6]. A two equation model of turbulence was used for Rayleigh numbers greater than 10^6. The results for Rayleigh numbers up to 10^6 were compared with the benchmark numerical work of de Vahl Davis [7].

Numerical solutions for transient natural convection in a 2-D square cavity with different sidewall temperatures were also obtained by Hyun and Lee [8]. They observed some oscillatory behavior at a period comparable to that of an internal gravity wave occurs when Pr>1 and Ra>Pr^4.

Experimental benchmark studies of low-level turbulence natural convection in an air filled vertical cavity were conducted by Karayiannis et al. [9, 10]. The dimensions of cavity are 0.75x0.75x1.5m giving two dimensional flow. The hot and cold vertical walls of the cavity are isothermal at 50 and 10 ^{o}C, resulting in

Rayleigh number of 1.58×10^9 and horizontal top and bottom walls are insulated. The studies showed that at the bottom of the hot wall (top of the cold wall) the turbulent heat flux was effectively zero. The absence of turbulent heat flux in these regions resulted in a boundary layer with the characteristics of a laminar flow. Experimentally obtained contour plot of the thermal field and a vector plot of the air flow in the cavity were reported for low turbulence natural convection. Ampofo repeats the same study with air filled partitioned square cavity by explaining the turbulence quantities [11, 12] and referring to the work of Penot and N'Dame [13]; he has reported that 2-D approximation of experimental natural convection in cavities should be valid if the horizontal aspect ratio of the cavity is greater than 1.8.

A work different from the studies mentioned so far wass a preliminary attempt to study transient natural convection phenomena in a two-dimensional cavity heated symmetrically from both sides with a uniform heat flux [14]. With the top of the cavity left open to atmosphere and bottom wall insulated, this situation leads to a well-mixed layer at the top, below which the fluid gets thermally stratified.

Although boundary conditions on the horizontal cavity surface are defined in numerical work as adiabatic or perfectly conducting, it is not easily realized in experiments and lie somewhere in between the above two limiting cases [15]. So it is very important to have the numerical visualization of the flow and simulation of the model in order to validate and verify the problem.

A numerical study was performed by Wansophark et al. [16] for the analysis of free and forced convection heat transfer. The study presents a combined algorithm between a segregated finite element method and a monotone streamline upwinding method for solving two-dimensional viscous incompressible thermal flows. The paper starts from briefly describing the set of the partial differential equations that satisfy the law of conservation of mass,

momentums and energy. Corresponding finite element equations are derived and element matrices are presented. The computational procedure used in the development of the computer program and the basic idea behind the adaptive meshing technique is then described. Finally, the finite element formulation and the computer program have been verified using examples that have prior numerical solutions, experimental results and empirical correlations.

Further extension of studies on natural convection in enclosures is conjugate natural convection and conduction. These problems are composed of natural convection of fluid and its solid conjugate inside a complex cavity and by using vorticity stream function method, the conduction effect of solid body on heat transfer is investigated [17, 18]. Moreover, experimental and numerical analyses of natural convection in enclosures with uniform volumetric sources or heat generating conducting bodies are available in literature. The fluid flow, heat transfer, streamlines and Nusselt numbers at the walls are investigated for various number of Rayleigh numbers in these studies and significant change in the buoyant flow parameters as compared to conventional non-conjugate investigations is observed [19, 20].

1.1.2. 3-D Studies

Although 2-D cavity model for a refrigerated space is good enough when the dimensional conditions are satisfied [13], the results may deviate from the experiments at the corners. On the other hand, 3-D modeling gives more realistic and accurate results.

One of the commonly used benchmark numerical solutions for natural convection in a cubical cavity was obtained by Wakashima et al. [21]. In the study; 3-D cavity has two differentially heated and isothermal vertical walls and also four adiabatic walls. The working fluid is air with Pr=0.71. In the computations, the high accuracy finite differences of fourth-order were

employed for the spatial discretization of governing equations and the boundary conditions. In addition the third-order backward finite difference was used in timewise discretization. The method is so called as time-space method. In this method the {n}-dimensional unsteady boundary-value problem is transformed into {n+1}-dimensional steady boundary-value problem, and the initial condition corresponds to the boundary condition at t=0 in the TSM calculation. It is unconditionally stable and the time step is chosen arbitrarily.

Transition to time-periodicity of a natural convection flow in a 3-D differentially heated cavity was studied by Janssen et al. [22]. Using finite volume method, scaling in the boundary layer along the wall in the steady flow regime was investigated. On the other hand; frequency calculation in the periodic flow regime was performed and it was observed that, the frequency calculated was almost the same as for the two-dimensional square cavity which was indicating the same instability mechanism responsible for the bifurcation.

Another numerical work based on the benchmark study of de Vahl Davis [5] was performed by Fusegi et al. [23]. In this study, a high-resolution finite difference analysis was reported on 3-D natural convection of air for the Rayleigh number range 10^3 to 10^6 in cubical enclosure. The details of the three dimensional flow and thermal characteristics were described and reasonable agreement with the experimental measurements was demonstrated.

An experimental study continued with an extension was conducted by Leong et al. [24-26] which is suitable for testing CFD codes. This experimental study involves natural convection within a differentially heated cubical cavity oriented at three different angles (diamond orientation in reference 26) and subjected to four different Rayleigh numbers, all in the range $10^5 \leq Ra \leq 10^8$. The cube sidewall temperature varied linearly with distance from the hot face. In view of the number of test cases reported and the relatively low experimental uncertainty, the problem appeared to be well suited as a benchmark for numerical validation.

Therefore a numerical benchmark study dealing with 3-D natural convection in an air-filled cavity oriented at three different angles (based on the previous experimental study of Leong et al.) was discussed at the ICHMT 2nd International Symposium on Advanced in Computational Heat Transfer in 2001 [27]. In this numerical benchmark study, ten teams submitted papers using various mesh sizes and computational techniques. Most teams reported the existence of oscillatory solutions for cases at high Ra where the heating was primarily from below. It was also observed that; computed Nu numbers agreed with measurements at Ra and at inclinations where the heating was at least partly from the side. However, no one set of participants produced Nu numbers that agreed with experimental results for all test cases.

Hsieh et al. presented an experimental work for transient buoyancy induced natural convection in the Rayleigh number range of 6.9×10^7-4.12×10^8 for aspect ratios of $A_H = 3$ and $A_W = 1.2$ inside a rectangular enclosure with silicone oil as the working fluid [28]. Time evolution of streak flow patterns was observed and temporal temperature distributions were outlined. Uncertainty analysis was also performed.

As similar to the 2-D case, 3-D analyses focused on temperature and velocity distribution determination across the enclosures caused by the heat source are available in literature [29, 30]. These studies named as conjugate heat transfer of natural convection and conduction may be numerical [29] or experimental [30], and able to investigate the effect of three-dimensionalities, heat transfer modes on fluid flow and the thermal characteristics in the enclosure.

1.1.3. Refrigerator Applications

Although various studies are available in the literature related to natural convection in enclosures, refrigerator applications are limited.

For refrigerators, simulation includes steady-state simulation and dynamic simulation. For steady-state simulation, the thermal capacity of foam insulation is neglected. For dynamic simulation, not only the refrigeration system, but also the refrigerated space (cabinet) is considered to be dynamic, so the simulation is complicated. Dynamic simulation of natural convection bypass two-circuit cycle refrigerator for both the component and system basis is performed by Lu et al. [31, 32]. Similarly, Penot et al. [33] investigated the turbulent convection in a large air filled cavity by the help of direct numerical simulation (DNS) and large eddy simulation (LES) methods which are supported by Chebyshev pseudo-spectral method and finite volume method respectively.

In a different study, the velocity and temperature distributions in commercial refrigerated open display cabinets are examined by applying finite element method. The stream function-vorticity formulation is the basis for the CFD code for the turbulence flow model [34]. The aim of the study is to reveal the influence of air curtain velocities on the efficiency and the code formed has been validated by comparison with experimental measurements performed in accordance with the EN 441 Standard.

Laguerre at al. [35] analyzed heat transfer by natural convection in domestic unventilated refrigerators. The study consisted of natural convection theories covering some cases such as rectangular empty cavity, vertical plates and air and heat transfer around an isolated object.

Based on reference [35], Laguerre et al. performed an experimental study of heat transfer by natural convection in a cavity selecting the application as a domestic refrigerator with the real dimensions [36]. Air temperature profile in the boundary layers and in the central zone of the empty refrigerator model was searched. The effects of temperature and the surface area of the cold wall were studied. Next, filling the refrigerator with four blocks of hollow spheres, the effect of obstacles on temperature profiles was investigated. The steady state

analyses were performed for the Ra number of about 10^8-10^9. Experimental work revealed that there was temperature stratification in the vertical direction with the cold zone at the top of the cavity. Additionally, air temperature was lower almost everywhere in the model containing blocks.

After the experimental study [36], in turn, Laguerre et al. performed the numerical simulation of air flow and heat transfer [37], experimental work of air flow [38], and PIV measurement of the flow field [39] in the domestic refrigerator. The effect of radiation was investigated in reference [37] for a 3-D enclosure with the dimensions close to an actual refrigerator and comparison of calculated air temperatures in numerical analysis and the experimental values showed good agreement when radiation was taken into account.

The experimental study [38] was focused on measurement of air velocity using particle image velocimetry (PIV) considering the influence of temperature and surface area of the cold wall and the obstacles filled inside. Circular air flow, downward along the cold wall and upward along the other walls was observed. The maximum value of the air velocity occurring near the bottom of the cold wall was 0.2 m/s and cold wall temperature effect on air velocity was more significant than the surface area. Moreover, the air velocity was lower almost everywhere in the filled refrigerator model than the empty one and the presence of blocks seemed to homogenize the air velocity.

As the next stage of the experimental work [38], Laguerre et al. compared the PIV measurement of the flow field with the CFD simulations [39]. In numerical model, temperature of the evaporator was assumed to be constant while a uniform overall heat transfer coefficient was used to describe the heat exchange with the room ambient air at constant temperature. Radiation between the walls of the cavity was also considered. The results obtained with the 3-D numerical simulations were in quite good agreement with the experimental airflow measurements.

1.2. Present Study

Maintaining a preset low temperature by spending the least amount of electricity is the most important characteristic of a refrigerator for evaluating its performance and optimizing the refrigerator's design for performance requires a well understanding the natural convection inside it. Considering the engineering problem of natural convection in domestic refrigerator applications, this study aims to simulate the fluid flow and temperature distribution in a single refrigerator compartment or the whole empty refrigerator by using the experimentally determined different temperature values as the specified constant wall temperature boundary conditions. Since the free convection in refrigerator applications is evaluated as a 3-D, turbulent, transient and coupled non-linear flow problem, it is rather difficult to realize the objective of the present work and a comprehensive study is a necessity.

Theory of natural convection in enclosures and governing continuity, momentum and energy equations on which the mathematical formulation of the problem relies will be explained in Chapter 2. Moreover, the basic assumption of Boussinesq to simplify the governing equations, the turbulence and radiation models used in numerical analyses will also be mentioned in this chapter.

The present study consists of some stages such as preliminary numerical work performed to understand the parameters affecting the analysis, experimental temperature measurements at the walls and midplane of the empty refrigerator and one of its compartments and a final numerical study to verify the experimental work by using the data obtained from the experiments as the boundary conditions of the domain. Detailed information about the 3-D models and the boundary conditions for the numerical analyses, the finite volume method utilized in the package program Fluent 6.3.26 [40], the experimental study done at research department of Arçelik Çayırova/İstanbul factory and the general concept of the related heat transfer analysis will be given in Chapter 3.

Chapter 4 will cover the results obtained from CFD analyses for the models explained in previous chapter. Temperature and velocity profiles with related heat transfer analysis for both including or omitting the radiation model will be presented at intermediate time steps and steady state time of the transient analyses performed and the results for each of the preliminary, single compartment and total refrigerator models will be discussed. In addition, effect of the radiation will be investigated by comparing the numerical study of a different full refrigerator model with the one similar in literature. While evaluating the radiation effect, convection boundary condition will be selected by defining overall heat transfer coefficient between ambient room air with constant temperature and inner surfaces of the walls.

The last chapter will include a brief summary of the present study, the conclusions and the future work that can be performed.

CHAPTER 2

NATURAL CONVECTION PHENOMENA

2.1. Theory

The convective heat transfer mode includes two basic mechanisms. The process is called forced convection if the motion of the fluid arises from an external mechanical means such as; a fan, a blower, the wind, pump, etc. The process is termed natural convection or free convection, if the fluid motion is caused by density differences which are created by temperature differences existing in the fluid mass in a gravitational field [41, 42].

The main difference between natural and forced convection lies in the nature of the fluid flow generation. Externally imposed flow is generally known in forced convection, whereas in natural convection it results from an interaction of the density difference with the gravitational (or some other body force) field, and depends on the temperature and concentration fields. Thus the motion is not known at the onset and has to be determined from the heat and mass transfer processes coupled with fluid flow mechanisms. Also, in practice, velocities in free convection are usually much smaller than those in forced convection [41]. The difference between the mechanisms of the natural and forced convection makes the numerical and experimental analysis of natural convection much more complicated than the forced convection. Therefore to study the free convection, special techniques and methods have been devised [41- 43].

Natural convection in enclosures with air inside is first tried to be understood by performing experimental studies. A variety of experiments are performed to figure out the mechanism of the natural convection. Then with the help of the knowledge obtained from benchmark experimental works, numerical codes are written to solve such a complicated physical phenomenon. For 2-D enclosures with specific boundary conditions, theoretical Nu number is compared with the experimental and numerical correlations derived from studies mentioned [42].

The present study is considering the enclosure as a 3-D cavity with different specified temperatures on the walls, therefore, the natural convection phenomenon of air inside the enclosure is affected by the interaction of all walls and the correlations derived may not be used for this situation.

Several simplifying physical assumptions are made to state the governing equations for the solution of the problem. These underlying assumptions are:

- The viscous dissipation effects and work performed by pressure forces are neglected,
- the thermophysical properties such as the thermal conductivity, coefficient of thermal expansion and viscosity are taken to be constant,
- the density has been taken as constant except in the buoyancy term in the vertical component of the momentum equation, following the Boussinesq approximation,
- heat generation per unit volume is neglected.

2.2. Boussinesq Approximation in Natural Convection

The governing equations for natural convective flow are coupled partial differential equations, and are of considerable complexity. In order to simplify these equations, a standard approximation of Boussinesq is introduced here.

In some literature studies, instead of this standard approximation natural convection analysis is based on the Boussinesq equations, in which the work of pressure forces are included [44-47]. Apart from the standard method, this approximation named as thermodynamic Boussinesq approach keeps the work of pressure forces and the heat generated by viscous friction in energy equation. However; except tall cavities (aspect ratio greater than 15), the work of pressure forces is negligible so that thermodynamic and standard models yield similar results. This fact leads to the application of standard Boussinesq approximation in the present thesis study since both the empty refrigerator and single compartment models are of the aspect ratio smaller than 15.

The origin of the simplification in standard Boussinesq approximation is due to the smallness of the volumetric thermal expansion coefficient so in general the variations in the density are small and can be ignored such as the one for the continuity equation. But the significant change in the value of density in the buoyancy term of the equation of motion can not be ignored. This is because the acceleration resulting from body force can be quite large, and sometimes much larger than the acceleration due to the inertial force in the equation of motion. Accordingly, one may treat density as a constant in all terms in the momentum equation except the one in the body force.

The Boussinesq approximation includes two aspects. First, the density variation in the continuity equation is neglected. Second, the density difference, which causes the flow, is approximated as a pure temperature effect. In fact, the density difference is estimated as in Equation 2.1.

$$\rho = \rho_0 (1 + \beta(T_0 - T)) \tag{2.1}$$

where;

β : volumetric thermal expansion coefficient,

ρ_0 : reference density,

T_0 : reference temperature values.

2.3. Governing Equations

A convective heat transfer process is governed by the basic conservation principles of mass, momentum and energy. Since their derivations are easily found in any standard heat transfer textbook, these equations will only be stated considering the assumptions made and explained in the previous section.

Continuity:

$$\frac{\partial \rho}{\partial t} + \rho(\frac{\partial u}{\partial x} + \frac{\partial v}{\partial y} + \frac{\partial w}{\partial z}) = 0 \tag{2.2}$$

x-momentum:

$$\rho(\frac{\partial u}{\partial t} + u\frac{\partial u}{\partial x} + v\frac{\partial u}{\partial y} + w\frac{\partial u}{\partial z}) = -\frac{\partial P'}{\partial x} + \mu(\frac{\partial^2 u}{\partial x^2} + \frac{\partial^2 u}{\partial y^2} + \frac{\partial^2 u}{\partial z^2}) \tag{2.3}$$

y-momentum:

$$\rho(\frac{\partial v}{\partial t} + u\frac{\partial v}{\partial x} + v\frac{\partial v}{\partial y} + w\frac{\partial v}{\partial z}) = -\frac{\partial P'}{\partial y} + \mu(\frac{\partial^2 v}{\partial x^2} + \frac{\partial^2 v}{\partial y^2} + \frac{\partial^2 v}{\partial z^2}) \tag{2.4}$$

z-momentum:

$$\rho(\frac{\partial w}{\partial t} + u\frac{\partial w}{\partial x} + v\frac{\partial w}{\partial y} + w\frac{\partial w}{\partial z}) = \frac{-\partial P'}{\partial z} + \mu(\frac{\partial^2 w}{\partial x^2} + \frac{\partial^2 w}{\partial y^2} + \frac{\partial^2 w}{\partial z^2}) + \rho_0 g\beta(T - T_0) \tag{2.5}$$

Energy:

$$\frac{\partial T}{\partial t} + u\frac{\partial T}{\partial x} + v\frac{\partial T}{\partial y} + w\frac{\partial T}{\partial z} = \alpha(\frac{\partial^2 T}{\partial x^2} + \frac{\partial^2 T}{\partial y^2} + \frac{\partial^2 T}{\partial z^2}) \tag{2.6}$$

where;

$P^{'}$: change in the hydrostatic pressure P_0 ,

In natural convection flows, the buoyancy force is the only body force due to a difference in density caused by temperature variation. The flow is initiated by variation of ρ . The temperature field is linked with the flow, and Equations 2.2 to 2.6 are coupled through the variation of the density ρ . Therefore, these equations which are set to start the solution must be solved simultaneously to give distributions of the physical variables; velocity, pressure and temperature, in space and time. The terms that are representing the change of variables with time in the governing equations will be zero when steady state is reached.

2.4. Turbulence

Most flows occurring in nature and in engineering applications are turbulent. An essential feature of turbulent flows is that the fluid velocity field varies significantly and irregularly in both position and time. In flows which are originally laminar, turbulence arises from instabilities at large Reynolds number. However; turbulence can not maintain itself but depends on its environment to obtain energy and the common sources of energy for turbulent velocity fluctuations are shear in the mean flow and other sources such as buoyancy. Therefore, turbulent flows are generally shear flows [48-51].

Irregularity or randomness is one of the characteristics of all turbulent flows. Another important feature of such kind of flow is the diffusivity of the turbulence which causes rapid mixing and increased rates of momentum, heat and mass transfer. Turbulent flows always occur at high Reynolds numbers and they are rotational and three dimensional. Moreover, dissipative structure of turbulent flows exists.

For engineering applications, there is no need to consider the details of turbulence; instead time-averaged effects are concerned even when the mean flow is unsteady. The process of time-averaging, however results in statistical correlations involving fluctuating velocities and temperatures to appear in the conservation equations. There is no direct way of knowing the magnitudes of these terms; so to approximating or modeling their effects in terms of quantities those can be determined is the best method [52].

In this study, k-ε turbulence model which belongs to two-equation models in the form of eddy viscosity model is used in numerical analysis. The k-ε model is the most widely used complete turbulence model and it is incorporated in most CFD codes. Another model may give slightly different results but it can not be stated whether k-ε model or the other model is giving more precise results. In addition to turbulent viscosity hypothesis, the k-ε turbulence model consists of:

- the model transport equation for k, turbulent kinetic energy,

$$k = 1/2(\overline{u'}^2 + \overline{v'}^2 + \overline{w'}^2) \tag{2.7}$$

- the model transport equation for ε, turbulent kinetic energy dissipation,

$$\varepsilon = k^{3/2}/L \quad \text{where } L \text{ is the length scale} \tag{2.8}$$

- the specification of turbulent viscosity, v_t

$$v_t = C_\mu \frac{k^2}{\varepsilon} \quad \text{where } C_\mu \text{ is the model constant} \tag{2.9}$$

Selected values for k and ε in the numerical analyses will be presented in Appendix B.

2.5. Radiation

Research on the analysis and numerical resolution of heat transfer and fluid flow phenomena where radiant heat exchange has an essential contribution, becomes a key aspect of CFD simulations. From this point of view; thermal radiation can strongly interact with convection in many situations of engineering interest. The influence of radiation on natural convection is generally stronger than that on forced convection because of the inherent coupling between the temperature and flow fields [53].

Literature studies show that the discrete ordinate method was successfully used to simulate the coupling of convection and radiation in a closed cavity for both participating and non-participating media [54-58].

Referring to reference [37], including or omitting the radiation effects, the determination of temperature and velocity profiles in a total refrigerator and a single compartment will be presented in this dissertation. Discrete ordinate (DO) method is used in reference [37] since the partition between the freezer compartment and the vegetable box is a glass shelf, and air inside is considered to be non-participating. For the sake of consistency the same method will be selected as the radiation model in the numerical analysis in the present study.

The general equation of heat transfer by radiation (in a given $\vec{s}$ direction) is:

$$\vec{\nabla} \cdot (I(\vec{r}, \vec{s}) \, \vec{s}) = 0 \tag{2.10}$$

where $I(\vec{r}, \vec{s})$ is radiative intensity in $\vec{s}$ direction (at $\vec{r}$ position) (W/m^2 per unit solid angle).

For a gray surface of emissivity ε_r, the net radiative flux leaving the surface is:

$$q''_{rad-out} = (1 - \varepsilon_r) \int\limits_{\vec{s} \cdot \vec{n} > 0} I_{in} (\vec{s} \cdot \vec{n}) d\Omega + \varepsilon_r \sigma T_s^4 \qquad (2.11)$$

where;

I_{in} : intensity of incident radiation in $\vec{s}$ direction (at $\vec{r}$ position)

$\vec{n}$: normal vector

T_s: surface temperature

Ω: solid angle

The walls in the models are gray and diffuse, therefore;

$$I_{out} = q''_{rad-out} / \pi \qquad (2.12)$$

The details of the benchmark literature study [37] and the parameters used in radiation analyses in the present work will be mentioned in the next two chapters.

CHAPTER 3

PHYSICAL MODEL AND ANALYSES

3.1. 3-D Model and Boundary Conditions

3-D models and boundary conditions used in preliminary numerical study and numerical studies based on experimental work for total refrigerator and one of its compartments will be presented in this section. In all analyses, 3-D models in which the temperature and velocity distributions of the air investigated are considered to be the cavities without any partitions or objects inside.

3.1.1. Preliminary Study

Different from the models in literature, refrigerated space is divided into compartments and one of the compartments is analyzed as a 3-D cavity in the preliminary study. Created model has dimensions of 20x50x60 cm height, depth and width respectively and corresponding letters for these dimensions are *c, a* and *b* in Figure 3.1.

The vertical walls are at T_{front} and T_{rear} respectively whereas top and bottom walls are indicated as T_{top} and T_{bottom}. Top wall temperature T_{top} will be the bottom horizontal wall temperature T_{bottom} of the upper compartment. Side walls are considered to be insulated which is nearly the real case in domestic refrigerators. For the air inside the enclosure, the governing equations are solved according to the boundary conditions specified in the whole domain.
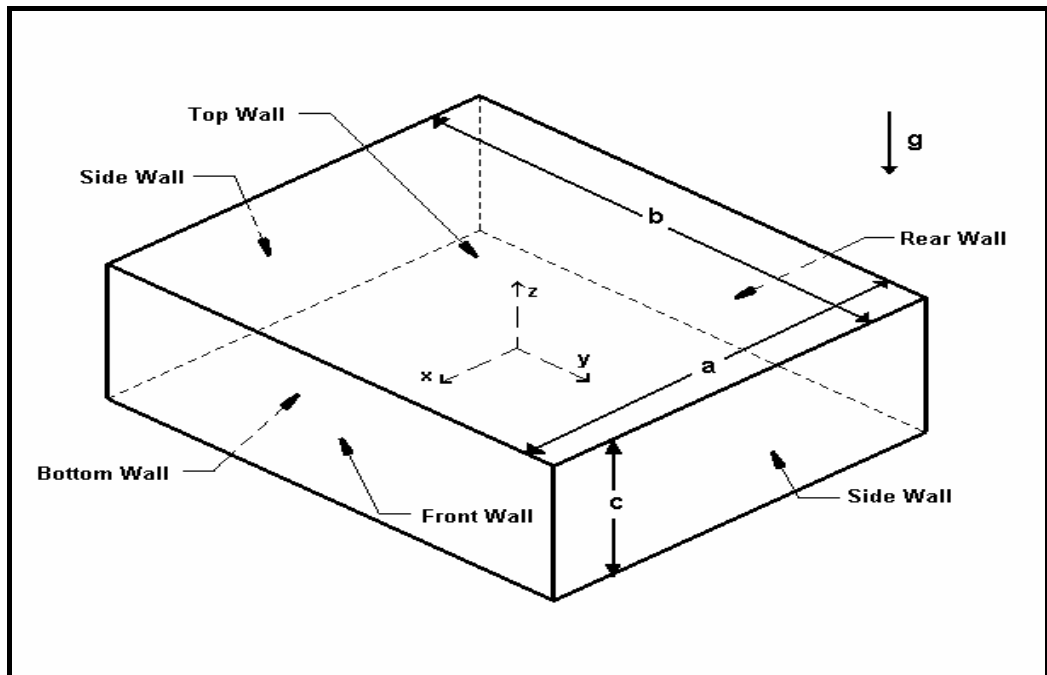
Figure 3.1. Schematic 3-D cavity model for the preliminary study

3-D model in this study has no mass flow from the boundaries so it is a closed cavity and it is heated from the front wall which is representing the door of the refrigerator and cooled from the back vertical wall which stands for the evaporator region. The model has different boundary conditions from those in literature such as velocity and temperature specified boundary conditions as well as the initial conditions of;

    i)   Temperature Boundary Conditions and Initial Condition:

$$T(\frac{-a}{2}, y, z, t) = T_{rear} \qquad\qquad T(\frac{a}{2}, y, z, t) = T_{front}$$

$$T(x, y, \frac{-c}{2}, t) = T_{bottom} \qquad\qquad T(x, y, \frac{c}{2}, t) = T_{top}$$

$$(\frac{\partial T}{\partial y})_{y=-b/2} = 0 \qquad\qquad (\frac{\partial T}{\partial y})_{y=b/2} = 0$$

$$T(x, y, z, 0) = T_i$$

ii) Velocity Boundary Conditions:

u=v=w=0 at all boundaries.

The initial and boundary conditions are determined for the unsteady analysis. Initial temperature is denoted to be 275 K and the values of the x, y and z velocity components are assumed to be zero respectively. Then, referring to Figure 3.1; the temperature values at the boundaries are $T_{top} = 279.20$ K, $T_{bottom} = 278.05$ K, $T_{front} = 279.85$ K, $T_{rear} = 272.85$ K and the side walls are assumed to be adiabatic [35, 59, 60].

In preliminary numerical work radiation effects are not taken into account while performing the analysis for the domain.

3.1.2. Numerical Study for a Single Compartment Based on Experimental Work

Starting with the temperature values obtained from the experimental work done in Arçelik, a close study to the preliminary numerical work is performed for a single compartment of 21.5x47x62 cm height, depth and width respectively. These values selected because they are the corresponding dimensions of the experimental study performed.

Same as the previous model, height, depth and width of the refrigerator compartment are represented with the letters *c, a* and *b* respectively in Figure 3.2. Dimension *d* shown in Figure 3.2 indicates the distance of the evaporator at the back surface from the side walls and it is 9.75 cm.
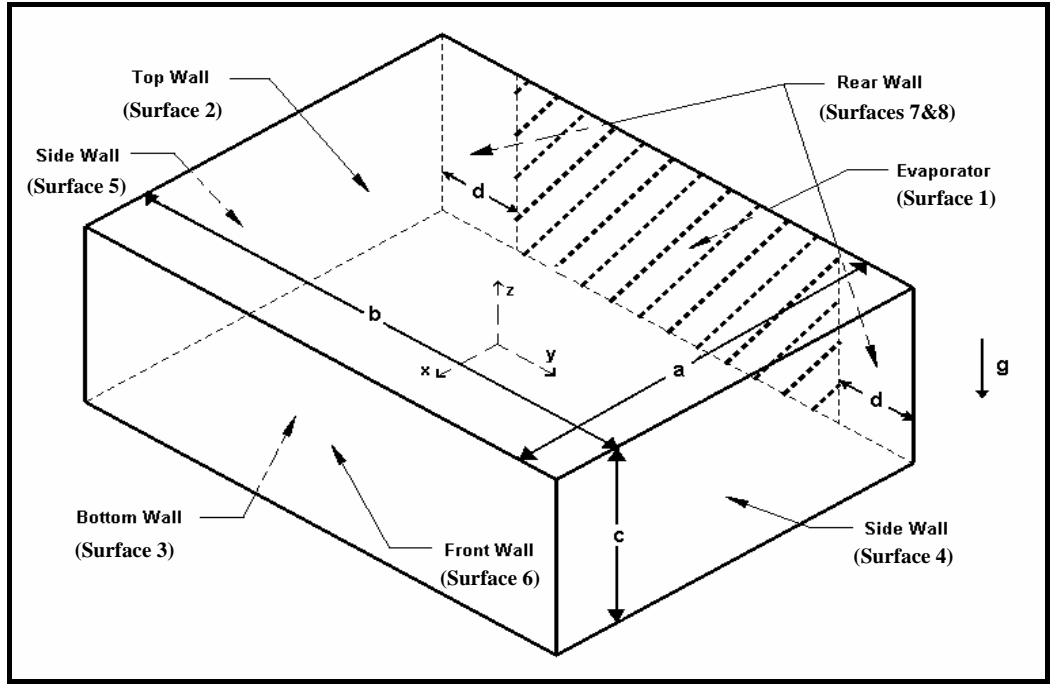
Figure 3.2. Schematic 3-D cavity model of a single compartment for the
numerical study based on the experimental work

It is again assumed that there is no mass flow across the boundaries. Initial
temperature and velocity assumptions for the fluid inside the cavity are the same
with the previous numerical analyses. With or without taking radiation effect
into consideration analyses are done for the boundary conditions of;

i) Temperature Boundary Conditions and Initial Condition:

$$T(\frac{-a}{2},\ \frac{-b}{2} < y < (\frac{-b}{2}+d) \cup (\frac{b}{2}-d) < y < \frac{b}{2},\ \frac{-c}{2} < z < \frac{c}{2},\ t)\ =\ T_{rear}$$

$$T(\frac{a}{2},\ y,\ z,\ t)\ =\ T_{front}$$

$$T(x,\ \frac{-b}{2},\ z\ ,\ t)\ =\ T_{left}$$

$$T(x,\ \frac{b}{2},\ z\ ,\ t)\ =\ T_{right}$$

$$T(x, y, \frac{-c}{2}, t) = T_{bottom}$$

$$T(x, y, \frac{c}{2}, t) = T_{top}$$

$$T(\frac{-a}{2}, (\frac{-b}{2}+d) < y < (\frac{b}{2}-d) <, \frac{-c}{2} < z < \frac{c}{2}, t) = T_{evap}$$

$$T(x, y, z, 0) = T_i$$

ii) Velocity Boundary Conditions:

$u=v=w=0$ at all boundaries.

where the wall temperature values obtained from the experimental study are to be; $T_{rear} = 282.82$ K, $T_{front} = 281.58$ K, $T_{left} = 281.79$ K, $T_{right} = 281.79$ K, $T_{bottom} = 280.24$ K, $T_{top} = 280.98$ K and $T_{evap} = 270.06$ K.

3.1.3. Numerical Study for Total Refrigerator Based on Experimental Work

For this case, a 3-D model with the same dimensions of the whole refrigerator cabinet analyzed in experimental work is created and temperatures of the walls as well as the evaporator region are used as boundary conditions at walls. Model has dimensions of 93x47x62 cm height, depth and width respectively.

Height, depth and width of the refrigerator are represented with the letters *c, a* and *b* respectively in Figure 3.3. Dimensions *f, e* and *d* shown in Figure 3.3 indicate the location of the evaporator at the back surface and these dimensions are 27 cm, 11 cm and 9.75 cm respectively.
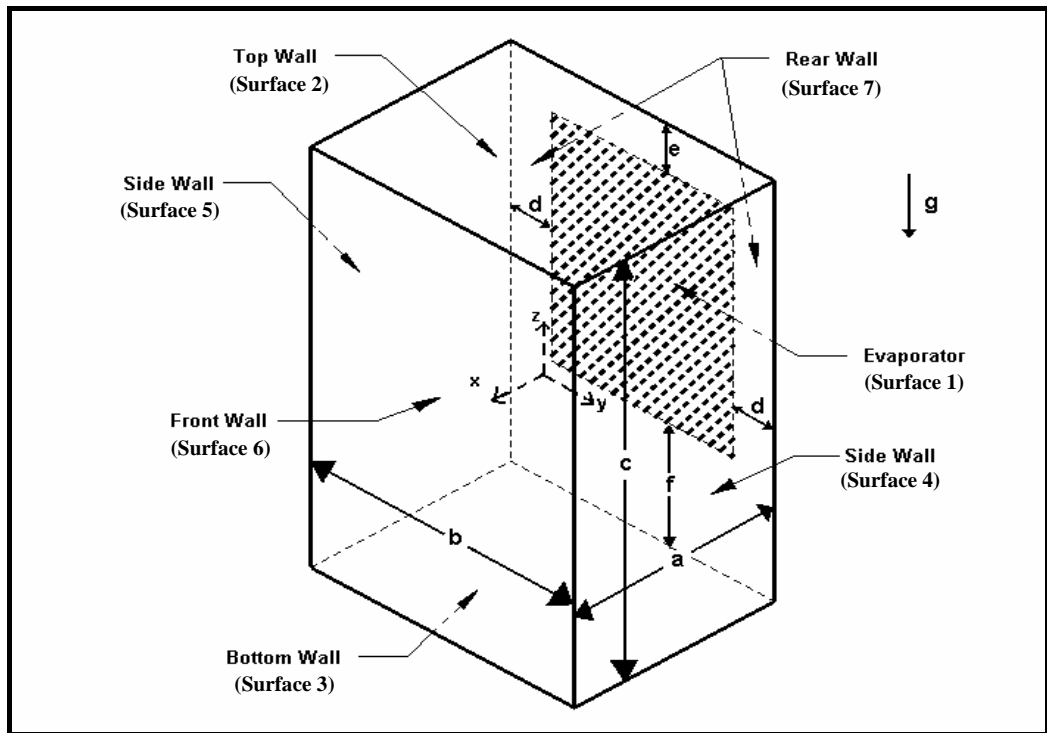
Figure 3.3. Schematic 3-D cavity model of the total refrigerator for the
numerical study based on the experimental work

Specified boundary conditions for the model are:

    i)   Temperature Boundary Conditions and Initial Condition:

$$T(\frac{-a}{2}, \frac{-b}{2} < y < (\frac{-b}{2}+d) \cup (\frac{b}{2}-d) < y < \frac{b}{2},$$

$$\frac{-c}{2} < z < (\frac{-c}{2}+f) \cup (\frac{c}{2}-e) < z < \frac{c}{2}, t) = T_{rear}$$

$$T(\frac{a}{2}, y, z, t) = T_{front}$$

$$T(x, \frac{-b}{2}, z, t) = T_{left}$$

$$T(x, \frac{b}{2}, z, t) = T_{right}$$

$$T(x, y, \frac{-c}{2}, t) = T_{bottom}$$

$$T(x, y, \frac{c}{2}, t) = T_{top}$$

$$T(\frac{-a}{2}, (\frac{-b}{2}+d) < y < (\frac{b}{2}-d) <, (\frac{-c}{2}+f) < z < (\frac{c}{2}-e), t) = T_{evap}$$

$$T(x, y, z, 0) = T_{i}$$

ii) Velocity Boundary Conditions:

u=v=w=0 at all boundaries.

Similar to the preliminary study; for unsteady, control mass analysis, initial temperature is denoted to be 275 K and the values of the x, y and z velocity components are assumed to be zero respectively. Wall temperature values obtained from experimental study are to be; $T_{rear} = 281.08$ K, $T_{front} = 280.65$ K, $T_{left} = 281.25$ K, $T_{right} = 281.25$ K, $T_{bottom} = 280.64$ K, $T_{top} = 281.16$ K and $T_{evap} = 273.85$ K. Numerical study for total refrigerator is performed either considering the radiation effect or neglecting it.

3.2. Numerical Approach

In order to obtain the temperature and velocity distributions inside the domain, numerical analyses are performed on the basis of finite volume method which is utilized in the package program Fluent 6.3.26. While executing the program, segregated pressure-based solver is used [40]. Different from the coupled solution method; governing equations are solved sequentially (i.e., segregated from one another) in this approach. Since the governing equations are non-linear and coupled, several iterations of the solution loop must be performed before a converged solution is obtained. The solver algorithm applied to all of the cells in the domain for each single iteration starts with the solution of momentum

equations after updating the fluid properties based on the current solution and then, pressure correction equation derived from the continuity equation and the linearized momentum equations is solved to obtain the necessary corrections to the pressure and velocity fields and the face mass fluxes such that continuity is satisfied. In this stage; the commonly used pressure-velocity coupling algorithm PISO, which stands for Pressure Implicit with Splitting of Operators is selected for the coupling of pressure and velocity field equations [61]. Next; equations for scalars such as turbulence, energy, species, and radiation are solved using the previously updated values of the other variables and solution loop ends with a check for convergence. The flowchart illustrating the segregated pressure based solver algorithm is presented in Appendix A.

3.2.1. Finite Volume Method

The main features of the finite volume method are the satisfaction of conservation principles in the control volume and over the whole domain, and a clear physical interpretation of the discretized governing equations. The closeness of the physical principles to the final mathematical forms needed for numerical calculation makes the finite volume method a natural one for a computational heat transfer treatment. In this method; computation point is the centroid of each cell and governing integral equations for the conservation of mass and momentum, and (when appropriate) for energy and other scalars such as turbulence and chemical species are solved after discretization. Surface and volume integrals are approximated by numerical quadrature and values at control volume faces are expressed in terms of nodal values by interpolation which results in an algebraic equation per control volume [40, 61].

The finite volume method consists of:

- Division of the domain into discrete control volumes using a computational grid.

- Integration of the governing equations on the individual control volumes to construct algebraic equations for the discrete dependent variables ("unknowns") such as velocities, pressure, temperature, and conserved scalars.
- Linearization of the discretized equations and solution of the resultant linear equation system to yield updated values of the dependent variables.

For a domain divided into many small cells, discretization can be applied to a general conservative form of all fluid flow equations for the transport of a scalar quantity Φ which is in the form of;

$$\frac{\partial}{\partial t}(\rho\Phi) + \nabla\bullet(\rho u\Phi) = \nabla\bullet(\Gamma\nabla\Phi) + S_\Phi \qquad (3.1)$$

This general differential equation composed of the unsteady, convection, diffusion and the source terms and integration of transport Equation 3.1 over a control volume leads to;

$$\int_{CV}\frac{\partial\rho\Phi}{\partial t}dV + \int_{CV}\nabla\bullet(\rho u\Phi)dV = \int_{CV}\nabla\bullet(\Gamma\nabla\Phi)dV + \int_{CV}S_\Phi dV \qquad (3.2)$$

Using Gauss divergence theorem, one may obtain;

$$\int_{CV}\frac{\partial\rho\Phi}{\partial t}dV + \oint\rho\Phi\vec{u}\bullet d\vec{A} = \oint\Gamma\nabla\Phi\bullet d\vec{A} + \int_{CV}S_\Phi dV \qquad (3.3)$$

where;

ρ : density,

$\vec{u}$: velocity vector,

$\vec{A}$: surface area vector,

Γ : diffusion coefficient for scalar quantity Φ,

$\nabla\Phi$: gradient of Φ,

S_Φ : source of scalar quantity Φ per unit volume.

Discretization of Equation 3.3 on a given cell yields [40];

$$\sum_f^{N_{faces}} \rho_f \vec{u}_f \Phi_f \bullet \vec{A}_f = \sum_f^{N_{faces}} \Gamma(\nabla\Phi)_n \bullet \vec{A}_f + S_\Phi V \tag{3.4}$$

where;

N_{faces} : number of faces enclosing a cell,

Φ_f : value of Φ converted through face f,

$\rho_f \vec{u}_f \bullet \vec{A}_f$: mass flux through face f,

$\vec{A}_f$: area vector of face f,

$(\nabla\Phi)_n$: magnitude of $\nabla\Phi$ normal to face f,

V: cell volume.

While applying finite volume method, Fluent stores discrete values of the scalar Φ at the cell centers. However, face values Φ_f are required for the convection terms in Equation 3.4 and must be interpolated from the cell center values. This is accomplished using an upwind scheme. In this thesis study; second order upwind discretization scheme is selected. In this approach, higher-order accuracy is achieved at cell faces through a Taylor series expansion of the cell-centered solution about the cell centroid. Thus when second-order upwinding is selected, the face value Φ_f is computed using the following expression:

$$\Phi_f = \Phi + \nabla\Phi \bullet \Delta\vec{s} \tag{3.5}$$

where;

Φ : cell-centered value in the upstream cell,

$\nabla\Phi$: gradient of cell-centered value in the upstream cell,

$\Delta\vec{s}$: the displacement vector from the upstream cell centroid to the face centroid.

This formulation requires the determination of the gradient $\nabla\Phi$ in each cell. This gradient is computed using the divergence theorem, which in discrete form is written as;

$$\nabla\Phi = \frac{1}{V} \sum_{f}^{N_{faces}} \tilde{\Phi}_f \vec{A} \qquad (3.6)$$

In this work; the face values, $\tilde{\Phi}_f$ are computed by taking the arithmetic average of the nodal values on the face by selecting node-based under gradient option in the solver panel of the package program [40].

Due to the fact that numerical simulations are transient, temporal discretization involves the integration of every term in the differential equations over a time step Δt. The integration of the transient terms results in a generic expression for the time evolution of the variable Φ as:

$$\frac{\partial\Phi}{\partial t} = F(\Phi) \qquad (3.7)$$

where the function F incorporates any spatial discretization.

This study involves first order implicit discretization because of the advantage of the fully implicit scheme that it is unconditionally stable with respect to time step size. Therefore, the discretization converts Equation 3.7 into;

$$\Phi^{n+1} = \Phi^n + \Delta t F(\Phi^{n+1}) \qquad (3.8)$$

where;

Φ^{n+1}: value of the scalar quantity Φ at the next time step, t+Δt,

Φ^n: value of the scalar quantity Φ at the current time step, t.

This implicit equation can be solved iteratively by initializing Φ^i to Φ^n and iterating Equation 3.9 until Φ^i stops changing (i.e., converges). At that point, Φ^{n+1} is set to Φ^n;

$$\Phi^i = \Phi^n + \Delta t F(\Phi^i) \qquad (3.9)$$

Since all the terms in the transport Equation 3.2 are discretized; a linearized form of this equation can be written as:

$$a_P \Phi = \sum_{nb} a_{nb} \Phi_{nb} + b \qquad (3.10)$$

where the subscript nb refers to the neighbor cells, and a_P and a_{nb} are the linearized coefficients for Φ and Φ_{nb}. In Equation 3.10; the coefficient a_{nb} contains the terms developed from the discretization of diffusion and convection terms in the main equation, whereas the coefficient a_P contains the terms developed from the discretization of diffusion, convection and time unsteady terms. Last term, b in Equation 3.10 involves the terms obtained from the discretization of unsteady, diffusion and source terms.

Similar equations can be written for each cell in the grid. This results in a set of algebraic equations with a sparse coefficient matrix and is solved by a point implicit (Gauss-Seidel) linear equation solver in the program.

Although the linearized set of equations are solved in each time step to obtain the velocity, temperature and other parameters for each cell, because of the nonlinearity of the governing equations of the problem it is necessary to control the change of Φ. This is typically achieved by under-relaxation, which reduces the change of Φ produced during each iteration. In a simple form, the new value of the variable Φ within a cell depends upon the old value, Φ_{old}, the computed change in Φ, $\Delta\Phi$, and the under-relaxation factor, α, as follows:

$$\Phi = \Phi_{old} + \alpha\Delta\Phi \qquad\qquad (3.11)$$

The under-relaxation factor, α presented in Appendix B is selected smaller than the default values for all computed variables in this study. This selection results in an improvement in accuracy and stability but total time consumed for the analyses increases.

The whole discretization scheme described so far for a scalar transport equation is used to discretize the continuity, momentum and energy equations in the present physical problem. However, there are still some annoying points. For instance; the pressure field and face mass fluxes are not known a priori and must be obtained as a part of the solution in the discretized momentum equation. Fluent uses a co-located scheme, whereby pressure and velocity are both stored at cell centers but the value of the pressure at the faces between neighboring cells is required. Therefore, an interpolation scheme is required to compute the face values of pressure from the cell values.

Since the simulations are based on a natural convection problem, it is necessary to pack the mesh in regions of high gradient to resolve the pressure variation adequately. For this reason the PRESTO (PREssure STaggering Option) scheme is selected in this work. This discretization scheme uses the discrete continuity balance for a "staggered" control volume about the face to compute the "staggered" (i.e., face) pressure.

The remaining issue in application of the selected solver (segregated solver in this study) for the solution is the determination of the pressure and velocity couling method. PISO algorithm mentioned above is used for coupling of pressure and velocity field solutions [40, 61, 62]. As an extension of SIMPLE method [63], the algorithm can be shortly described as:

a) Guess the pressure field p^*

b) Solve momentum equations to obtain u^*, v^*, w^*

c) Solve the pressure correction equation

d) Correct p from,

$$p^{**} = p^* + p'$$

e) Calculate u, v, w from their starred values using the velocity correction equations,

$$u^{**} = u^* + u'$$
$$v^{**} = v^* + v'$$
$$w^{**} = w^* + w'$$

f) Make a second correction for p, u, v, and w as;

$$p^{***} = p^{**} + p''$$
$$u^{***} = u^{**} + u''$$
$$v^{***} = v^{**} + v''$$
$$w^{***} = w^{**} + w''$$

g) Solve the discretization equation for other variables, such as temperature and turbulence quantities

h) Treat the corrected pressure p as a new guessed pressure p^*, return to step b, and repeat the steps until a converged solution is achieved.

Dimensions of the models as well as the operating and boundary conditions lead to a turbulent flow inside, which is the case for the refrigerator applications of the cavity analyses [9, 35, 36]. In the present study, k-ε turbulence model is

used for the solution of the problem as explained in Chapter 2. Although the obtained results are meaningful, the investigation of turbulent natural convection remains challenging. The strong coupling between flow and temperature fields and interaction between boundary layers and core flow make computation very stiff and converge difficult. In addition; the flow in a cavity, in particular for cooling of electronics or of refrigerator compartments, is likely to be transitional. This causes problems for most of the Reynolds-averaged Navier-Stokes (RANS) based turbulence models, which are calibrated in fully turbulent flow conditions. When the turbulence level in the core region of cavity is low for buoyancy-driven flows, most of the models tend to relaminarize the flow and, as a consequence, underpredict the near wall turbulence intensities and boundary layer thicknesses [64].
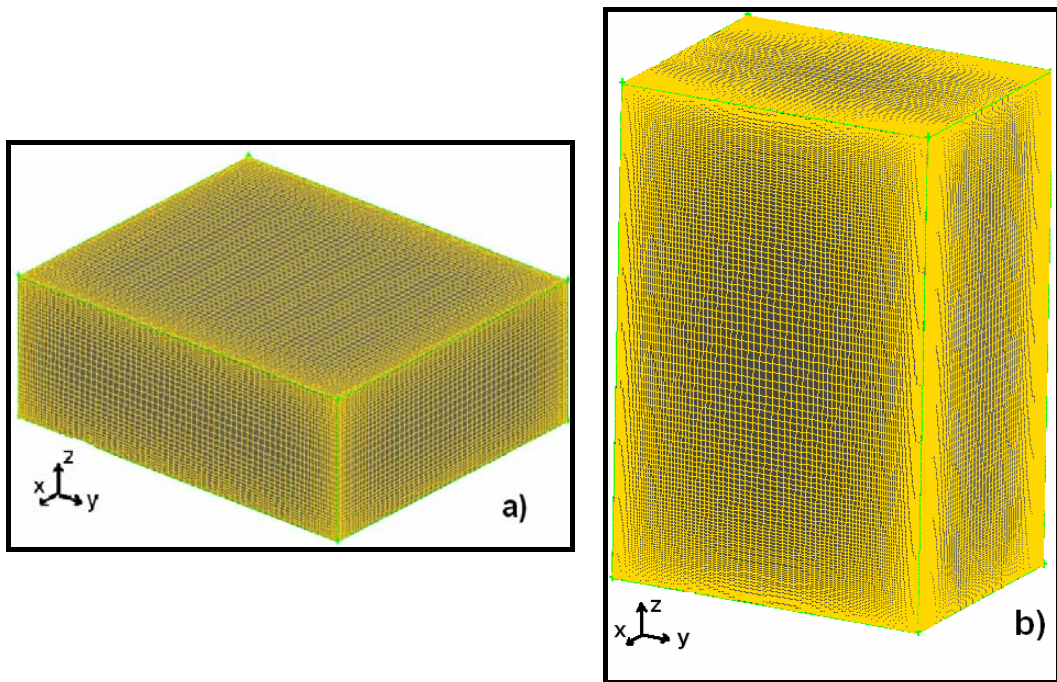
Figure 3.4. Meshed model of 3-D geometries, a) the preliminary study and the single compartment, b) the total refrigerator

Formulation of numerical methods is developed on the basis of hexahedral meshes for all three cases shown in Figure 3.4. Model cavities' meshes are clustered from central region of the domain to the corners which are critical and dominating the solution of the natural convection problem in a closed enclosure. The growth rate of the cells from the six corners to the center of the domain is 1.06.

Characteristics of the 3-D cavity models in numerical analyses and the total number of cells in these models used for the simulations are submitted in Table 3.1.

Table 3.1. Number of cells used for the simulations

	Mesh Number			
	Height	**Width**	**Depth**	**Total**
Preliminary Study	37	75	66	183150
Single Compartment	37	75	66	183150
Total Refrigerator	133	103	78	1068522

Screenshots of the solver algorithm, materials selected with its properties, operating and sample boundary conditions specified for each analysis, solution controls, viscous model selected, radiation model chosen when applied, solution initialization and residual monitors are presented in Appendix B.

3.3. Experimental Work

Since the cavity analyses in literature are generally numerical and different from the present study, it is necessary to perform experiments in order to form a base

for the boundary conditions of the numerical analysis and check the obtained results of the numerical solutions.

In the experimental part, 4243 TMB model static (without ventilation) household refrigerator (with outer dimensions 173x70x68 cm) in the research department of Arçelik Çayırova factory is used and the temperatures of the walls and specified points at different locations inside are measured. So it will also be possible to substitute the values of the temperature boundary conditions in the numerical analysis with the experimental ones.

Temperature measurements are made only on one side of the symmetry plane of the domain as shown in Figures 3.5 and 3.6 for both single compartment and total refrigerator. Omega, T-type copper-constantan thermocouples with a temperature measuring range of –250 °C to 350 °C and HP, Agilent 34970A model data logger are used in measurements [65, 66].

Temperatures of 58 specified points (5 points each for top and bottom walls, 12 points each for the other walls and symmetry plane) are measured for the total refrigerator and 54 point measurements (9 points for all walls and symmetry plane) are performed for single compartment. Compartment's bottom wall is 39 cm above the bottom of the whole refrigerator so one part of the back wall is completely the evaporator region. Temperature values are continuously measured and data is recorded every ten seconds through three days for compartment case and one day for the whole refrigerator.

On the other hand; it is obvious that measuring the air velocity experimentally is difficult. Actually in a few work, the air velocity in the cavity was measured with the help of a probe but for such a cavity of the present work the probe inserted may disturb the flow due to the dimensions of the compartment and the x, y and z velocity magnitudes. That is why; the velocity results obtained in

numerical work will be compared with the results of the similar studies in literature.

The real errors in experimental data are those factors that are always vague to some extent and carry some amount of uncertainty. A reasonable definition of experimental uncertainty may be taken as the possible value the error may have [67]. Expected uncertainty including the measurement, switching and transducer conversion errors in this experimental study arises from the uncertainties in T-type thermocouples used and the data logger integrated and these uncertainty values (standard limits of error) are ± 1 $^{\circ}$C for both [66, 67].

Some pictures of the experimental set-up and the schematic view of the locations of the T-type thermocouples used in the experiments are presented in Figures 3.5-3.7. The coil seen in Figures 3.5 and 3.6 is not actually a working condenser coil. It is there just for fixing the thermocouples on the symmetry plane.

For both models, red colored thermocouples are positioned on the top wall, whereas yellow, blue, black, orange and green colored ones are located on side, back, bottom, symmetry and front surfaces respectively. On the surfaces which are parallel, thermocouples are located opposing to each other. Given dimensions which are in centimeters indicate the exact locations of the thermocouples in Figure 3.7. One can easily understand from Figure 3.7 that, numbering of thermocouples starts with the thermocouple **t1** at the top wall close to the back and symmetry planes and continues in the order of side, back, bottom, symmetry and front surfaces.
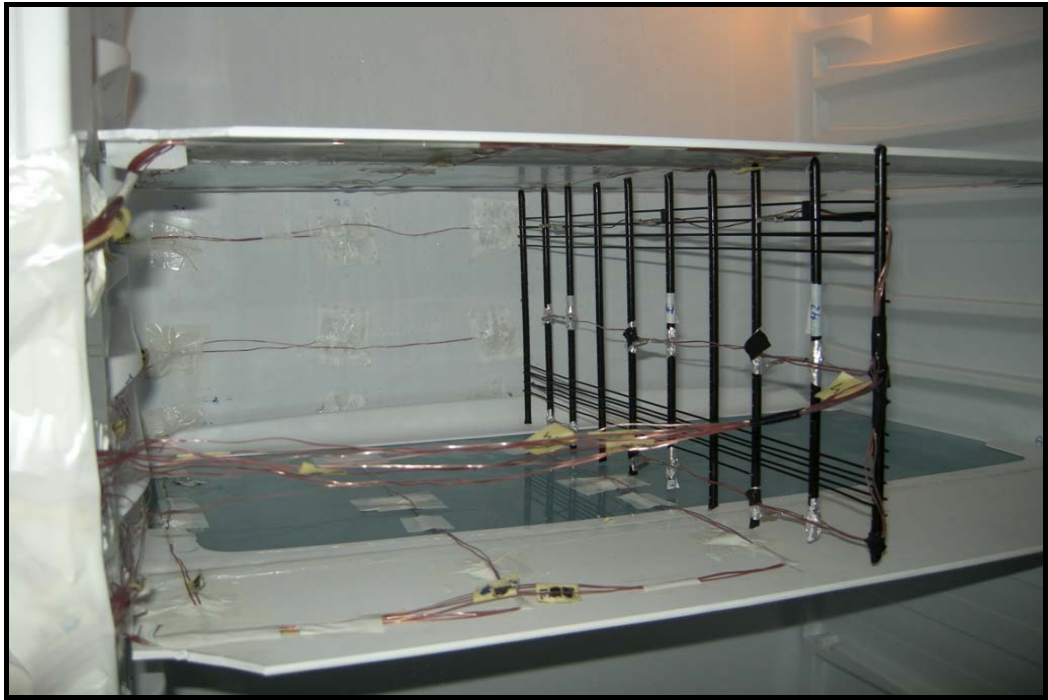
Figure 3.5. Experimental set-up for the single compartment

Figure 3.6. Experimental set-up for the total refrigerator
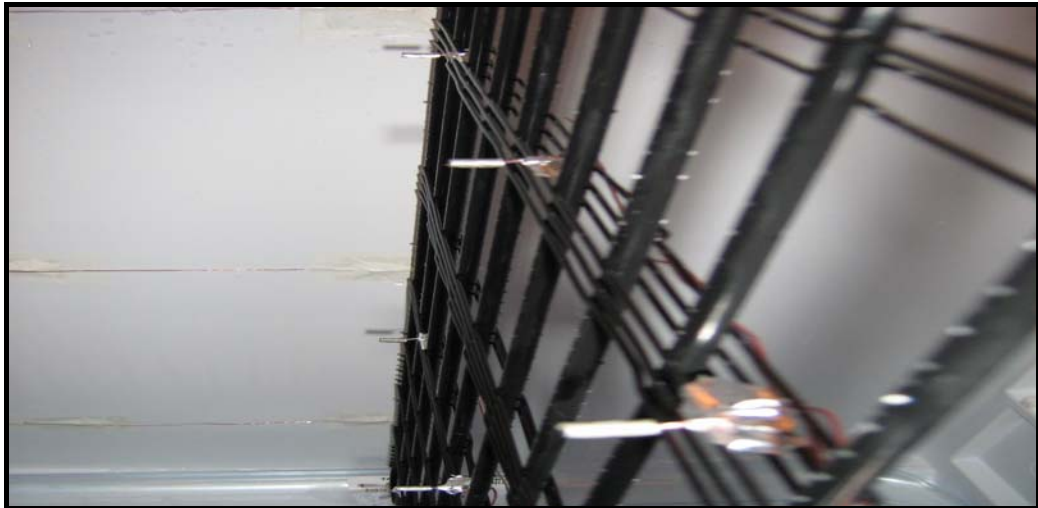
Figure 3.6.*Continued*, Experimental set-up for the total refrigerator
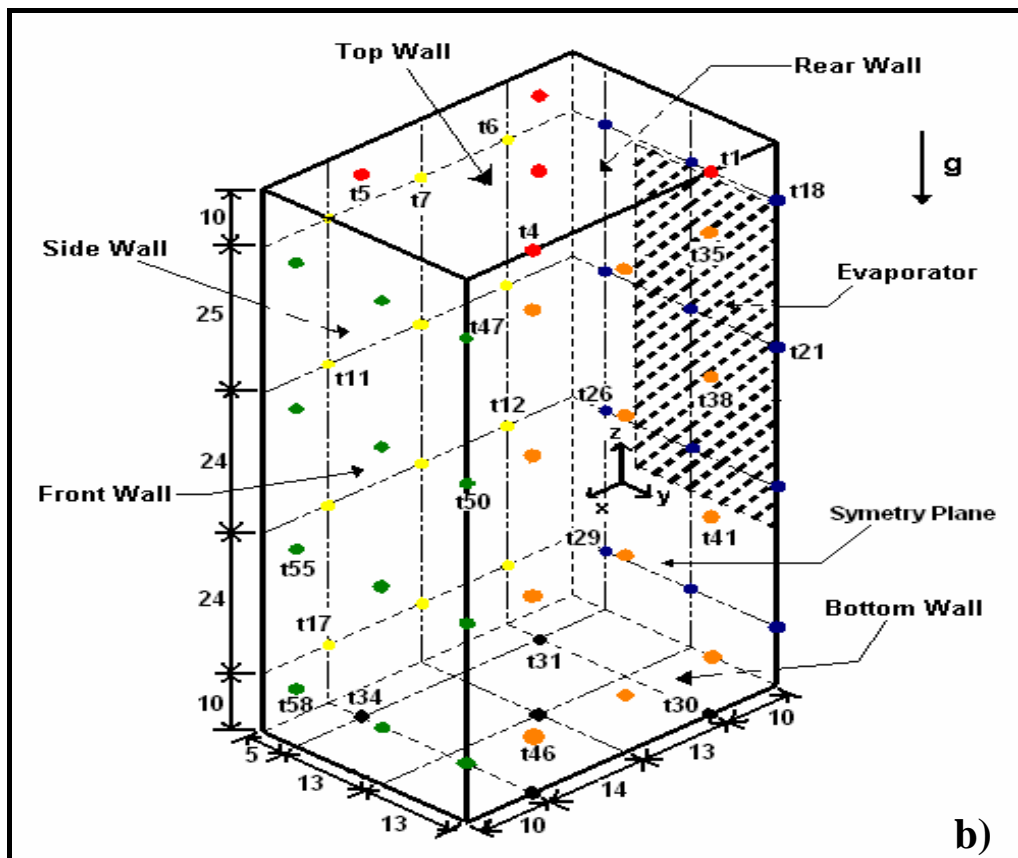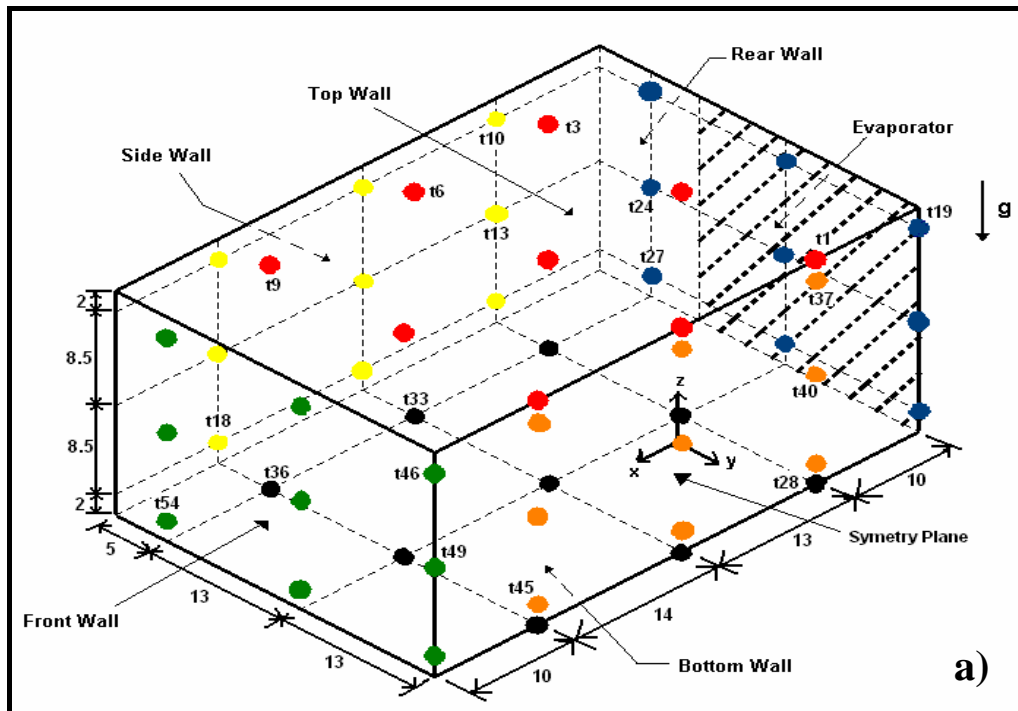
Figure 3.7. Schematic view of the thermocouple locations, a) the single
compartment, b) the total refrigerator

3.4. Heat Transfer Analysis

After performing the numerical analysis to obtain the temperature and velocity distributions inside the domain, now it is possible to evaluate both the heat flux and heat transfer coefficient at the walls and total heat transfer rates from the walls.

3.4.1. Heat Flux

Since temperature distribution has been determined, heat fluxes from the walls at any instant can be calculated from;

$$q^{''} = q^{''}_{conv} + q^{''}_{rad} \qquad (3.12)$$

where;

$q^{''}_{conv}$: the convective heat flux,

$q^{''}_{rad}$: the radiative heat flux.

While calculating the convective heat flux, Fourier's law can be used;

$$q^{''} = -k(\frac{\partial T}{\partial n})_{wall} \qquad (3.13)$$

where;

k : the thermal conductivity of the fluid inside,

n : the normal vector to the wall.

However for turbulent flows, Fluent uses the law-of-the-wall for temperature derived using the analogy between heat and momentum transfer [40, 68].

The law-of-the-wall for mean velocity yields,

$$U^* = \frac{1}{\kappa}\ln(Ey^*) \tag{3.14}$$

where;

$$U^* \equiv \frac{U_P C_\mu^{0.25} k_P^{0.5}}{\tau_w / \rho} \tag{3.15}$$

$$y^* \equiv \frac{\rho C_\mu^{0.25} k_P^{0.5} y_P}{\mu} \tag{3.16}$$

κ : von Karman constant (0.4187),

E : empirical constant (9.793),

U_P : mean velocity of the fluid at point P,

k_P : turbulence kinetic energy at point P,

y_P : distance from point P to the wall,

μ : dynamic viscosity of the fluid.

The logarithmic law for mean velocity is known to be valid for $30 < y^* < 300$. In Fluent, the log-law is employed when $y^* > 11.225$. When the mesh is such that $y^* < 11.225$ at the wall-adjacent cells, Fluent applies the laminar stress-strain relationship that can be written as;

$$U^* = y^* \tag{3.17}$$

Reynolds' analogy between momentum and energy transport gives a similar logarithmic law for mean temperature. As in the law-of-the-wall for mean velocity, the law-of-the-wall for temperature employed in Fluent comprises the following two different laws:

- linear law for the thermal conduction sublayer where conduction is important,
- logarithmic law for the turbulent region where effects of turbulence dominate conduction.

The law-of-the-wall implemented has the following composite form:

$$T^* = \Pr y^* + \frac{1}{2}\rho\Pr\frac{C_\mu^{0.25}k_P^{0.5}}{q_{conv}^"}U_P^2 \qquad y^* < y_T^* \tag{3.18}$$

$$T^* = \Pr_t(U^* + P) + \\ \frac{\rho C_\mu^{0.25}k_P^{0.5}}{2q_{conv}^"}(\Pr_t U_P^2 + (\Pr - \Pr_t)U_c^2) \qquad y^* > y_T^* \tag{3.19}$$

where P is computed by using the formula given by Jayatilleke [69];

$$P = 9.24\left[(\frac{\Pr}{\Pr_t})^{3/4} - 1\right]\left[1 + 0.28e^{-0.007\Pr/\Pr_t}\right] \tag{3.20}$$

and,

k_P : turbulence kinetic energy at point P,

ρ : density of the fluid,

c_P : specific heat of the fluid,

$\Pr$: molecular Prandtl number,

$\Pr_t$: turbulent Prandtl number (0.85 at the wall),

U_c : mean velocity magnitude at $y^* = y_T^*$.

T^* is also related to wall temperature T_{wall} and adjacent cell temperature T_P as;

$$T^* \equiv \frac{(T_{wall} - T_P)\rho c_p C_\mu{}^{0.25} k_P{}^{0.5}}{q_{conv}^{"}} \qquad (3.21)$$

The non-dimensional thermal sublayer thickness, y_T^*, in Equations 3.18 and 3.19 is computed as the y^* value at which the linear law and the logarithmic law intersect, given the molecular Prandtl number of the fluid being modeled.

The procedure of applying the law-of-the-wall for temperature is as follows. Once the physical properties of the fluid being modeled are specified, its molecular Prandtl number is computed. Then, given the molecular Prandtl number, the thermal sublayer thickness, y_T^*, is computed from the intersection of the linear and logarithmic profiles, and stored.

During the iteration, depending on the y^* value at the near-wall cell, either the linear or the logarithmic profile in Equations 3.18 and 3.19 applied to compute the wall heat flux $q_{conv}^{"}$.

The function for P given by equation Equation 3.20 is relevant for the smooth walls. For the rough walls, however, the modified form of this function is used. Details of law-of-wall for mean velocity and temperature in turbulent flows are given in literature [40].

While obtaining the heat flux values, area weighted average of the flux at each facet on the corresponding wall is calculated by the computer program.

3.4.2. Effective Heat Transfer Coefficient

For such kind of a physical problem the second parameter related to heat transfer analysis is the convective heat transfer coefficient. After computing the

heat fluxes to or from the walls it is very simple to calculate effective heat transfer coefficient for each wall from the formula;

$$h_{eff} = \frac{q^{''}}{T_{wall} - T_{ref}}$$
(3.22)

In Equation 3.22, T_{ref} is the reference temperature and it is taken as the temperature of the geometric center of the cavity for that time instant of analysis and $q^{''}$ is the total heat flux. If radiation is not included in the analysis, such as the case of preliminary study, then the effective heat transfer coefficient is equal to the convective heat transfer coefficient.

In the next chapter of the report, effective heat transfer coefficients at the front and rear walls as well as some of the other walls are presented.

3.4.3. Heat Transfer Rates

The methodology used in the computer program to calculate heat fluxes and heat transfer coefficients for the walls performs the calculations based on area weighted average of the quantity searched so it may cause small errors. Therefore; calculating the total heat transfer rate gives more meaningful results. Moreover the results of this computation will also reveal the magnitude of radiation heat transfer and offers whether the analysis would reach to steady state or not.

CHAPTER 4

MODEL RESULTS AND DISCUSSION

In this chapter, first the results of the numerical analysis for the preliminary model cavity and related heat transfer analyses will be outlined. Then analyses performed in literature for the whole empty refrigerator and the one done using Fluent with design parameters in the present work to determine the contribution of radiation transfer will be compared. Next, experimental study made to define the constant temperature boundary conditions for the following numerical analyses of a single compartment and total refrigerator will be discussed and numerical analyses including the heat transfer studies will be outlined.

4.1. Results of Preliminary Numerical Analysis

Preliminary numerical analysis was performed to form a CFD model for the natural convection problem in a cavity. The preliminary analysis presented here is an extension of a verification study of the created numerical model. Before the preliminary study, previous studies had been performed and analyzed in order to reveal the impact of three parameters (mesh size, temperature difference between vertical walls and initial z velocity) on the solution of the problem in parallel to the work in literature [4, 16, 70].

The first parameter was the mesh size. To obtain a solution which is independent of mesh size, minimum number of mesh points (or nodes) necessary for the model was investigated. In the numerical analysis performed

for the determination of the necessary mesh points, the initial temperature was denoted to be 275 K and the values of the x and y velocity components were assumed to be zero and z velocity component was assumed as 0.01 m/s respectively. Referring to Figure 3.1; the wall temperatures were assumed to be $T_{top} = 279.20$ K, $T_{bottom} = 278.05$ K, $T_{front} = 279.85$ K, $T_{rear} = 272.85$ K with the adiabatic side walls [35, 59, 60]. The numerical analysis was performed for all coarse meshed, finer meshed and finest meshed control volumes. Total number of cells, mesh faces, mesh edges and mesh nodes of the three control volumes are tabulated in Table 4.1.

Table 4.1. The mesh characteristics of models used for the simulations

	Numbers of Mesh			
	Faces	**Edges**	**Nodes**	**Total**
Coarsed Meshed Cavity	9050	472	60480	55836
Finer Meshed Cavity	20334	712	193496	183150
Finest Meshed Cavity	27872	868	289674	275520

It was observed that, solutions for the finer meshed and the finest meshed volumes were the same, therefore, the finer meshed domain with 183150 volume elements was used for the preliminary analysis.

The second parameter which affects the solution of the free convection problem is the temperature difference between the boundaries. In order to observe the dependence of the solution on temperature difference, the initial temperature and the velocity values as well as the boundary conditions were kept the same but only the front wall temperature of the cavity was increased from $T_{front} = 279.85$ K to $T_{front} = 304.85$ K. Since the temperature difference was very large compared to the previous condition, the development of the temperature

isotherms in the cavity were very weak at the time instants considered before. Whereas, these profiles were not changing so much which resulted in a much longer time to reach steady state. That is why, for the preliminary study, front wall temperature was decided to be $T_{front} = 279.85$ K which is a similar situation to what happens in a real domestic refrigerator application.

It was aimed to observe the effect of the third parameter, initial z velocity, therefore; to visualize this dependence, initial temperature and velocity values as well as the boundary conditions were kept the same as in the first case but only the z velocity component was assumed to be 0.001m/s instead of 0.01m/s. The performed analysis showed that, the characteristics of the velocity profiles and temperature profiles did not change compared to the analysis done with *w*=0.01 m/s but a decrease in velocity magnitudes with decreasing initial z velocity was observed and the development of the flow inside the compartment slowed down.

Although the physical problem is symmetric with respect to the x-z midplane, the velocity profiles on x-y midplane had not been symmetrical so far. To prevent this misleading occurrence it was decided to apply a new method. Instead of defining in the whole cavity; the initial z velocity was specified in a small region close to the front wall. Due to the fact that the finer meshing of the compartment fits to the physical problem better, analysis of the new approach was focused on finer meshed cavity and at the end of the analysis it was revealed that, patching a small volume with an initial z velocity onto the whole volume with zero velocity gives more physically meaningful results. However, there was still a small deviation from the symmetric velocity distribution.

As the final work before the preliminary study; taking *w*=0 m/s as an initial condition, the analysis had been repeated for finer meshed cavity and it was observed that; nearly an exact symmetric velocity distribution on x-y midplane had been reached, therefore; initial z velocity dependence of the problem had

been observed and assumption of $u=v=w=0$ m/s velocity initial condition in the preliminary analysis was made.

In this section, the results from the analysis of the finalized form of the preliminary numerical model will be presented.

4.1.1. Temperature and Velocity Profiles

Considering $\beta=0.0032$ K^{-1}, the transient analysis is performed and temperature and velocity profiles inside the compartment are obtained.
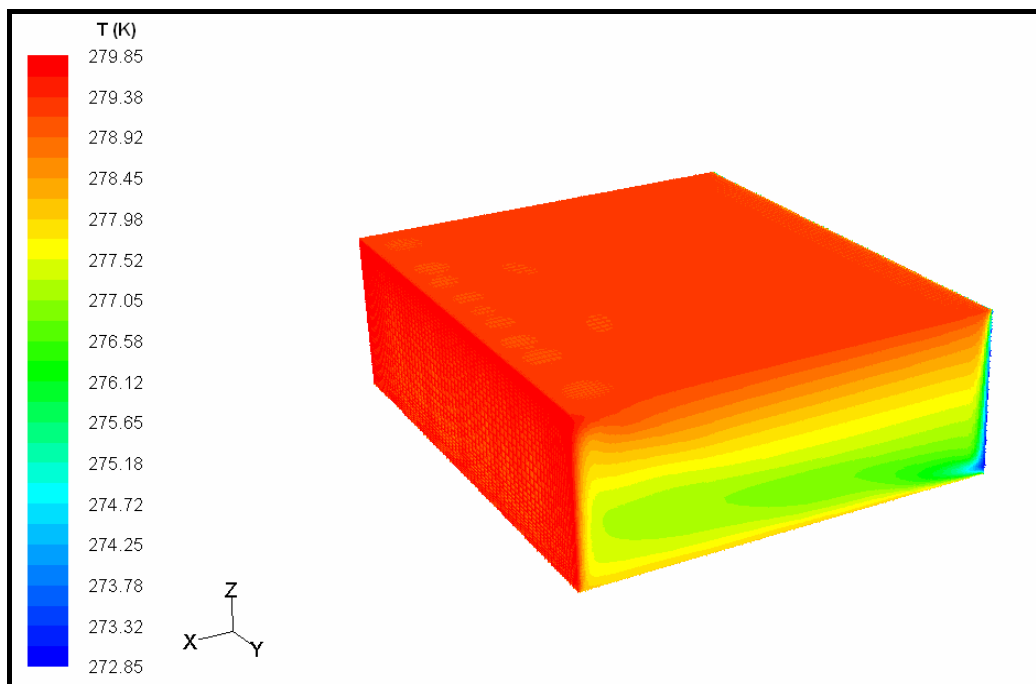

Figure 4.1. Temperature profile for the preliminary analysis, t=150 s

In Figure 4.1, the temperature profile at the time instant of 150 seconds shows free convection characteristics. Hot air heated at the front wall rises to the top, interacts with the relatively cold top wall and descents a little bit and then

continues to diffuse straight to the back side of the compartment as presented in Figure 4.2. On the other hand, a complicated velocity distribution developing mainly at front and rear vertical walls is observed at this time instant. The flow is symmetric with respect to x-z plane.
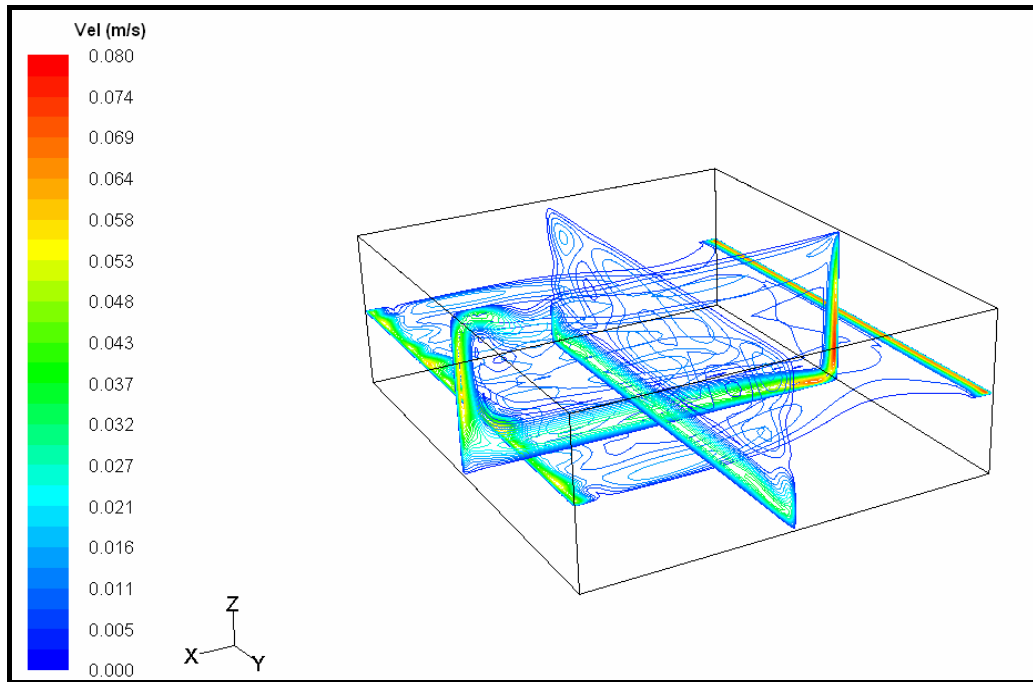
Figure 4.2. Velocity contours at midplanes for the preliminary analysis, t=150 s

In Figures 4.3 and 4.4, it is presented that, at the time of 5 minutes, the temperature profile is not different from the previous time instant. The only change is that the hot streams of air above the compartment influence the nearly stagnant air below and result in an increase in the temperature of the air around the center of the cavity. Additionally, velocity profile is not changing so much but a better organized developing flow with slightly increased magnitudes is observed. After 300 seconds, temperature profile is almost the same but velocity value is increasing up to 0.081 m/s. Temperature profile and velocity contours inside the compartment are presented in Figures 4.5 and 4.6 for the time instant of 600 seconds and in Figures 4.7 and 4.8 for the time instant of 3600 seconds.
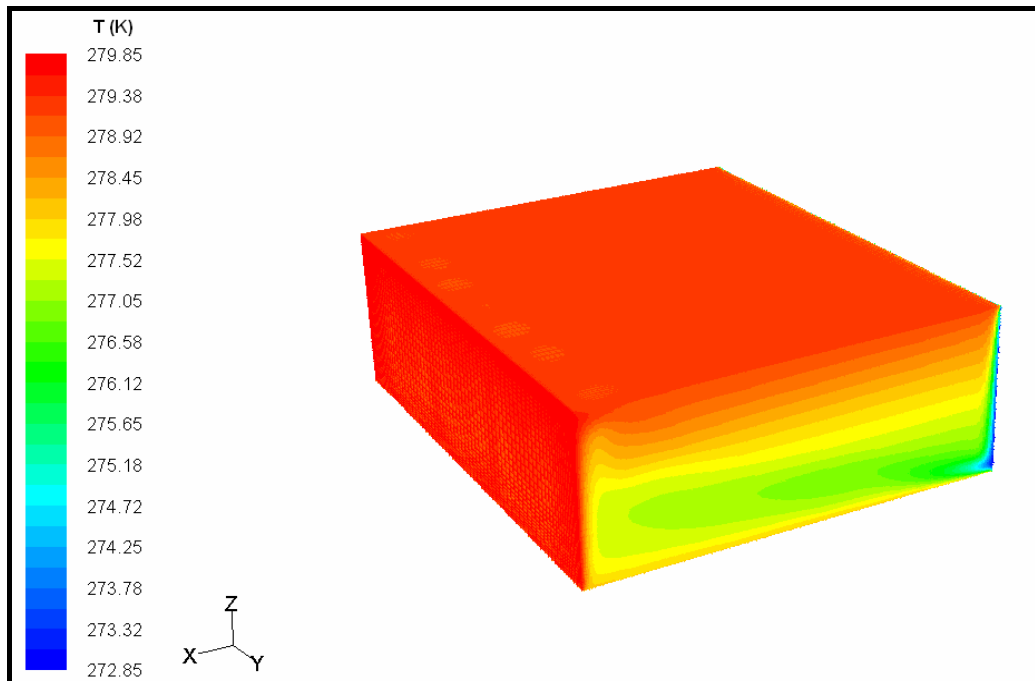
Figure 4.3 Temperature profile for the preliminary analysis, t=300 s
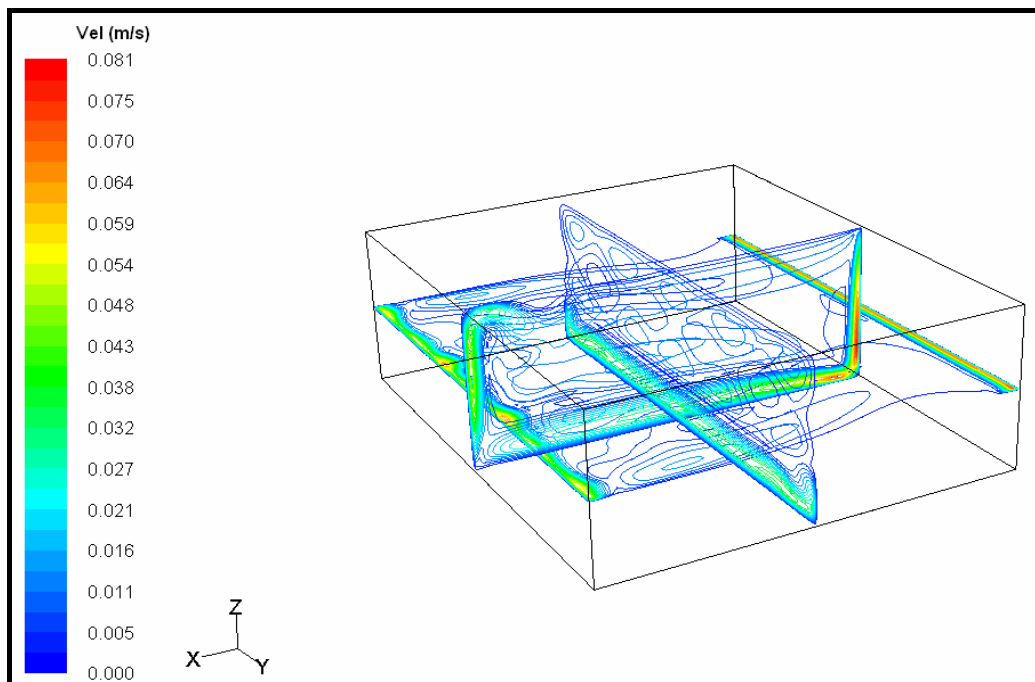
Figure 4.4. Velocity contours at midplanes for the preliminary analysis, t=300 s
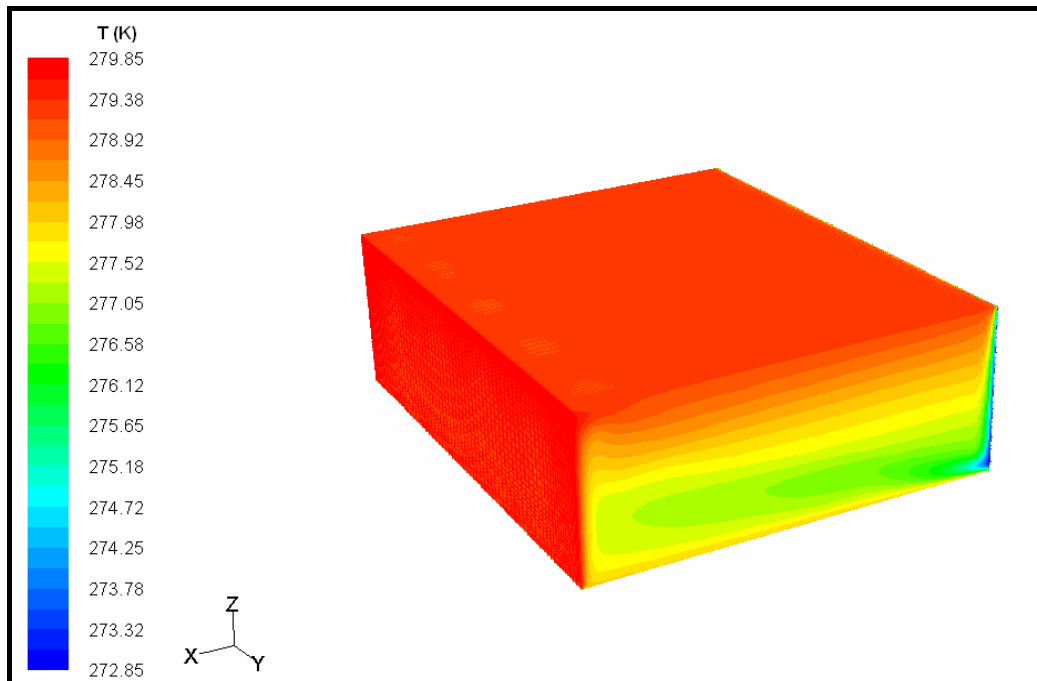
Figure 4.5. Temperature profile for the preliminary analysis, t=600 s
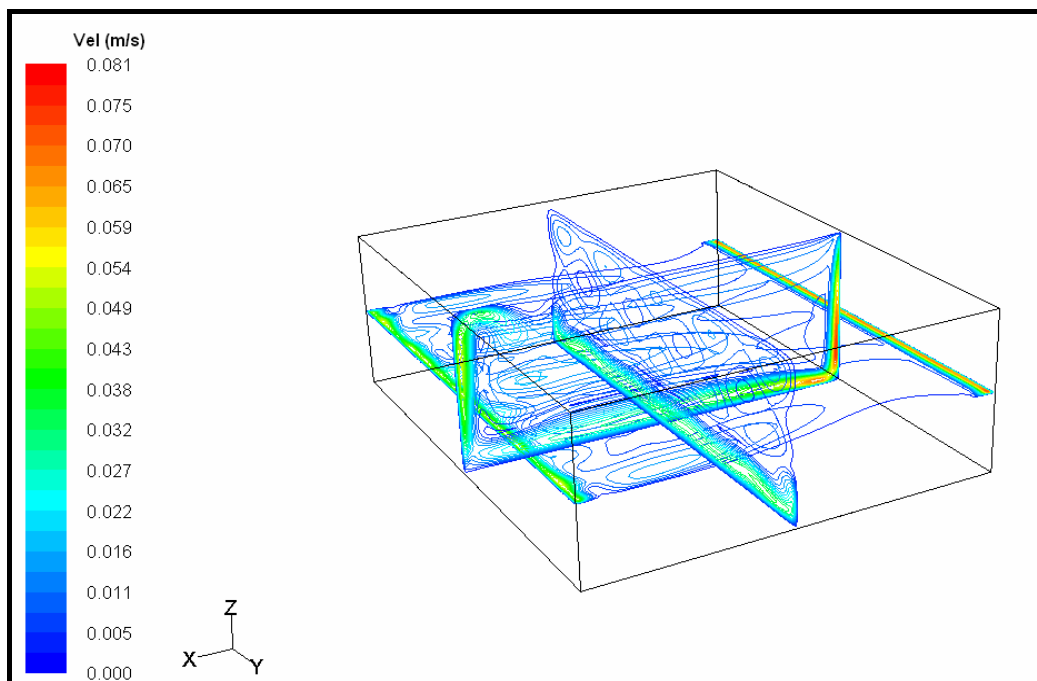
Figure 4.6. Velocity contours at midplanes for the preliminary analysis, t=600 s
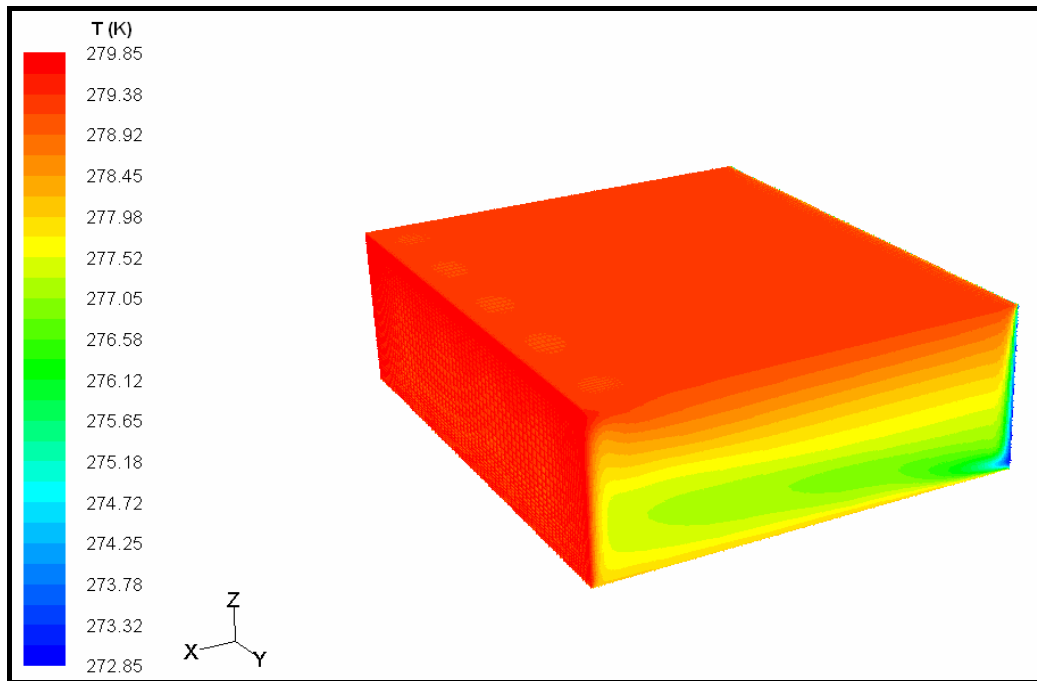
Figure 4.7. Temperature profile for the preliminary analysis, t=3600 s
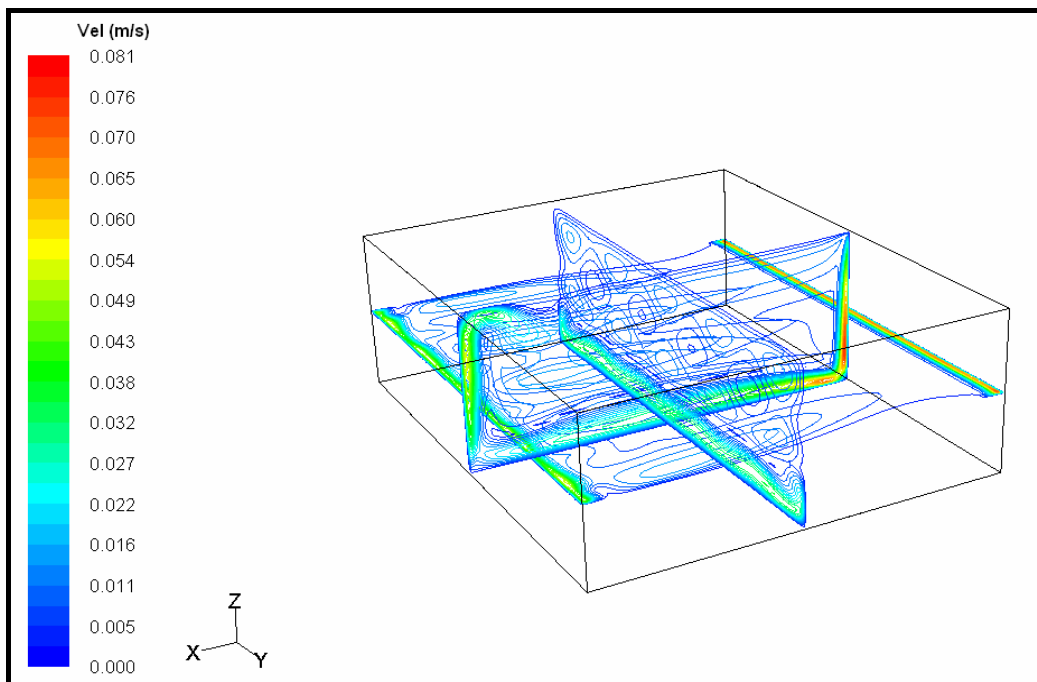
Figure 4.8. Velocity contours at midplanes for the preliminary analysis, t=3600 s

To visualize the velocity boundary layers at the walls and the flow directions more clearly at steady state, the velocity vectors at the symmetry plane of the cavity (x-z midplane) at the time of 3600 s is presented in Figure 4.9.
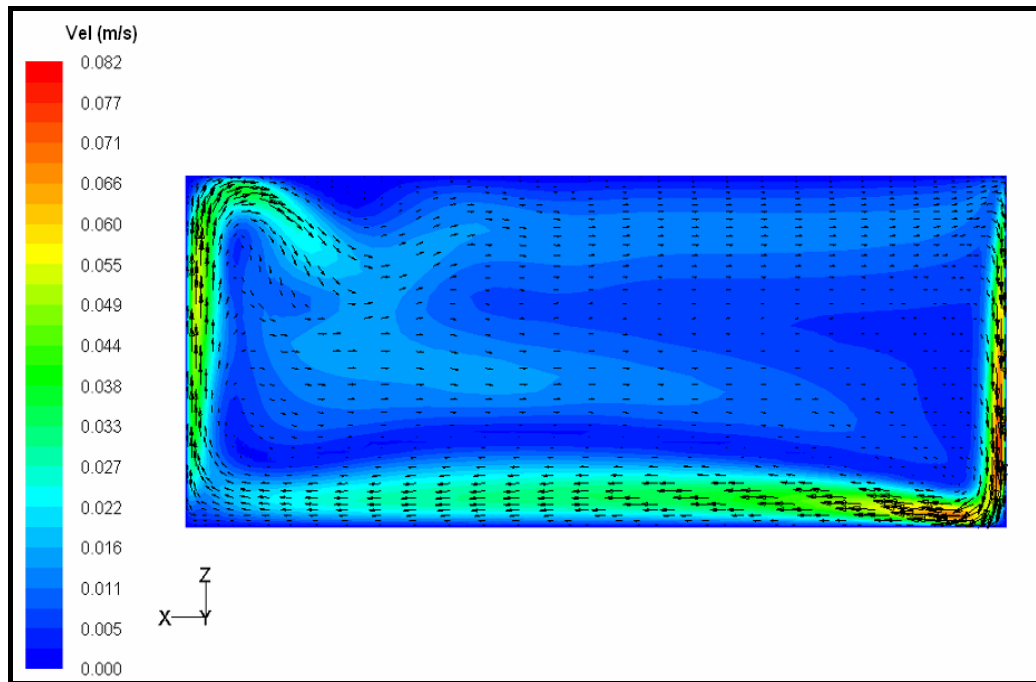
Figure 4.9. Velocity vectors at the symmetry plane for the preliminary analysis, t=3600 s

4.1.2. Heat Transfer Analysis

Heat transfer analysis explained in the previous chapter is performed for the model without radiation. As an extension of the numerical analyses summarized in the previous section, the heat flux, total heat transfer rates from the walls and convective heat transfer coefficient at the walls are determined. While obtaining the heat flux values, area weighted average of the flux at each face of the corresponding wall is calculated by the computer program.

Time dependent heat flux values for all walls are evaluated by using Equation 3.18 or 3.19 with Equation 3.21 and plotted in Figure 4.10.
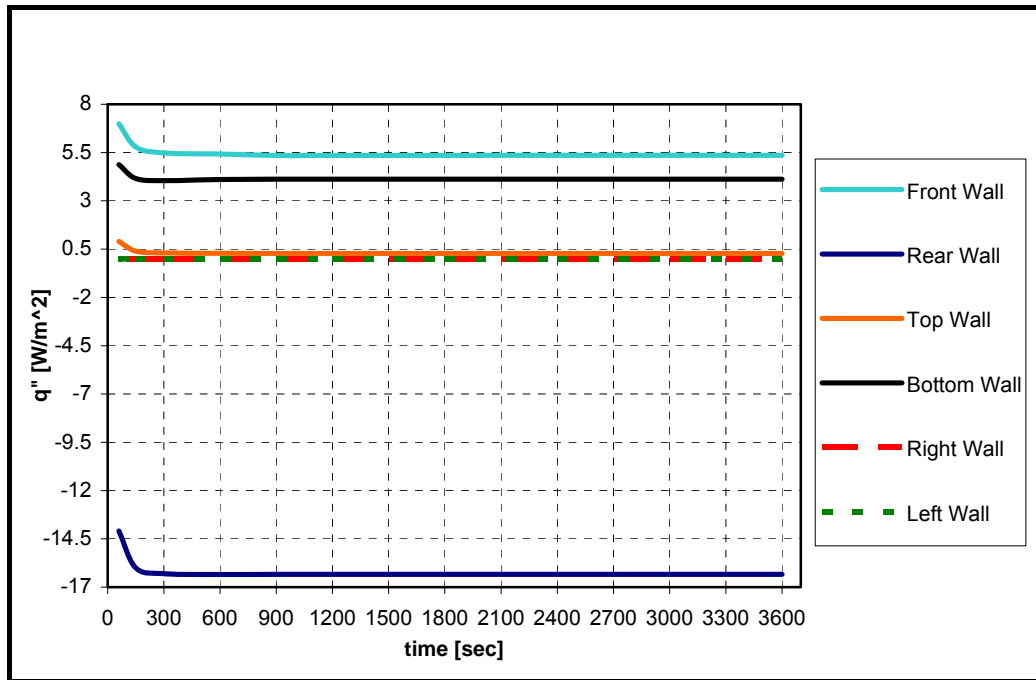
Figure 4.10. Time dependent heat flux values for the preliminary analysis

In Figure 4.10, it is shown that heat flux values are constant after 150 seconds. Moreover, the absolute heat flux values at the front and rear walls are larger than the others since they are the boundaries driving the natural convection inside.

Time dependent convective heat transfer coefficients for all walls are evaluated by using Equation 3.22. As observed in Figure 4.11, convective heat transfer coefficient values are not changing with time after 300 seconds. Only change is observed at the bottom wall between the time instant of 300 seconds and 900 seconds. Moreover, heat transfer coefficient value at the bottom wall is larger than the others since the temperature difference between the bottom wall and the geometric center is smaller than the other walls.
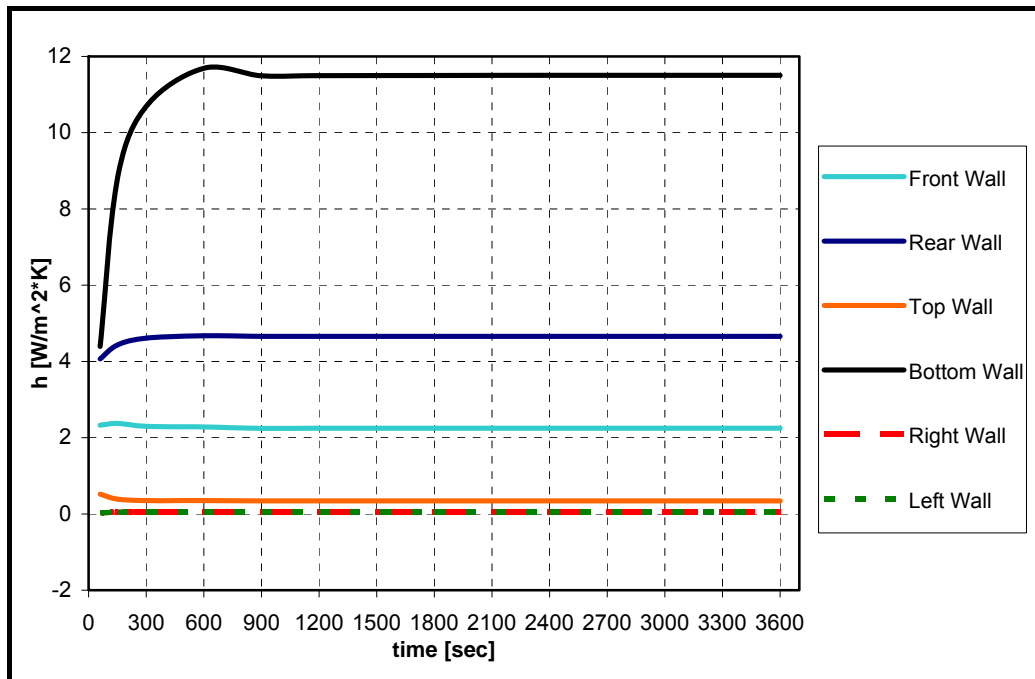
Figure 4.11. Time dependent convective heat transfer coefficient values for the preliminary analysis

Next, the steady state time is taken as t=3600 seconds, and by calculating the values of heat flux and convective heat transfer coefficient parameters at 4 equally spaced lines (9 cm distance between each) on front and rear walls presented in Figure 4.12, variations of them with respect to spatial coordinate z are plotted.

In Figure 4.13, it is revealed that heat flux values are not changing from the symmetry plane to side wall for both front and rear walls. Moreover, this value decreases from bottom to top for the hot front wall and opposite for the rear cold wall which is the result of the boundary layer development on those surfaces. This fact is supported by h(z) graph in Figure 4.14. Convective heat transfer coefficient value increases from the bottom to the top at the rear wall due to an increase in corresponding heat flux value as mentioned before and the case is reverse for the front wall.
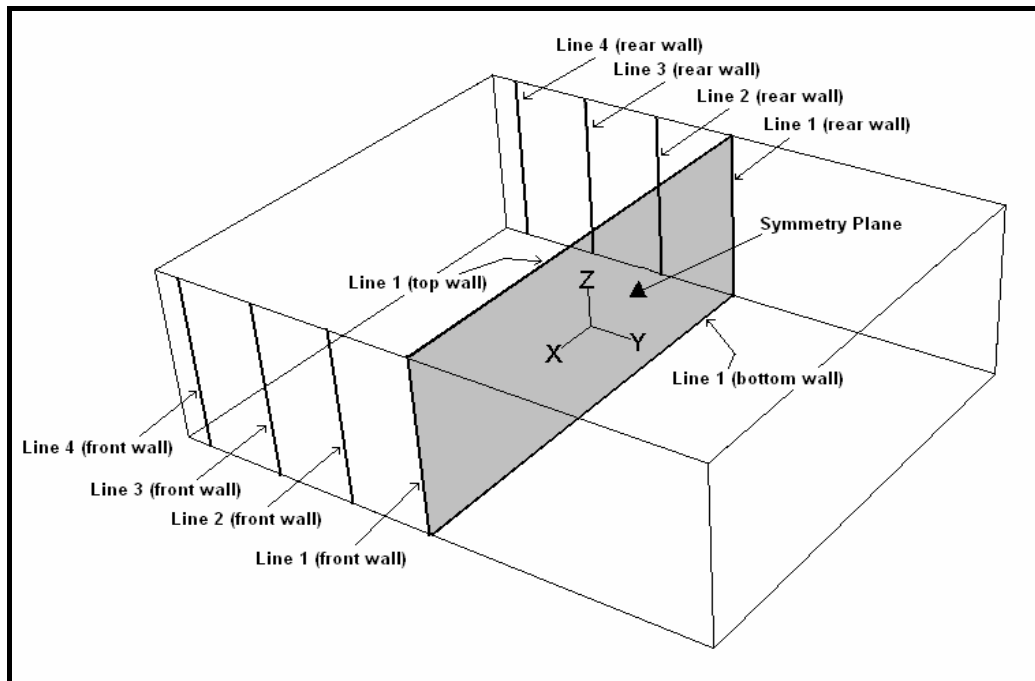
Figure 4.12. Configuration of the reference lines used for s.s. heat
transfer analysis in the preliminary analysis
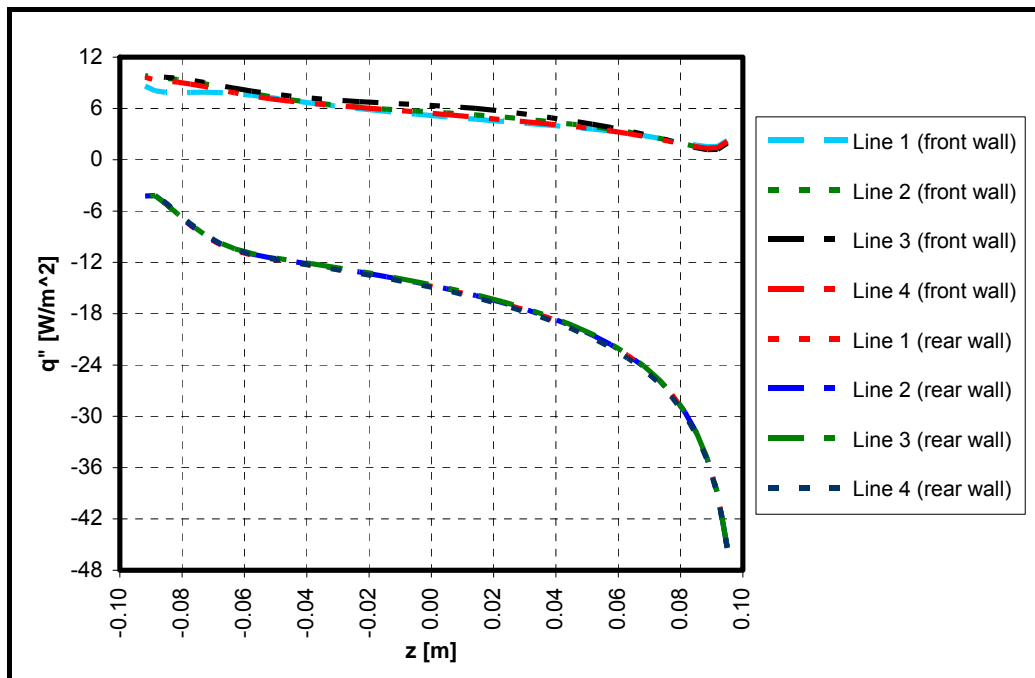
Figure 4.13. Steady state heat flux values at the front and the rear walls for the
preliminary analysis
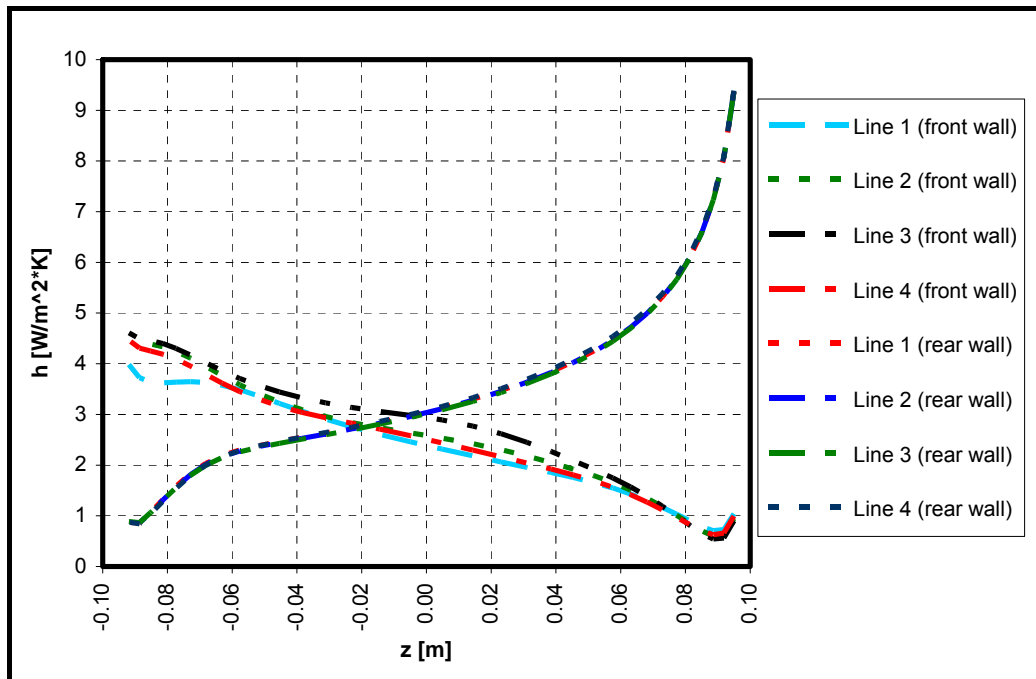
Figure 4.14. Steady state convective heat transfer coefficient values at the front and the rear walls for the preliminary analysis

To compare the values of q″ and h for bottom and top walls with the ones obtained for front and rear walls, q″(x) and h(x) are presented only for the lines, Line 1 (top wall) and Line 1 (bottom wall), shown in Figure 4.12.

In Figure 4.15, it is shown that, the heat flux value is high on Line 1 for the bottom wall at the region close to the rear wall because this region is in contact with the cold air flowing downward on the rear wall. However, a sharp decrease in the heat flux value is observed through the reference line and it converges to zero at the location where bottom wall intersects with the front wall. On the other hand; q″(x) is not changing and nearly zero on the top wall which means very small amount of heat transfer on the top wall. Since effective heat transfer coefficient which is the same with the convective heat transfer coefficient in the preliminary analysis (radiation heat flux is taken as zero) is determined by dividing the heat flux value by a constant temperature difference, the characteristics of the graph in Figure 4.16 is similar to the one in Figure 4.15.
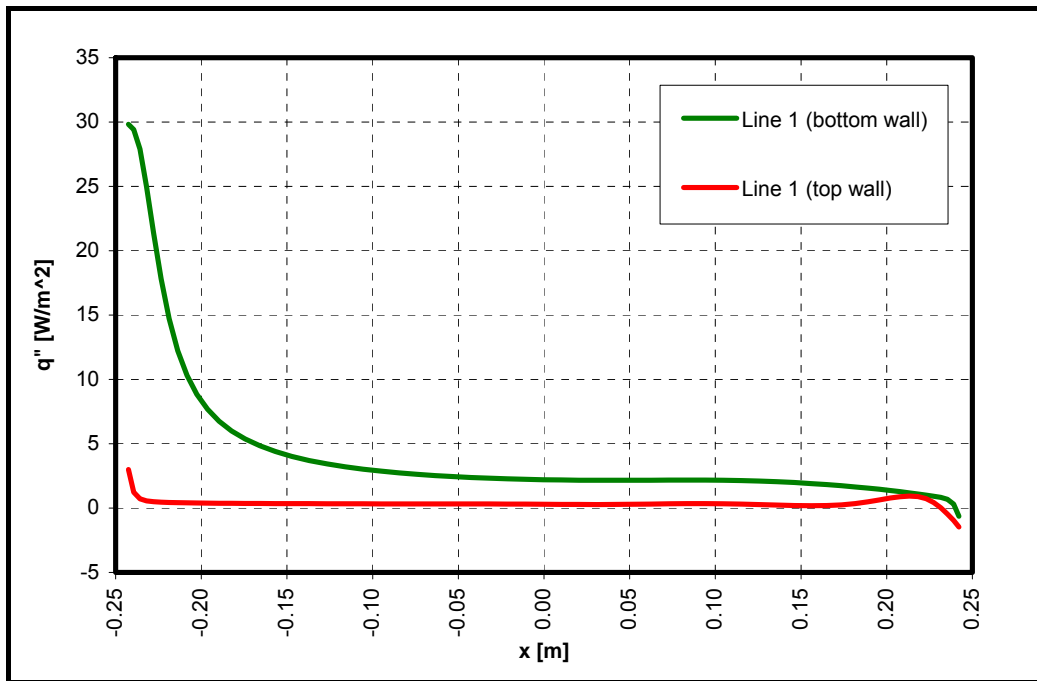
Figure 4.15. Steady state heat flux values at the bottom and the top walls for the preliminary analysis
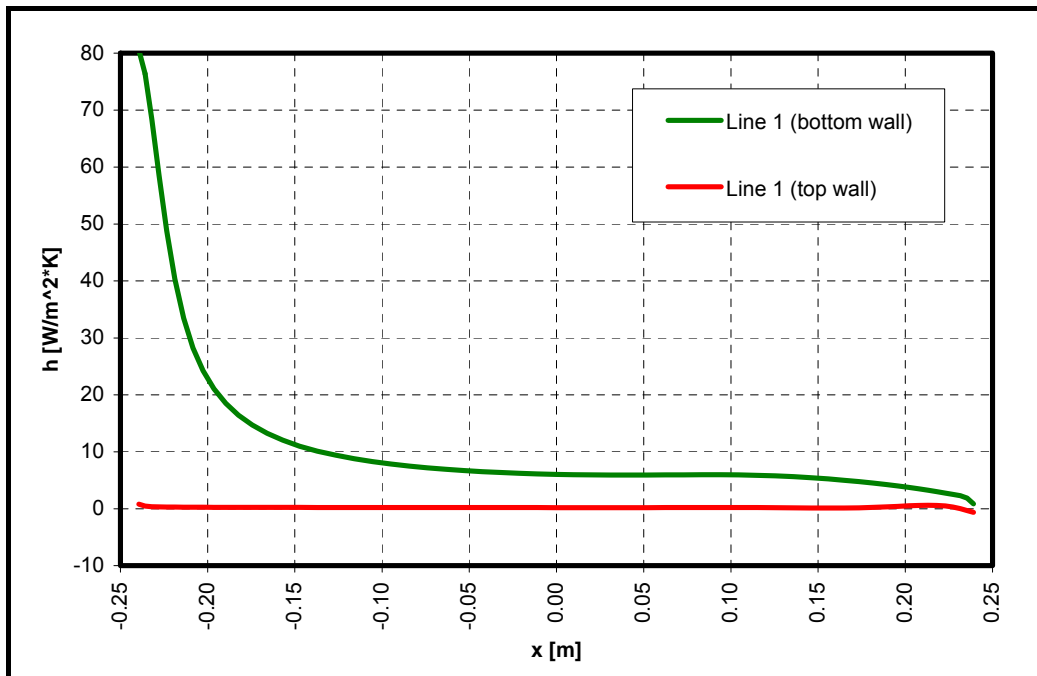

Figure 4.16. Steady state convective heat transfer coefficient values at the bottom and the top walls for the preliminary analysis

Finally, heat transfer rate from the system is calculated at time t=3600 s and it is checked whether this time instant is good prediction for the steadiness or not. The total heat transfer rates in Watts from all boundaries are tabulated in Table 4.2.

Table 4.2. Total heat transfer rates (in Watts) for preliminary analysis, t=3600 s

Front Wall	0.67973787
Rear Wall	-2.1345682
Top Wall	0.16646683
Bottom Wall	1.2884793
Left Side Wall	0
Right Side Wall	0
Residual of the Energy Balance	*0,0001158*

Table 4.2 supports that the time instant 3600 s is a very good prediction for the steadiness of the analysis.

4.2. Evaluation of Radiation Effect

Preliminary study was performed omitting the radiation in the numerical model. However obtained temperature and velocity profiles in the cavity and heat transfer analysis revealed that radiation heat transfer may be significant although the temperature differences between the walls are small. For this reason evaluation of radiation effect is searched.

A recent literature study which is parallel to present study investigated the numerical simulation of air flow and heat transfer in domestic refrigerators [37]. In that study, the refrigerating compartment was analyzed for three configurations: i) empty refrigerator, ii) refrigerator equipped with glass shelves

and iii) refrigerator loaded by product. The characteristics of the refrigerator in reference [37] are presented in Table 4.3.

Table 4.3. Characteristics of the refrigerator [37]

External dimensions (height x width x depth)	149 cm x 60 cm x 59 cm
Internal dimensions (height x width x depth)	136 cm x 52 cm x 44 cm
Dimensions of the evaporator	90 cm x 48 cm
Thermostat setting	+ 5 ^{o}C
Number of Shelves	4

Both experimental and numerical approaches were used and the numerical simulations were executed using Fluent 6.1 by taking into account and by neglecting radiation heat transfer. The constant evaporator temperature and 3-D laminar air flow conditions were assumed. Numerical results presented in [37] showed temperature stratification in the refrigerating compartment (warm zone at the top and cold zone on the bottom) for all configurations. It was also observed that calculated air temperature and the experimental values showed a good agreement when radiation was taken into account. In the literature study, it is said that Rayleigh number based on the height of the evaporator and the temperature difference between the internal air and cold wall (evaporator) surface was estimated about 6×10^{8}, therefore laminar flow assumption was made in the simulation. Additionally, Boussinesq approximation was used and thermal boundary conditions based on experimental data were as follows:

- Overall heat transfer coefficient between ambient room air and interior of the wall (U=0.34 W/m^{2}K),
- constant ambient room air temperature (T$_{amb}$=20 ^{o}C),
- constant evaporator temperature (T$_{evap}$=-0.5 ^{o}C).

The resolution parameters and number of cells used were also presented and they are tabulated in Tables 4.4 and 4.5.

Table 4.4. Resolution parameters used in the simulations [37]

	Relaxation factor	Type of discretization
Pressure	0.8	Presto
Density	1	-
Gravity forces	1	-
Momentum	0.2	Second order upwind
Energy	1	Second order upwind
Radiation	1	-
Pressure-velocity	-	Simple

Table 4.5. Number of cells used for the simulations [37]

	Mesh number			
	Height (136 cm)	Half width (26 cm)	Depth (44 cm)	Total
Empty refrigerator	138	28	66	255024
Refrigerator with shelves	222	28	66	410256
Refrigerator with shelves & products	240	62	74	1101120

Discrete ordinate method (DO) was selected for radiation. The steady state temperature and velocity fields on the symmetry plane for all configurations were shown and a comparison between experimental and predicted non-dimensional temperature results was done.

In order to verify the results in literature and check the numerical approach in the analyses performed so far in the present work, the simulation presented in the reference [37] is repeated for empty refrigerator. The model with the same

dimensions and number of cells inside is formed and only the numerical simulation taking the radiation into account is performed. However k-ε turbulence model and PISO pressure-velocity coupling algorithm are used with two different internal emissivity values of 0.9 and 0.85. Although the emissivities of the walls are not specified in the literature study [37], the value of 0.9 is selected based on the reference [39]. The analysis with the internal emissivity value of 0.85 is performed to determine the effect of selected internal emissivity value on radiative and total heat transfer rates.

In Figure 4.17, steady state temperature profiles on symmetry plane in the literature study and present work performed for the emissivity value of 0.9 are presented respectively.
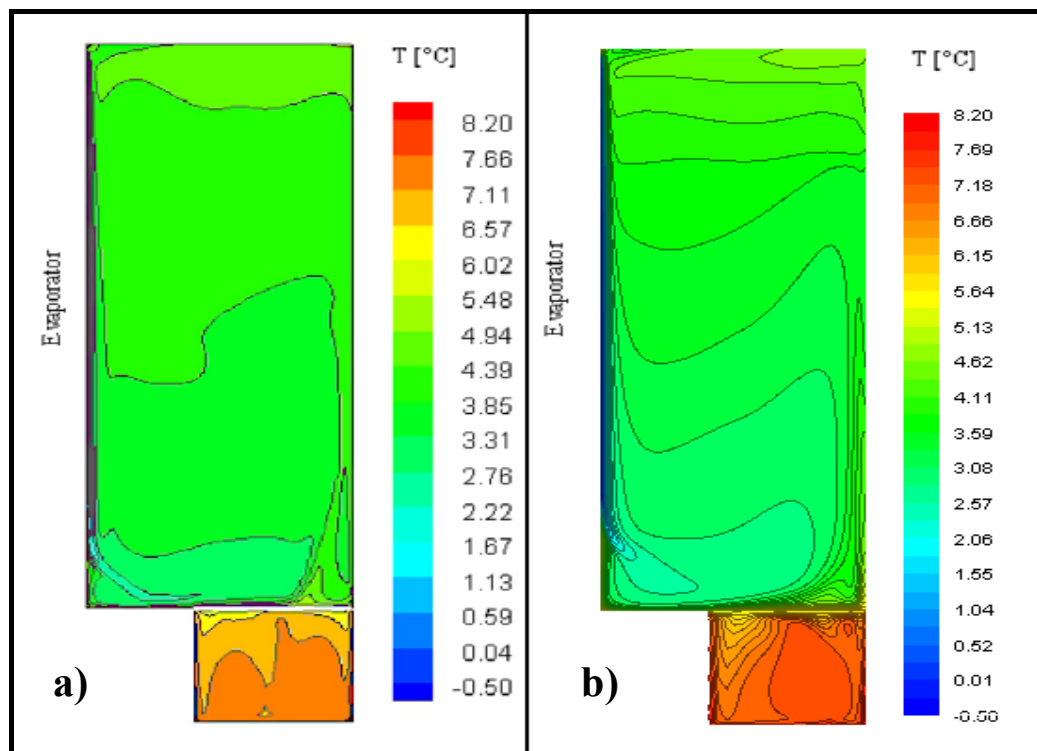

Figure 4.17. Temperature profiles on the symmetry plane,
a) literature [37], b) present study

Thermal stratification is observed in the literature study [37] and the the case with $\varepsilon = 0.9$ of the present study with the cold zone at the bottom of the refrigerating compartment and the warm zone at the top. Moreover; the maximum temperature in the main cavity is determined as 8.2 ^{o}C in both [37] and the present work.

It is observed from Figure 4.18 that the velocity magnitudes on the symmetry plane determined in [37] and the present work differ from each other. This may be due to the turbulent flow assumption, corresponding pressure-velocity coupling method and emissivity values selected for the walls in the analysis.
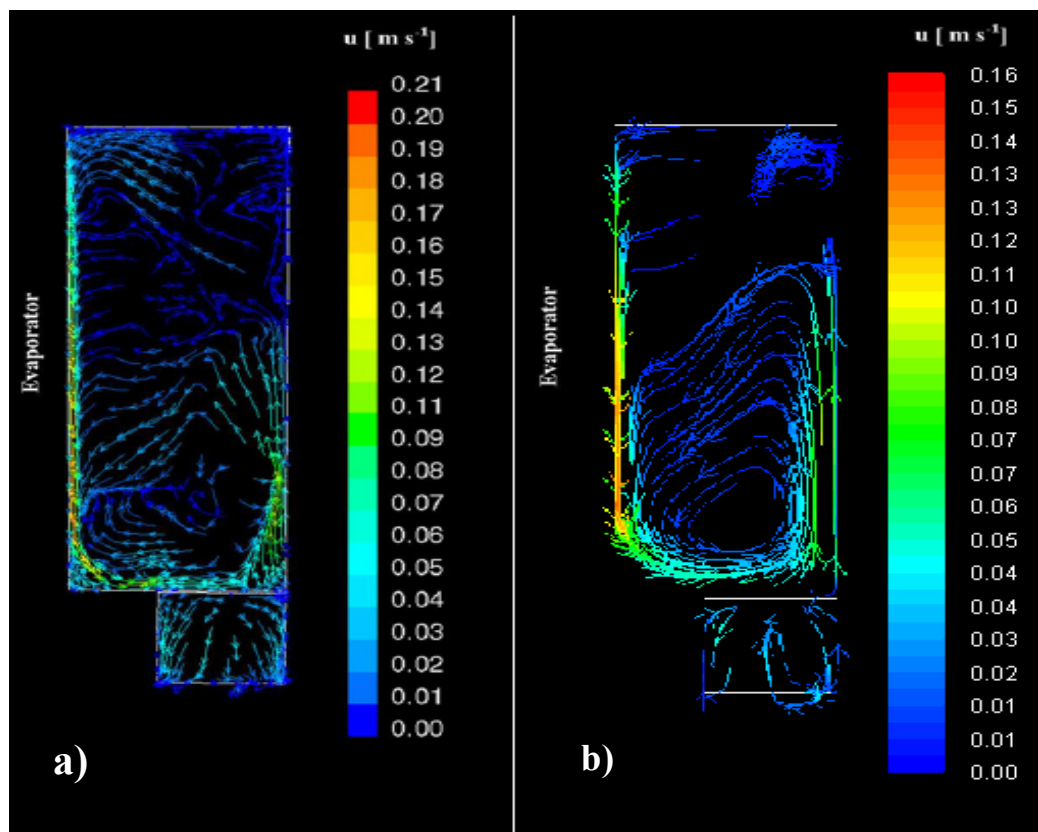

Figure 4.18. Velocity path lines on the symmetry plane,
a) literature [37], b) present study

In Figure 4.19, experimental temperature values measured 21.5 cm away from the evaporator on the symmetry plane in [37] are compared with the numerical simulations performed including radiation or omitting it for both literature study [37] and present work. In [37] results, the experimental and predicted dimensionless air temperature results overlap when radiation is taken into account. Present study with $\varepsilon = 0.9$ or $\varepsilon = 0.85$ cases give very close results also.
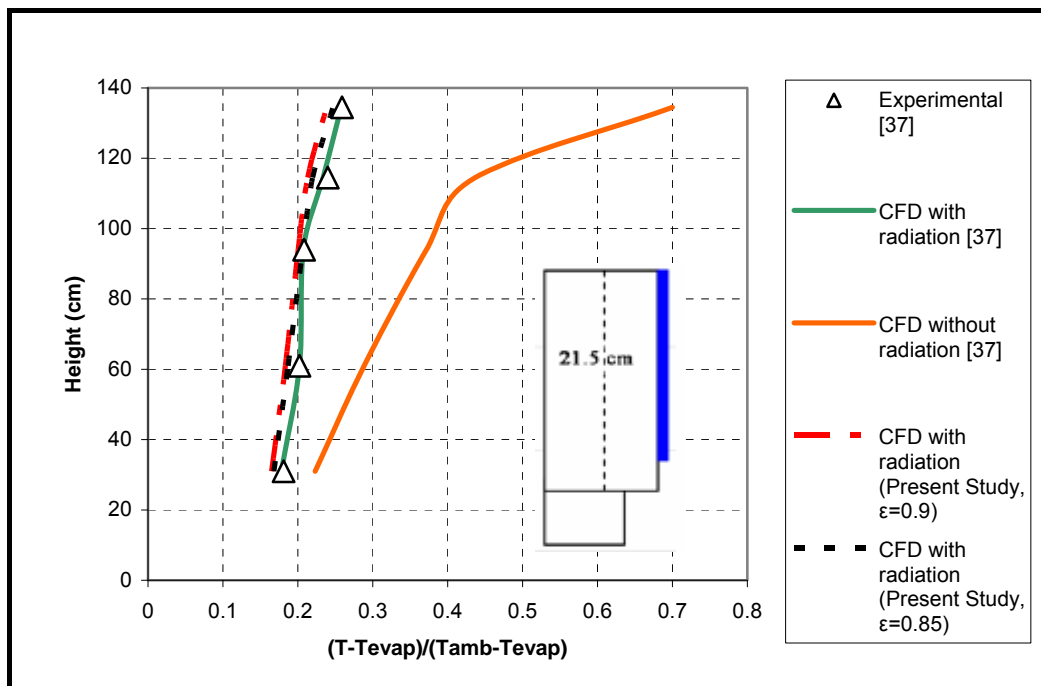
Figure 4.19. Experimental air temperatures and predicted values obtained by the simulation with and without radiation in literature [37] and present study

Since in the present work the numerical study in literature has been repeated only for the case in which the radiation is included; Figure 4.19 outlines just the comparison of non dimensional experimental values with the predicted ones at the same locations considered in literature [37].

It is observed that defining overall heat transfer coefficient between external air and interior of the wall as the thermal boundary condition makes the computational time much longer with respect to the previous numerical studies.

In Table 4.6, the results of the present study show that radiative heat transfer between the walls is comparable to the convective one for both of the selected internal emissivities when the steady state time of 6000 s is considered.

Table 4.6. Radiative and total heat transfer rates (in Watts) for the present study, t=6000 s

	Rad. Heat Transfer Rate		Tot. Heat Transfer Rate	
	ε=0.9	ε=0.85	ε=0.9	ε=0.85
Front Wall	2.83	2.76	3.59	3.56
Rear Wall	-8.37	-8.10	-11.47	-11.32
Top Wall	1.19	1.18	1.20	1.18
Bottom Wall	0.41	0.40	1.06	1.05
Left Side Wall	2.11	2.03	2.87	2.85
Right Side Wall	2.11	2.03	2.87	2.85
Residual of the Energy Balance	*0.28*	*0.30*	*0.12*	*0.17*

With the recent work performed in parallel to the study in literature [37], it is shown that the model created, the turbulent flow assumption, the selected discretization method, the number of cells used (especially for finer meshed cavities) in numerical analysis are successfully determined. Additionally, CFD analysis performed by taking the radiation into account proves that radiation heat transfer between the walls is significant and may be comparable to the convection heat transfer in domestic refrigerator applications. For this reason further numerical works for single compartment and total refrigerator with experimentally obtained wall temperature boundary conditions will be performed including radiation model or omitting it.

4.3. Results of Experimental Analysis for 3-D Models

Using the set of temperature data obtained from the experimental study in Arçelik; constant temperature wall boundary conditions are determined for the following numerical analyses. While determining the isothermal wall temperature in numerical analyses, the arithmetic average of all temperature values measured by the thermocouples in experiments belonging to corresponding refrigerator wall is evaluated. Referring to Figure 3.7, sample temperature distributions at the locations of the thermocouples positioned on the side wall of the compartment and total refrigerator are specified in Figures 4.20 and 4.21 respectively. Since the data was taken in ten-second intervals for one or three days, representing all data leads to a very confusing graph, therefore, the temperature data acquiesced for 2 hours is used for the graph.
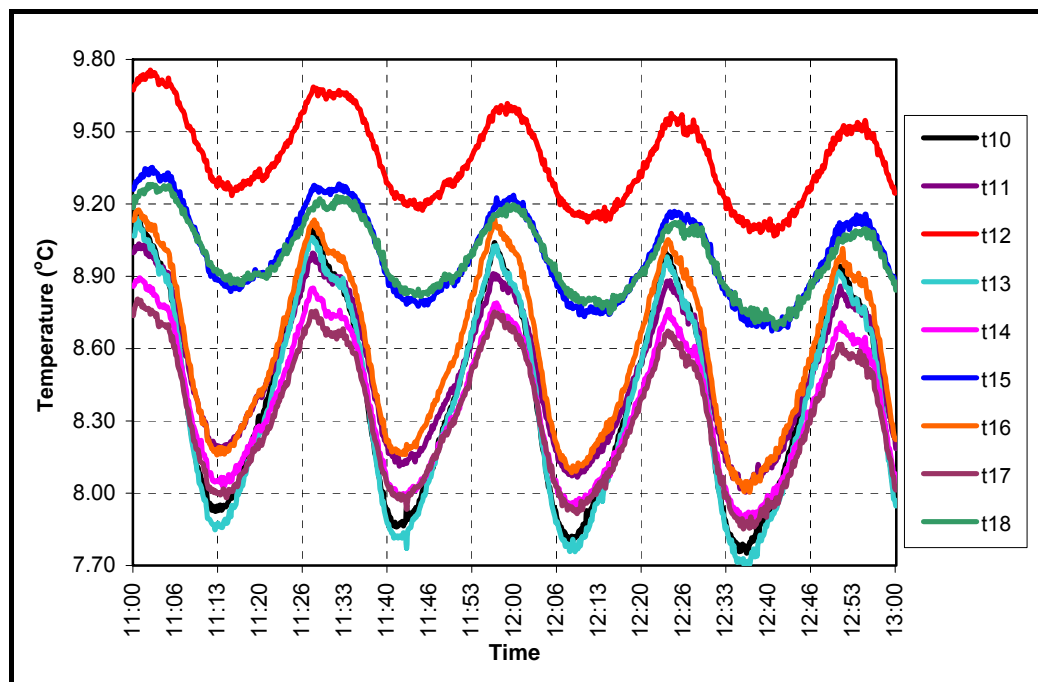

Figure 4.20. Temperature distribution on the side wall of the single compartment

In Figure 4.20, the temperature distribution on the side wall of the single compartment is presented. When it is analyzed, temperature values measured by thermocouples t12, t15 and t18 are higher than the others. These thermocouples are on the same vertical line which is nearest to the front wall (door) of the refrigerator; therefore they may be affected from the ambient room air. Temperature values measured by the thermocouples, t10, t13 and t16 are lower than the values measured by t12, t15 and t18. These thermocouples are also positioned on a vertical line close to the relatively hot rear wall. On the other hand; t11, t14 and t17 which are located on the vertical line at the middle of the side wall measure the lowest temperatures. The fluctuations in the temperature measurements decrease from back to front, because thermocouples close to the evaporator are to be affected by the compressor. Although the experiments were done in a temperature-controlled room, the room air temperature decreases from 20.7 ^{o}C to 20.2 ^{o}C for the time interval considered in Figure 4.20. In parallel to the change in the room air temperature, temperature values measured by thermocouples on the compartment side wall are slightly decreasing.
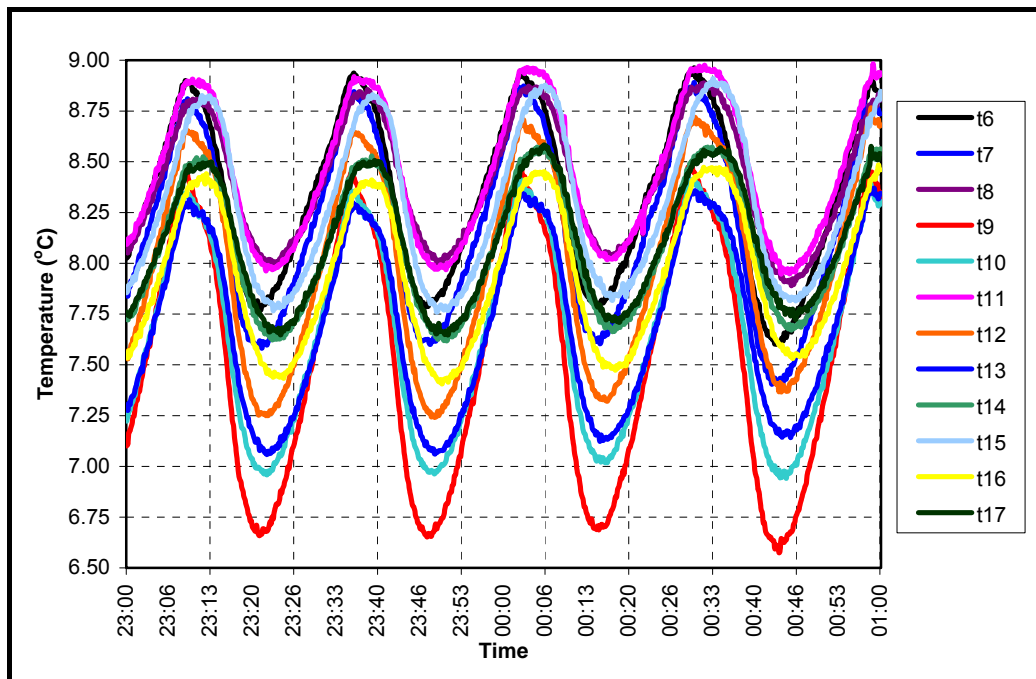

Figure 4.21. Temperature distribution on the side wall of the total refrigerator

Considering the thermocouple locations for the total refrigerator presented in Figure 3.7; in Figure 4.21 it is presented that, on the side wall of the total refrigerator cabinet, highest temperature values are measured by thermocouples, t11, t6 and t8 and t7 due to the contact with hot air at the top of the volume. Hot rear wall affects the temperature values measured by the thermocouples, t12 and t15. They measure slightly smaller temperatures. Relatively cold air results in a small decrease in the temperature values of t14, t17 and t16. Temperatures of the points of thermocouples, t13 and t10 are lower than the others but still higher than the temperature value indicated by t9. The lowest temperature is measured by t9 because it is very close to the evaporator.

Both of the Figures 4.20 and 4.21 imply that the compressor is on about 15 minutes. Additionally, its off time is nearly the same. If the insulation were better, the latter time interval would be larger than the former.

Two-hour temperature distributions for all walls and symmetry plane of both the single compartment and the total refrigerator are presented in Appendix C.

4.4. Results of Numerical Analysis of a Single Compartment

Results of the numerical analysis performed for a single compartment whose dimensions and experimentally determined temperature boundary conditions were explained in section 3.1.2 will be the scope of this section.

4.4.1. Temperature and Velocity Profiles

A time dependent natural convection analysis is performed for either including or omitting the radiation and corresponding temperature and velocity profiles have been determined at the midplanes.
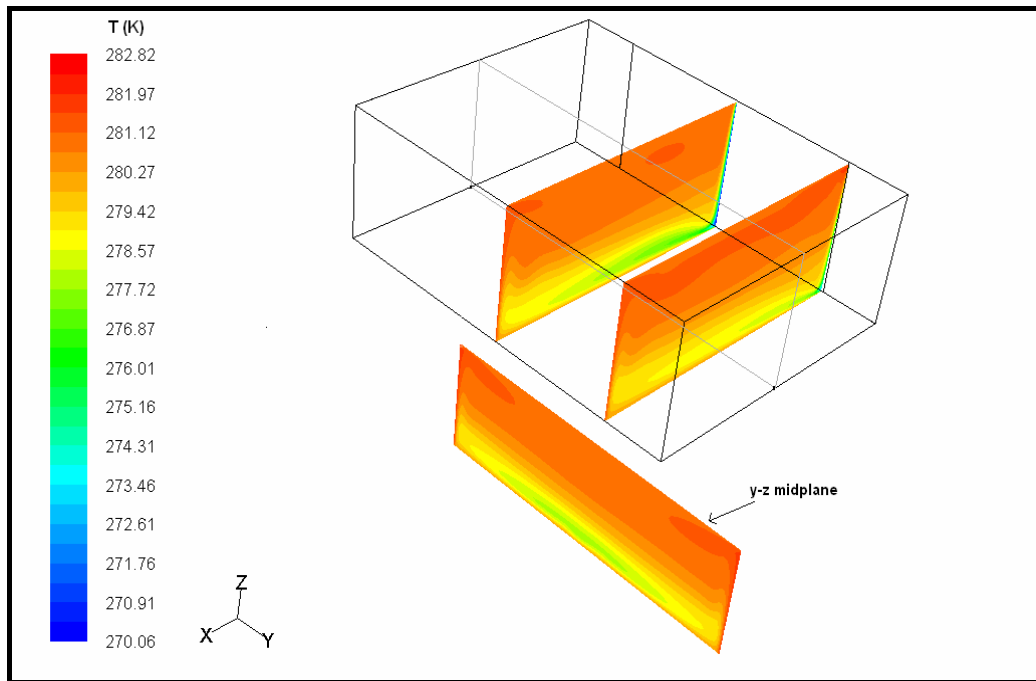
Figure 4.22. Temperature profile for the single compartment analysis, t=150 s
(with radiation)
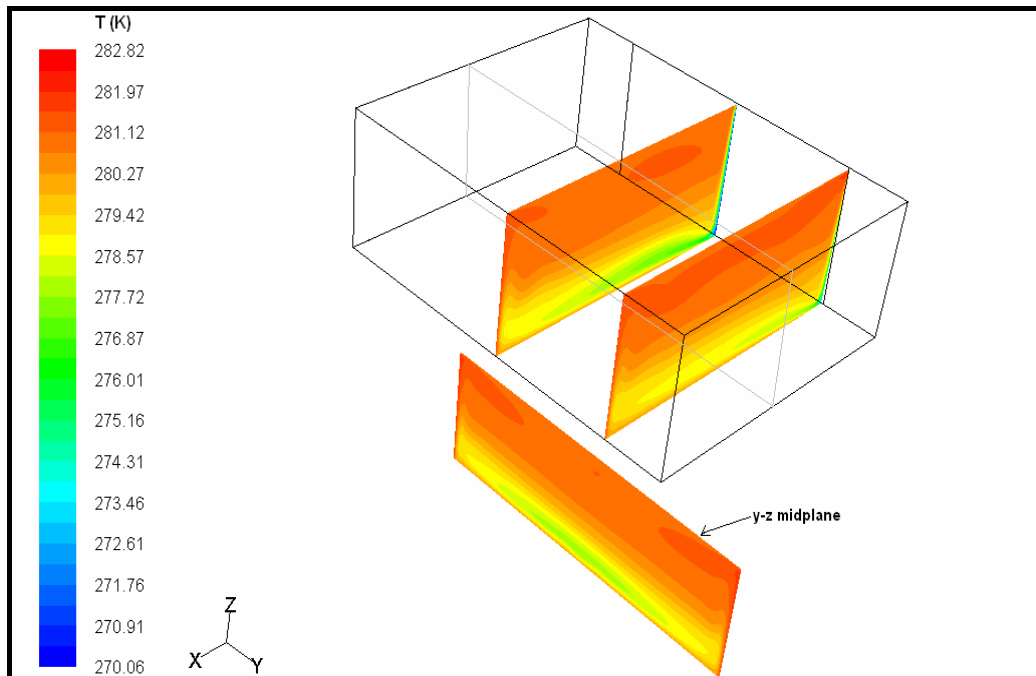
Figure 4.23. Temperature profile for the single compartment analysis, t=150 s
(without radiation)

The temperature and velocity profiles are searched and visualized at three different planes; x-z midplane which is the symmetry plane orthogonal to the evaporator and front wall, a plane parallel to symmetry plane and perpendicular to evaporator at its one end and y-z midplane of the cavity. The results obtained for the y-z midplane are shifted below the domain in order to make the whole picture clear.

In Figures 4.22 and 4.23, at t=150 seconds, the temperature profile in the compartment is nearly the same for the cases, radiation included or omitted. Moreover, on the symmetry plane of the problem (x-z midplane) the onset of the flow is faster. Natural convection characteristics are significant. Boundary layers developing on the evaporator and bottom wall are observed. Although the maximum temperature is the same in Figures 4.22 and 4.23, maximum velocity value in the domain is 0.119 m/s for the radiation included analysis and it is 0.124 m/s for the analysis where radiation is not taken into account.
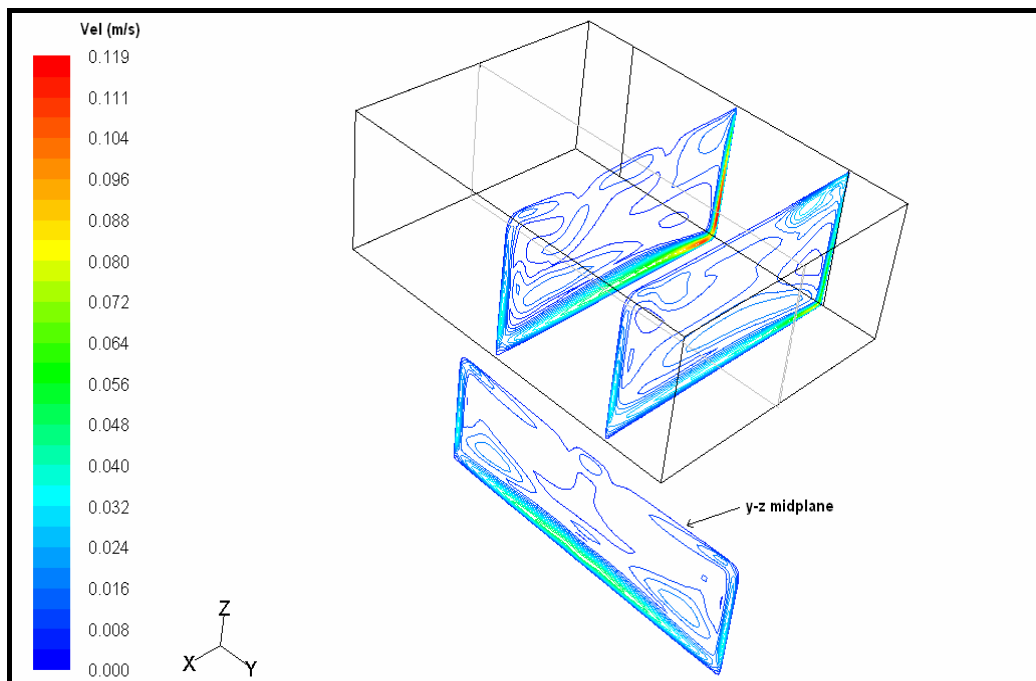

Figure 4.24. Velocity profile for the single compartment analysis, t=150 s
(with radiation)
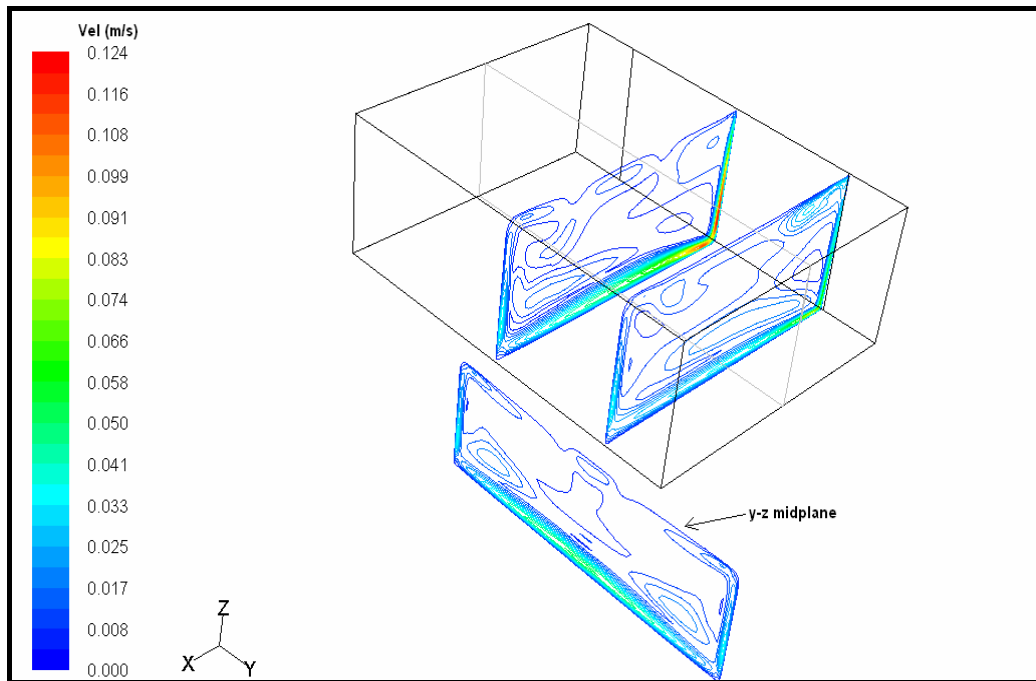
Figure 4.25. Velocity profile for the single compartment analysis, t=150 s
(without radiation)

It is presented in Figures 4.26 and 4.27 that, at the time of 5 minutes, the temperature profile is not different from the previous time instant for both radiation included or omitted analyses. The only change is that stratification is more clearly observed. Additionally, in Figures 4.28 and 4.29 velocity profiles are not changing so much but a more organized developing flow with slightly increased magnitudes is observed.

At the time instants of 600 to 3600 seconds, temperature and velocity profiles are not changing for both cases. For completeness, temperature profile inside the compartment and velocity contours for the time instants of 600 and 3600 seconds are presented in Figures 4.30 to 4.37.
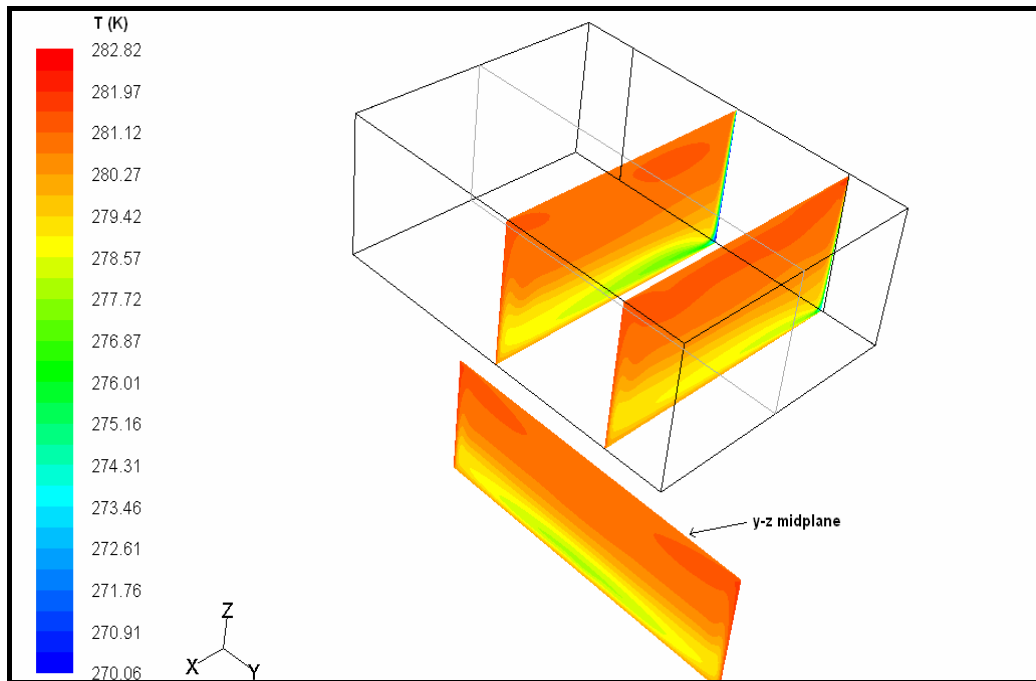
Figure 4.26. Temperature profile for the single compartment analysis, t=300 s
(with radiation)
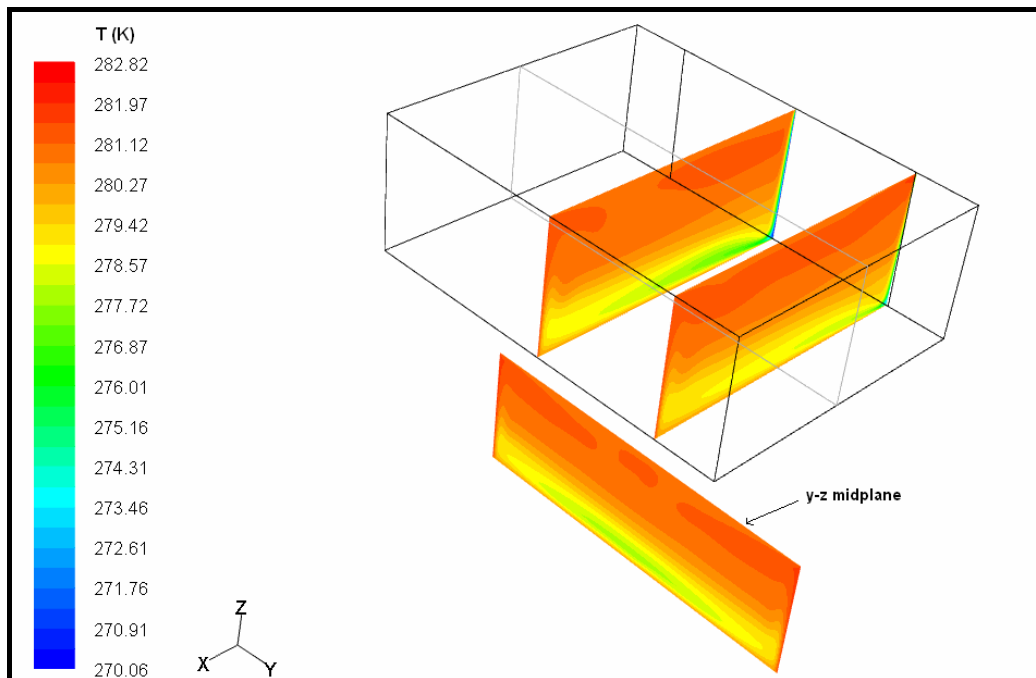
Figure 4.27. Temperature profile for the single compartment analysis, t=300 s
(without radiation)
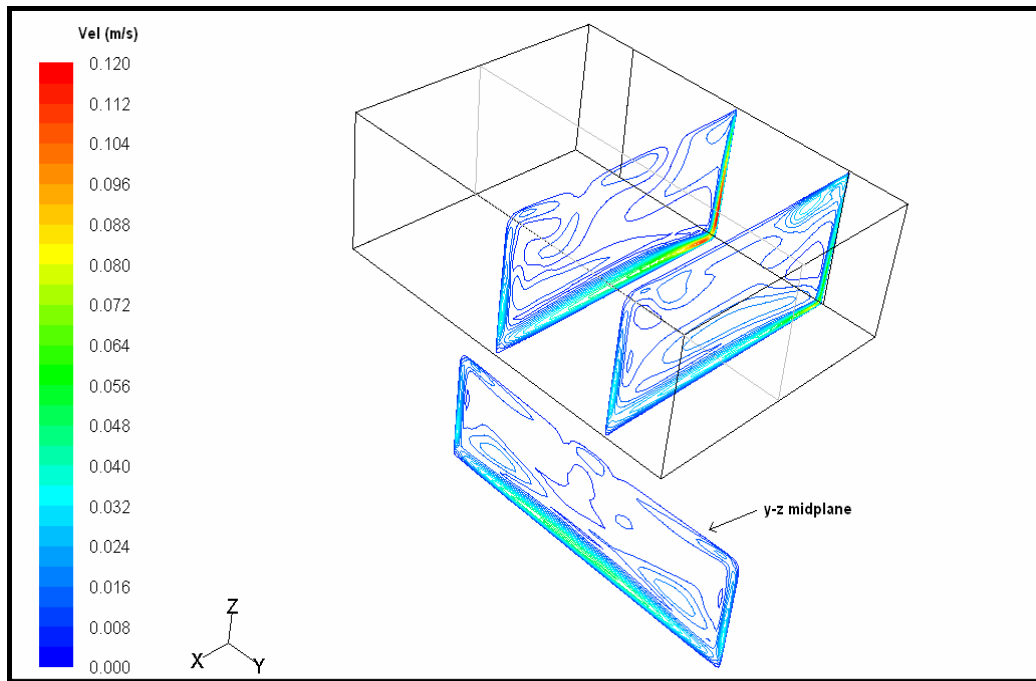
Figure 4.28. Velocity profile for the single compartment analysis, t=300 s
(with radiation)
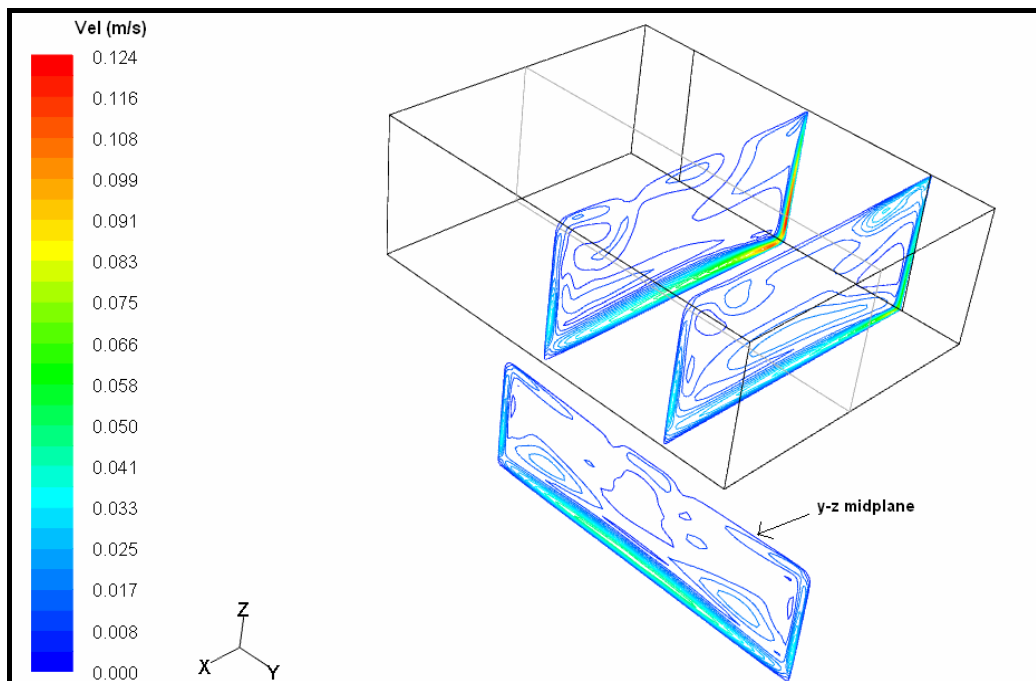
Figure 4.29. Velocity profile for the single compartment analysis, t=300 s
(without radiation)
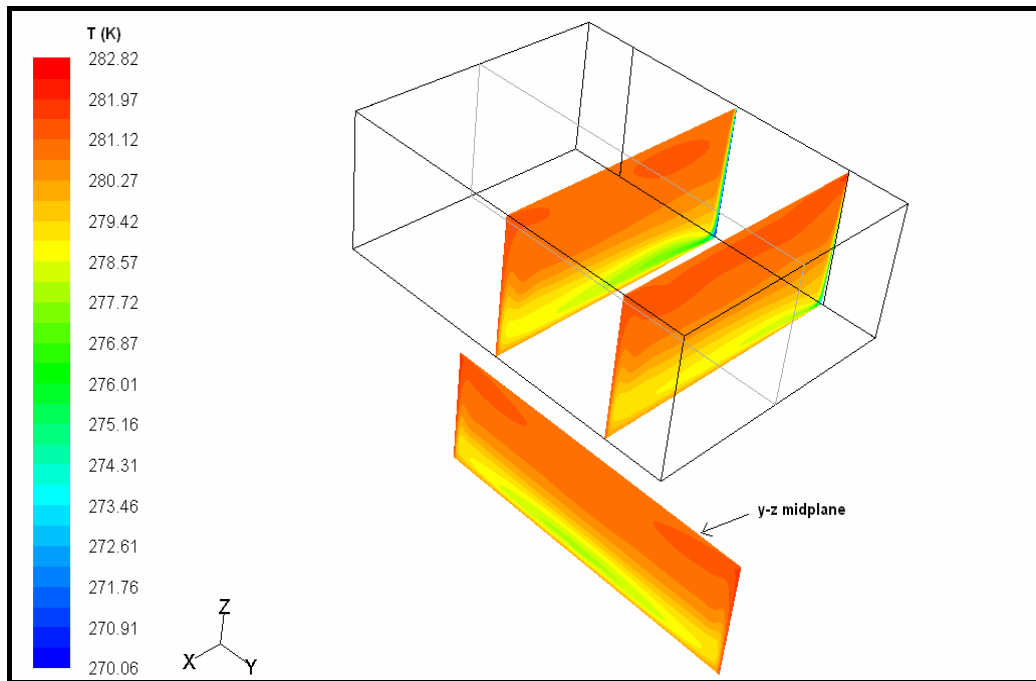
Figure 4.30. Temperature profile for the single compartment analysis, t=600 s
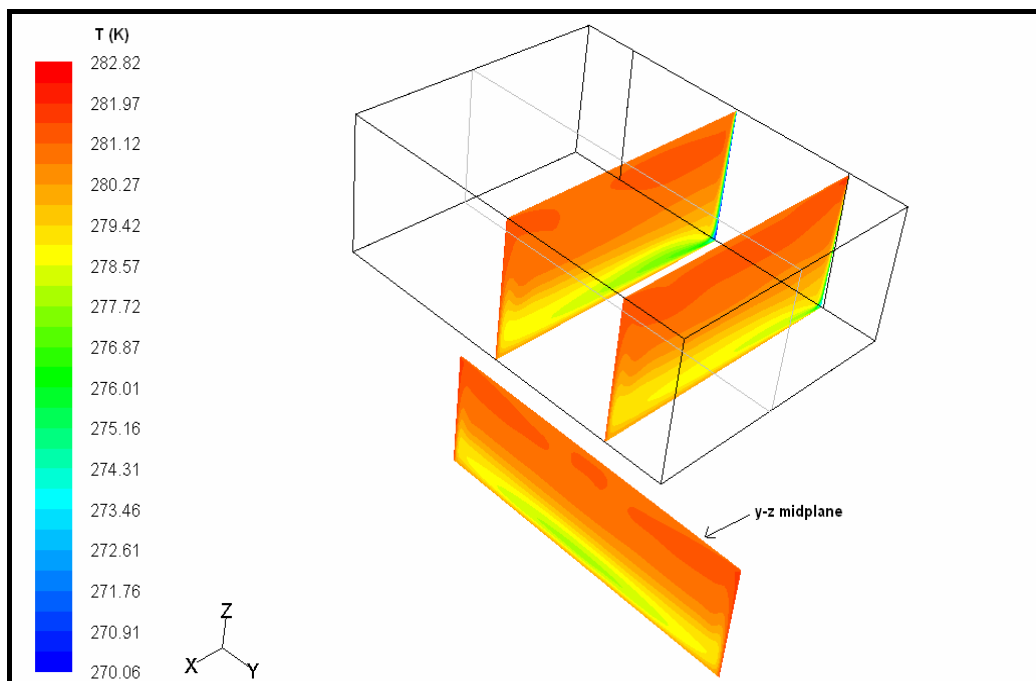
(with radiation)

Figure 4.31. Temperature profile for the single compartment analysis, t=600 s
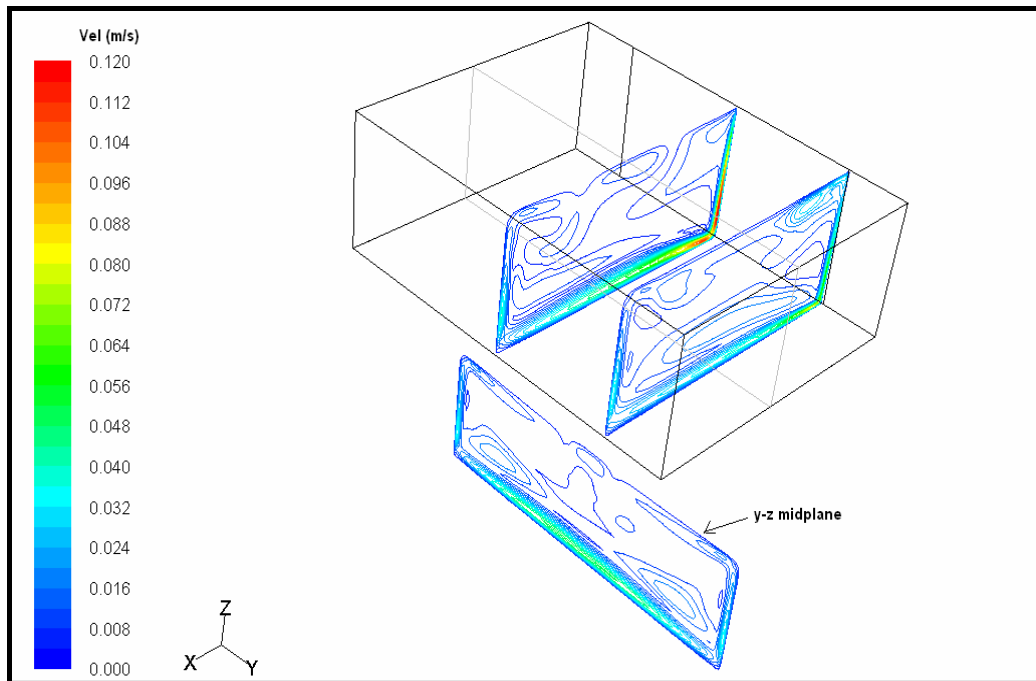
(without radiation)

Figure 4.32. Velocity profile for the single compartment analysis, t=600 s
(with radiation)
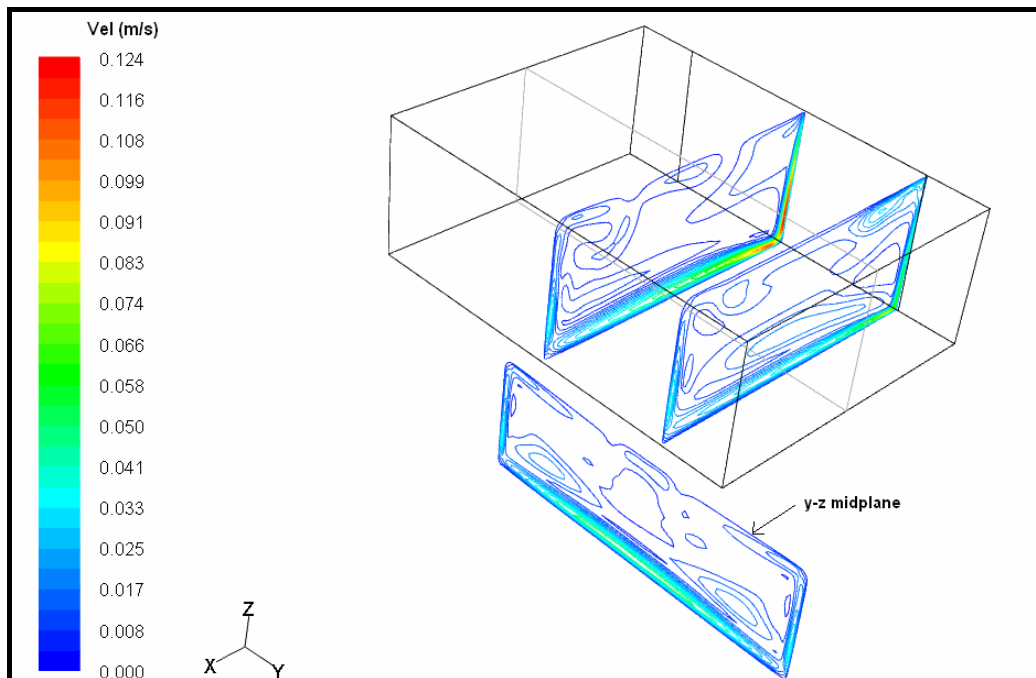
Figure 4.33. Velocity profile for the single compartment analysis, t=600 s
(without radiation)
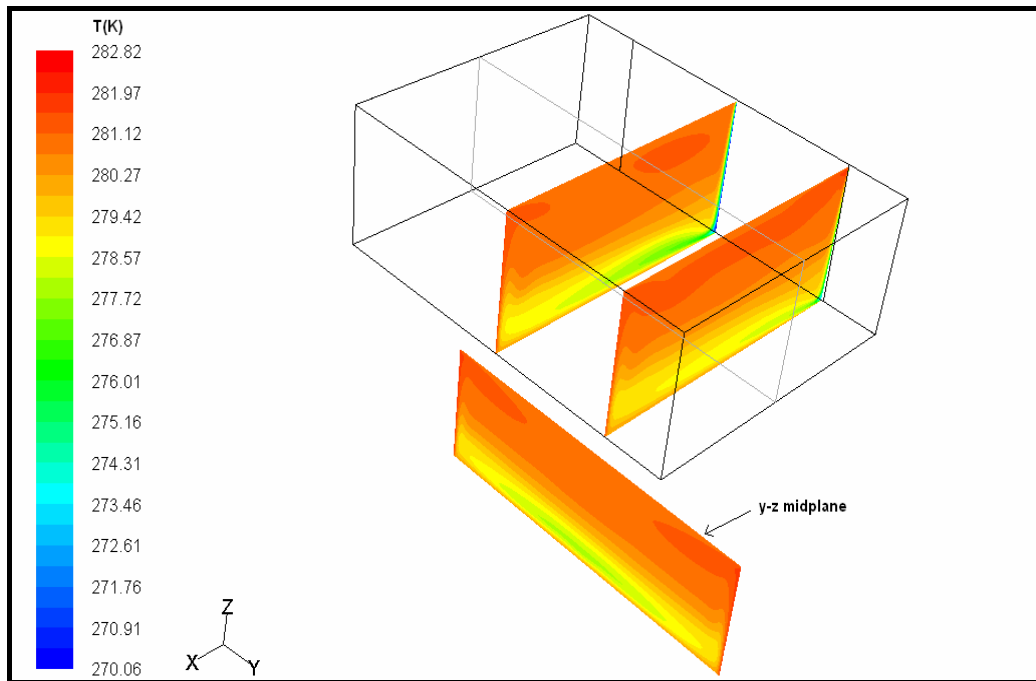
Figure 4.34. Temperature profile for the single compartment analysis, t=3600 s
(with radiation)
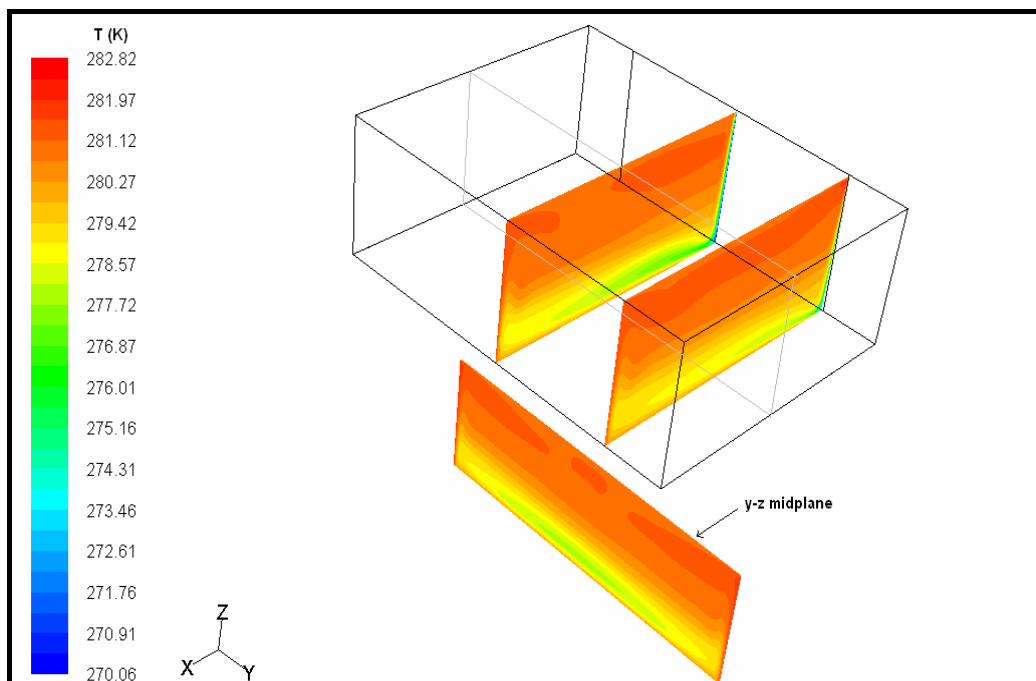
Figure 4.35. Temperature profile for the single compartment analysis, t=3600 s
(without radiation)
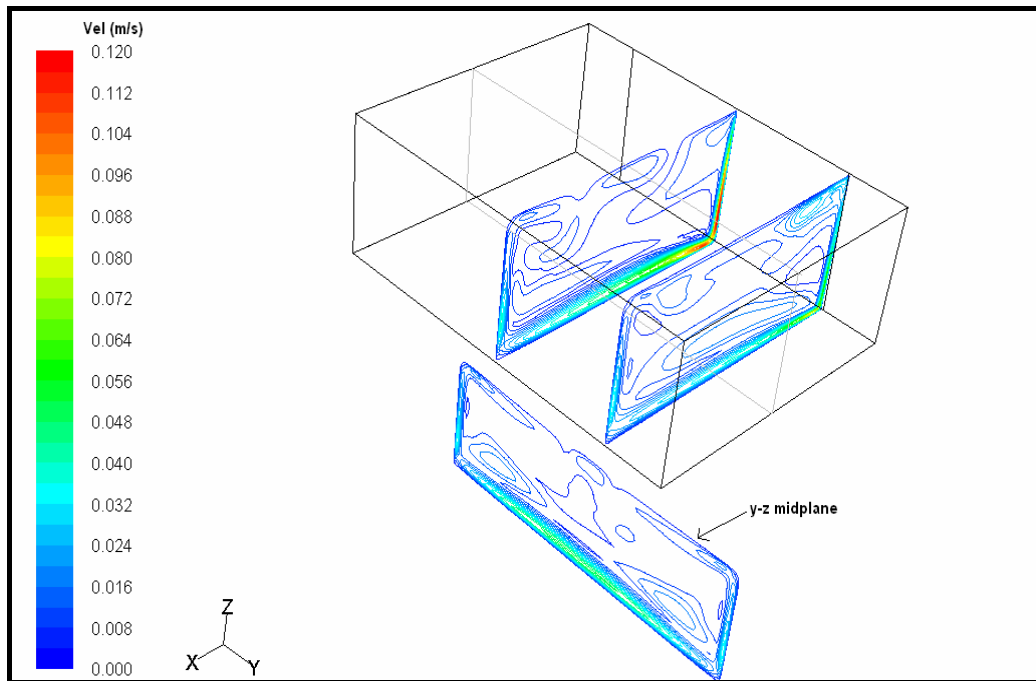
Figure 4.36. Velocity profile for the single compartment analysis, t=3600 s
(with radiation)
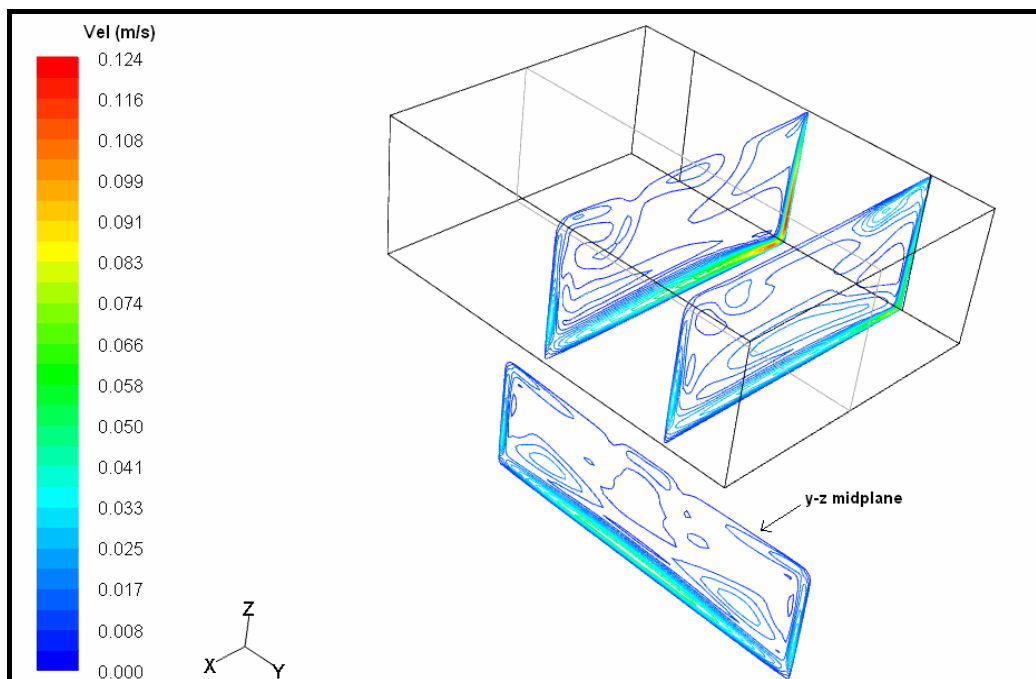
Figure 4.37. Velocity profile for the single compartment analysis, t=3600 s
(without radiation)

When the results presented in Figures 4.32 and 4.33 or 4.36 and 4.37 are compared, radiation only affects the maximum velocity value. Except the maximum velocity value, the circulation loops formed, boundary layers developed on the walls are the same for both of the analyses, radiation included or neglected. However, the time to reach steady state decreases when radiation is taken into account as an additional heat transfer mechanism; i.e. it is nearly 5 minutes and 3 minutes for the analysis without radiation and with radiation respectively. On the other hand; run time of the single compartment numerical analysis with radiation is three times the computation time of numerical analysis for the same domain without radiation.

The velocity boundary layers at the walls and the flow directions can be compared in detail for the symmetry plane of the cavity (x-z midplane) at the time of 3600 s. As expected, at steady state, the velocity distribution for both cases converges to the same profile inside the compartment.
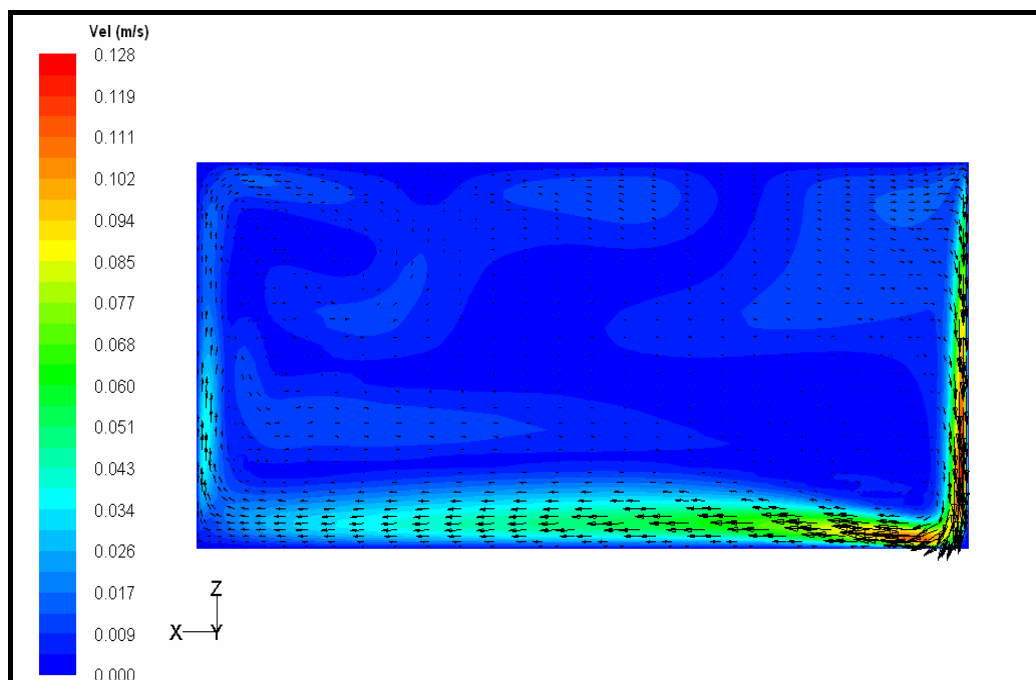
Figure 4.38. Velocity vectors at the symmetry plane for the single compartment analysis, t=3600 s (with radiation)
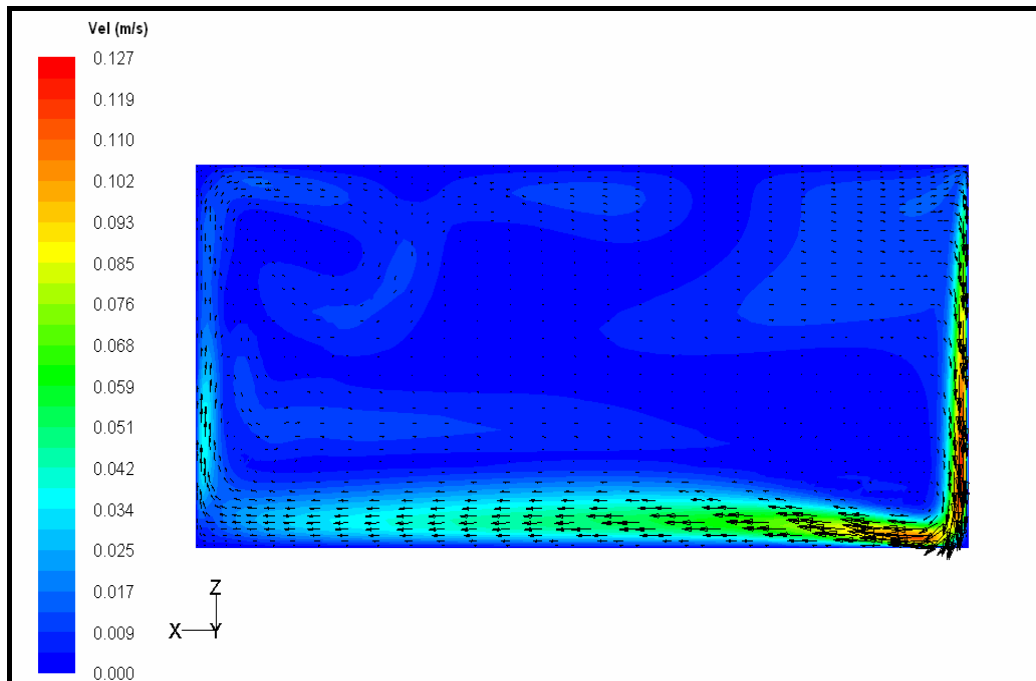
Figure 4.39. Velocity vectors at the symmetry plane for the single compartment analysis, t=3600 s (without radiation)

4.4.2. Heat Transfer Analysis

Heat transfer analysis formulated in the previous chapter is performed for the single compartment models with or without radiation. Time dependent heat flux and the effective heat transfer coefficient are determined. Total heat transfer rates from the walls and change of the heat flux and the effective heat transfer coefficient with spatial coordinates are also examined for similar reference lines of the preliminary numerical analysis. The effective heat transfer coefficient is the convective heat transfer coefficient for the analysis that does not include radiation. While obtaining the heat flux values, area weighted average of the flux at each face of the corresponding wall is calculated by the computer program and reference temperature is again the geometric center temperature of the domain.
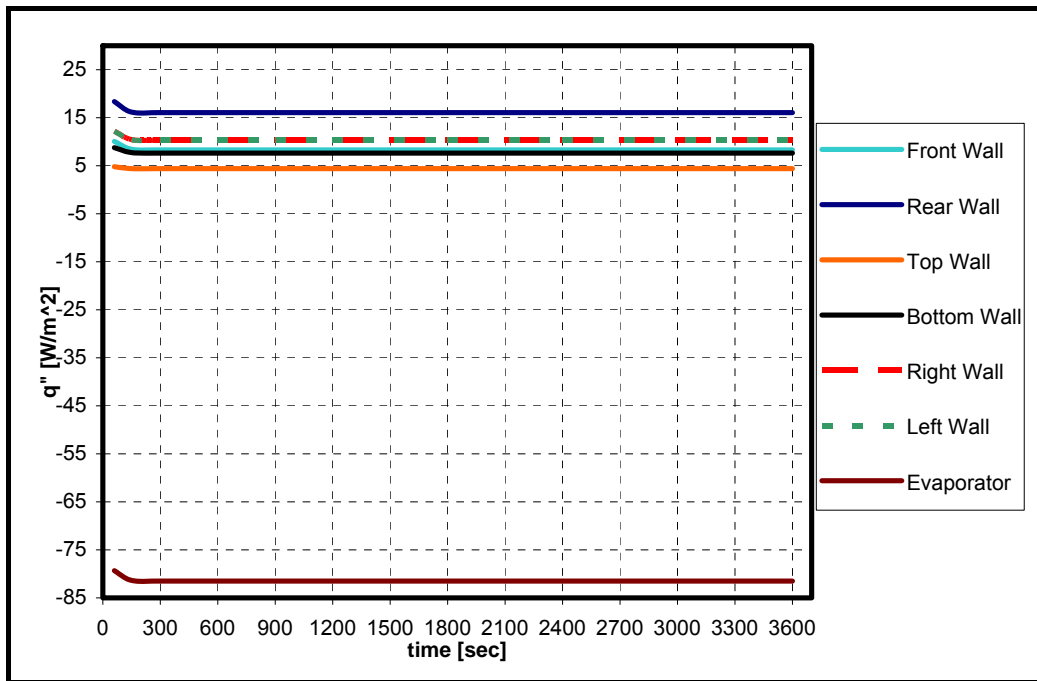
Figure 4.40. Time dependent heat flux values for the single compartment
analysis (with radiation)
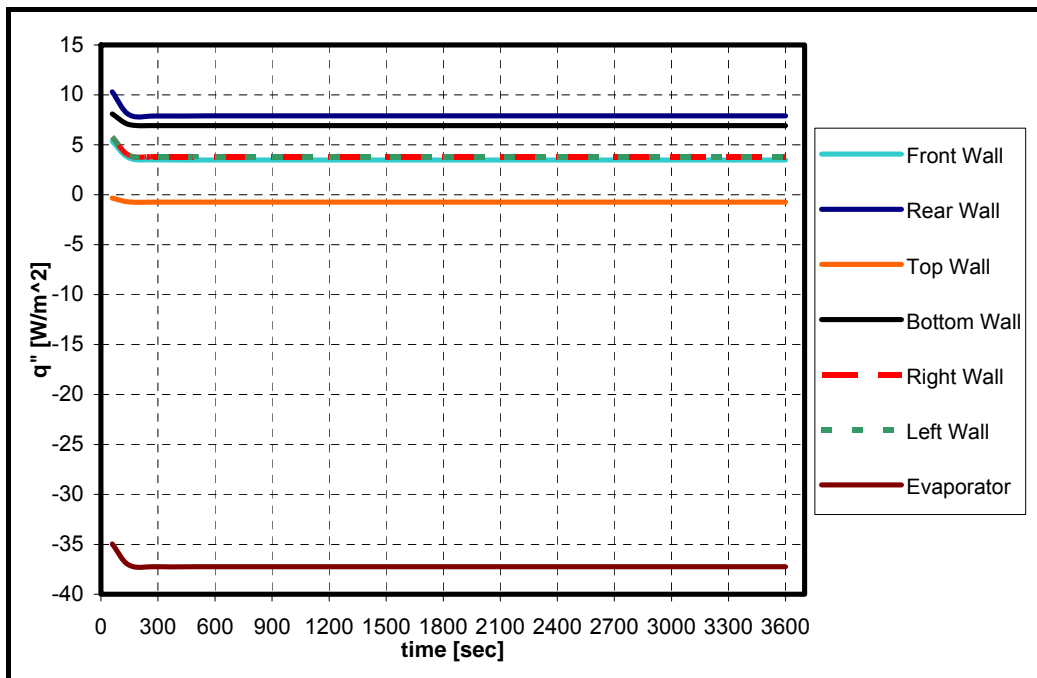
Figure 4.41. Time dependent heat flux values for the single compartment
analysis (without radiation)

In Figures 4.40 and 4.41, the heat flux values are reaching to steady state at 300 seconds and the radiative heat flux value is comparable to the convective one at all time instances. Additionally, the absolute heat flux value at the evaporator is much more than the other walls since its temperature is about 11 $^{\circ}$C lower than the other walls.

Time dependent effective heat transfer coefficients for all walls are plotted in Figures 4.42 and 4.43. In figures it is presented that effective heat transfer coefficient values are not changing with time after 300 seconds for both cases but due to the radiative heat flux on the front wall the effective heat transfer coefficient on this wall is greater than the others. On the other hand; the effective heat transfer coefficient value for the evaporator is about 10 W/m^{2}K for radiation included analysis whereas convective heat transfer coefficient value for evaporator is about 5.5 W/m^{2}K.
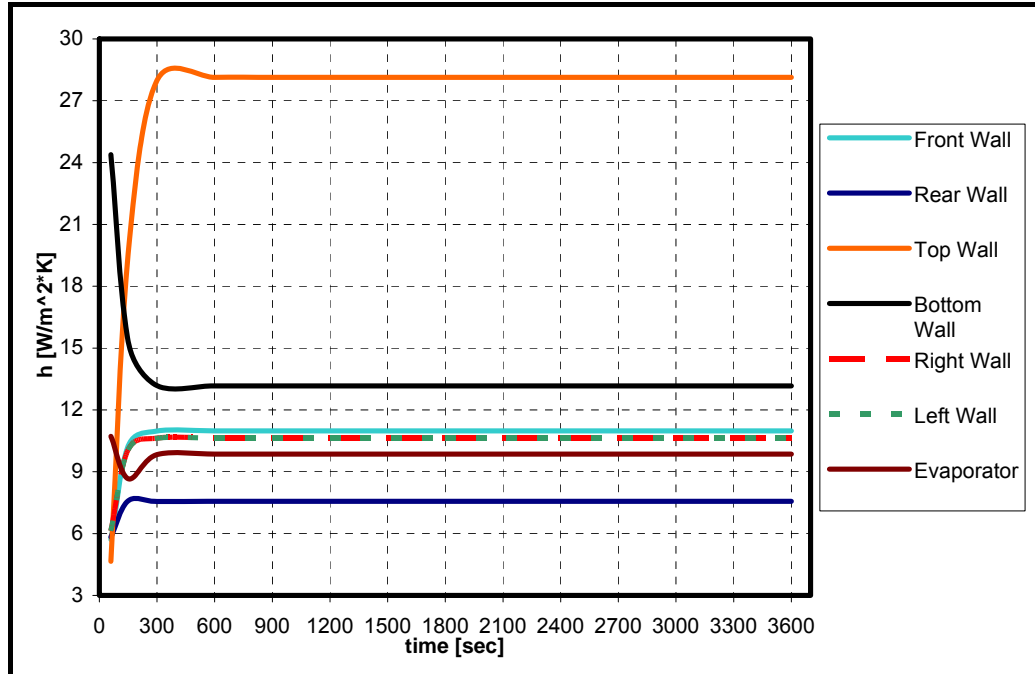
Figure 4.42. Time dependent effective heat transfer coefficient values for the single compartment analysis (with radiation)
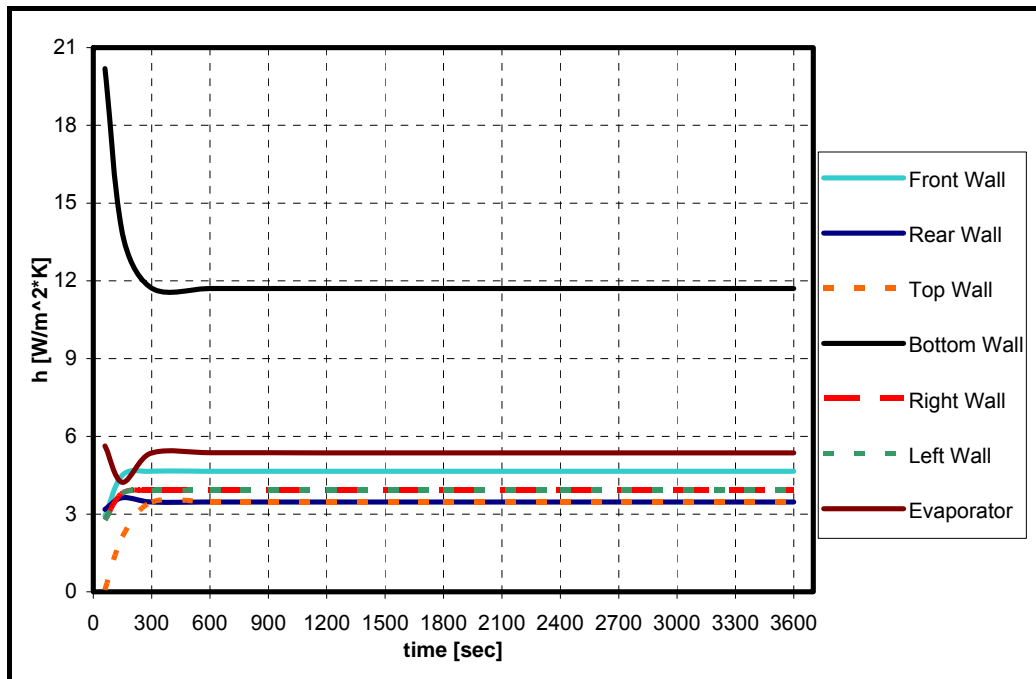
Figure 4.43. Time dependent effective (convective) heat transfer coefficient values for the single compartment analysis (without radiation)

For the time of 3600 seconds, q" and h variations with spatial coordinates are obtained for the reference lines shown with the evaporator edge in Figure 4.44. Heat flux and effective heat transfer coefficient parameters are calculated for three and four vertical equidistance lines (9 cm between each) on evaporator and front wall respectively. Then, these are calculated only for the lines, Line 1 (top wall) and Line 1 (bottom wall), on top and bottom walls. In all the calculations, both of with or without radiation cases are considered.

In Figure 4.45, it is indicated that that heat flux values are not changing with y direction (from center to the edge) on the evaporator for both radiation and without radiation cases. Moreover, total heat flux values of both radiation included or omitted analyses increase from bottom to top which is reflecting the direction of flow of air on the evaporator. On the other hand; radiative heat flux is not changing with z because it only depends on the temperature of the walls and the evaporator.
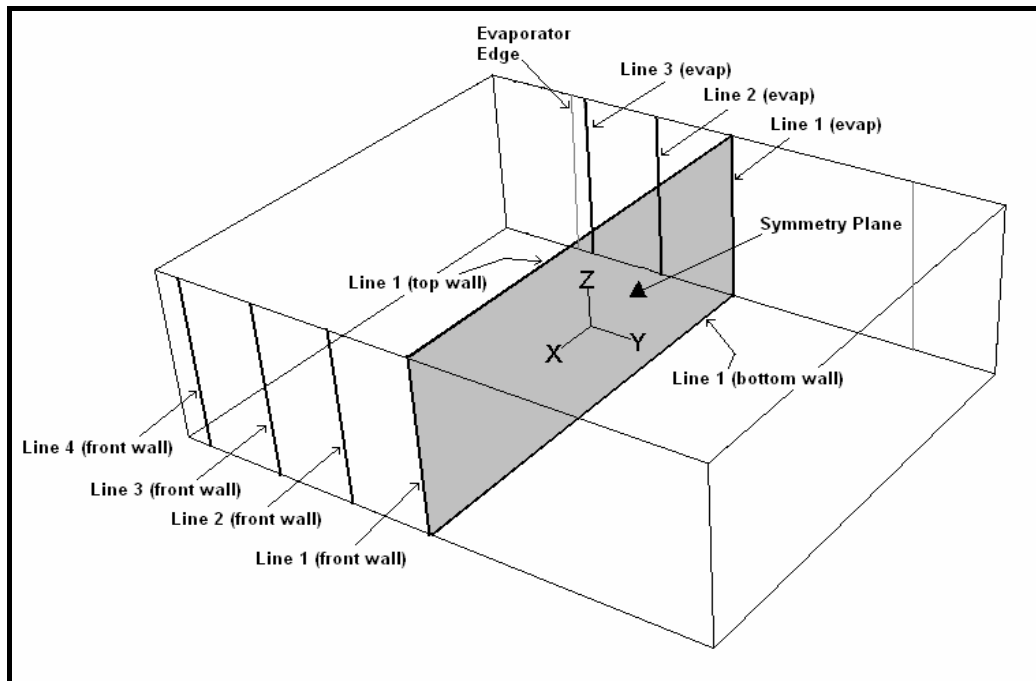
Figure 4.44. Configuration of reference lines used for s.s. heat transfer

analysis in the single compartment analysis
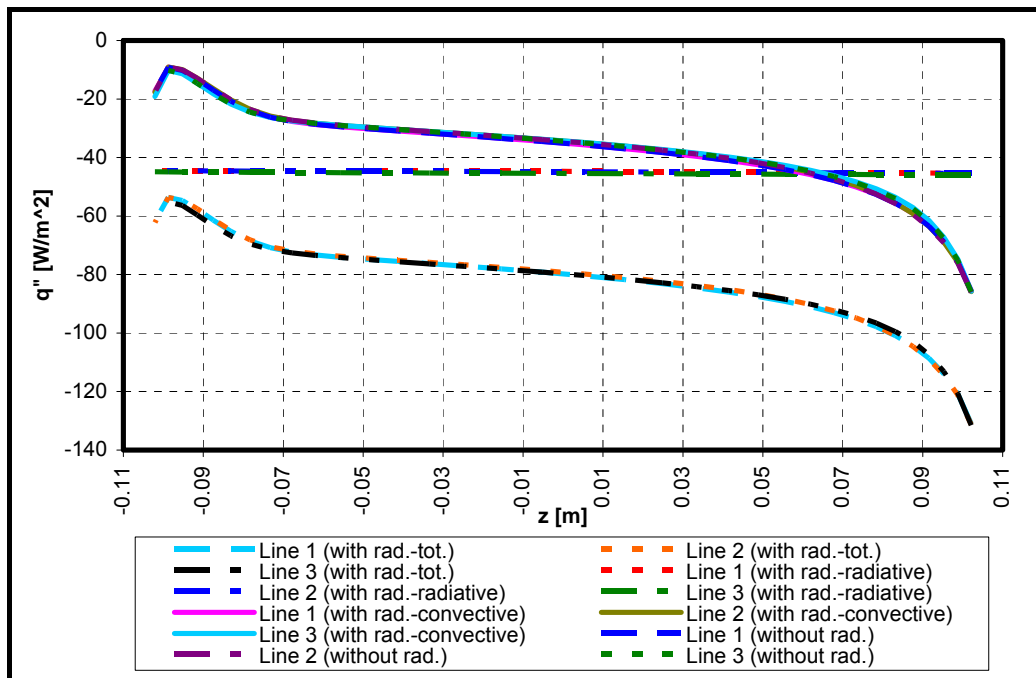
Figure 4.45. Steady state heat flux values at the evaporator for the single

compartment analysis
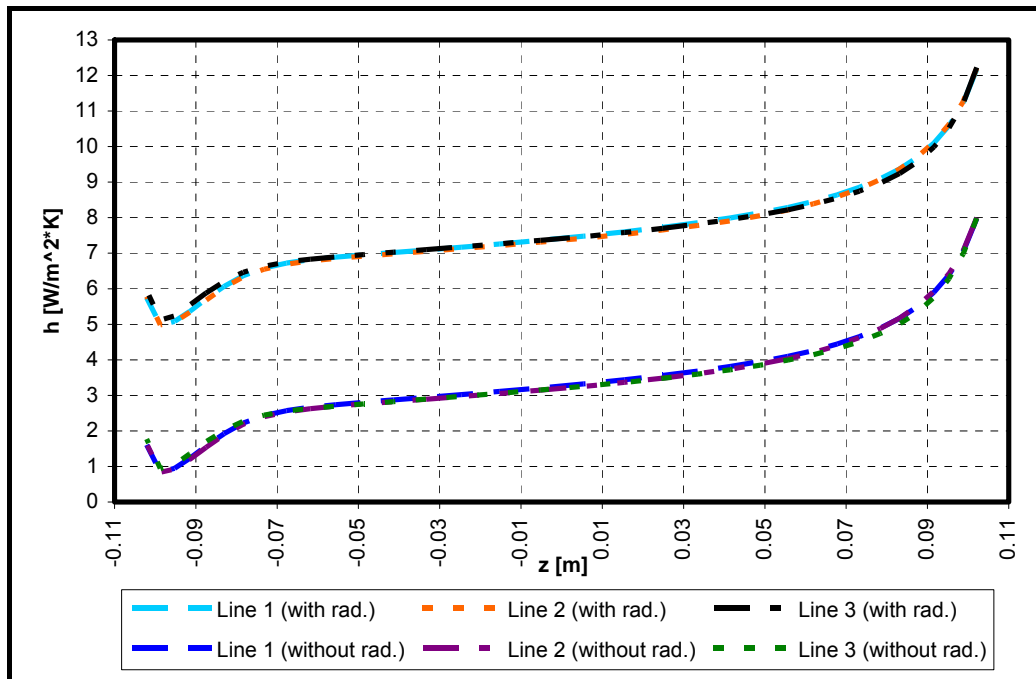
Figure 4.46. Steady state effective heat transfer coefficient values at the
evaporator for the single compartment analysis

Parallel to the heat flux values; it is presented in Figure 4.46 that effective heat transfer coefficient values increase from bottom to top at the evaporator wall for the cases of radiation included or omitted. Due to the radiative heat flux, the effective heat transfer coefficient value is about 2.5 times greater than the convective one obtained from the analysis in which radiation is not considered.

It is shown in Figure 4.47 that the total heat flux is from the front wall to the air inside and it is decreasing from bottom to top, but there is a slight increase after z=0.03 m. Additionally, the total heat flux value is decreasing from line 1 to line 4 on the wall. Similar characteristics are observed for the radiative component of the flux. The radiative heat flux from the wall is decreasing from bottom to top until z=0 m and then it is increasing. This may be due to a greater temperature difference between the upper and lower quarter regions of the front wall with the other walls and evaporator as presented in Figures 4.34 and 4.35.
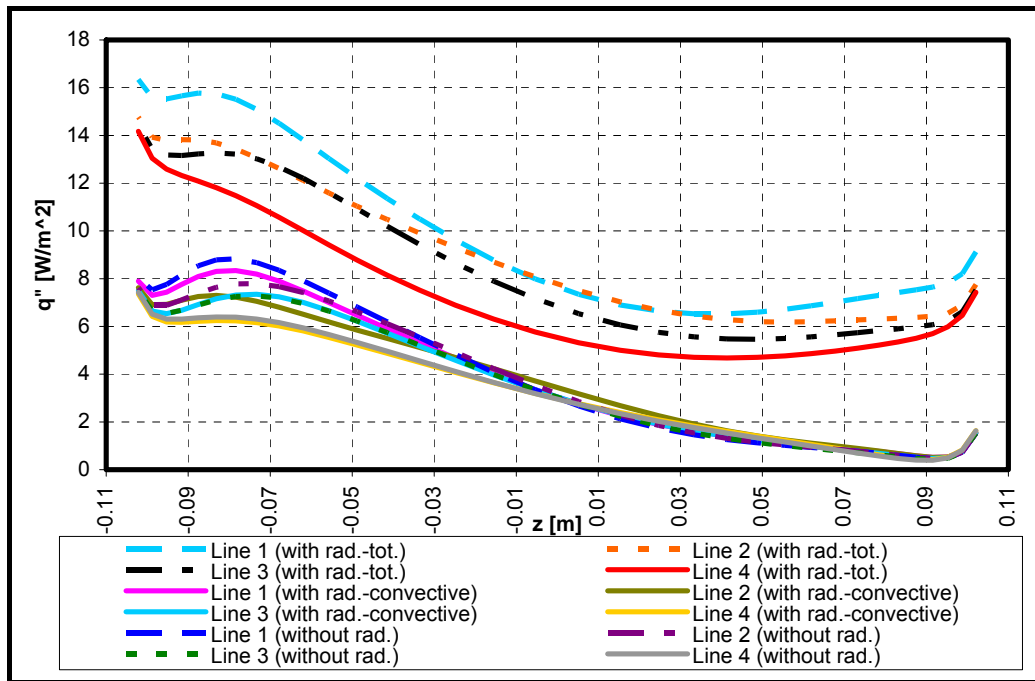
Figure 4.47. Steady state heat flux values at the front wall for the single compartment analysis
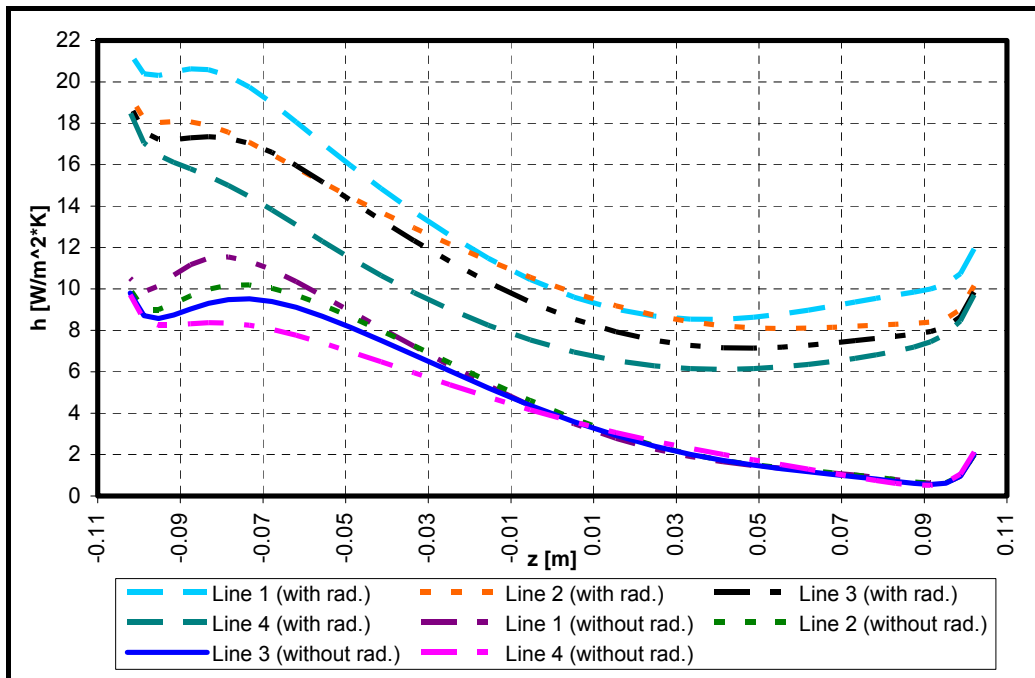

Figure 4.48. Steady state effective heat transfer coefficient values at the front wall for the single compartment analysis

In Figure 4.47, convective heat flux values obtained from the radiation included analysis are the same with ones found in analysis without radiation.

Since the effective heat transfer coefficient is the ratio of the heat flux to a constant temperature difference, the characteristic of the graph in Figure 4.48 is similar to the one in Figure 4.47. The magnitude of the effective heat transfer coefficient is about 3 times the magnitude of the convective heat transfer coefficient for all reference lines on the front wall.

In Figures 4.49 and 4.50, q"(x) and h(x) are presented respectively only for Line 1 (top wall) and Line 1 (bottom wall), shown in Figure 4.44. In Figure 4.49, the total heat flux from the bottom wall is high at the region close to the back wall but it decreases very rapidly and becomes constant after x=0 m. On the other hand; for the line 1 on the top wall the heat flux values are smaller than the values for bottom wall and the convective heat flux values are nearly zero.
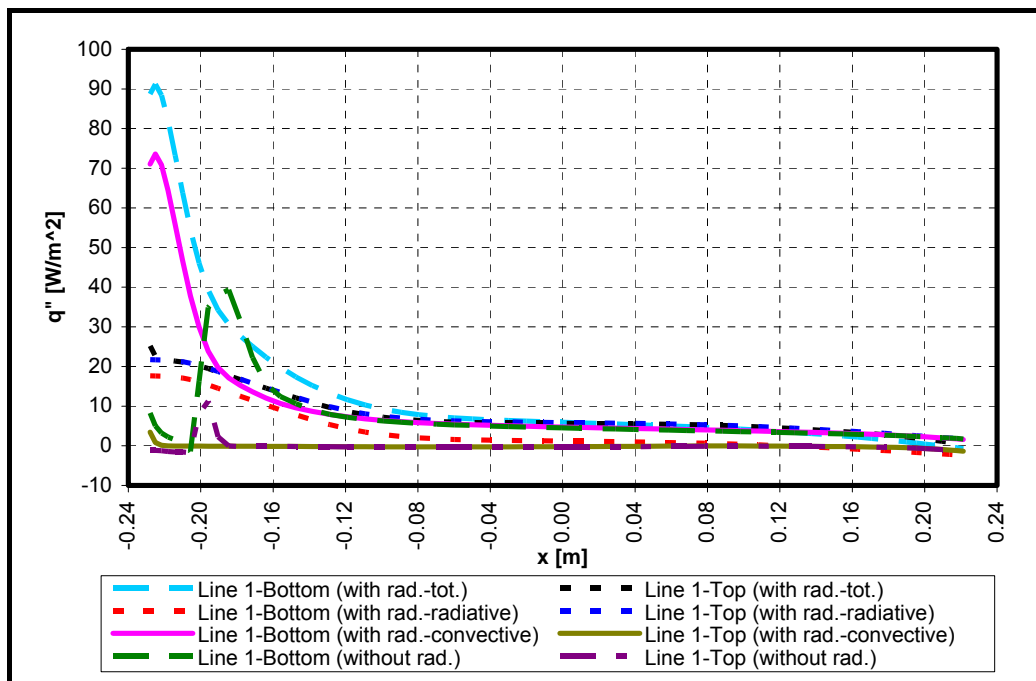

Figure 4.49. Steady state heat flux values at the bottom and the top walls for the single compartment analysis
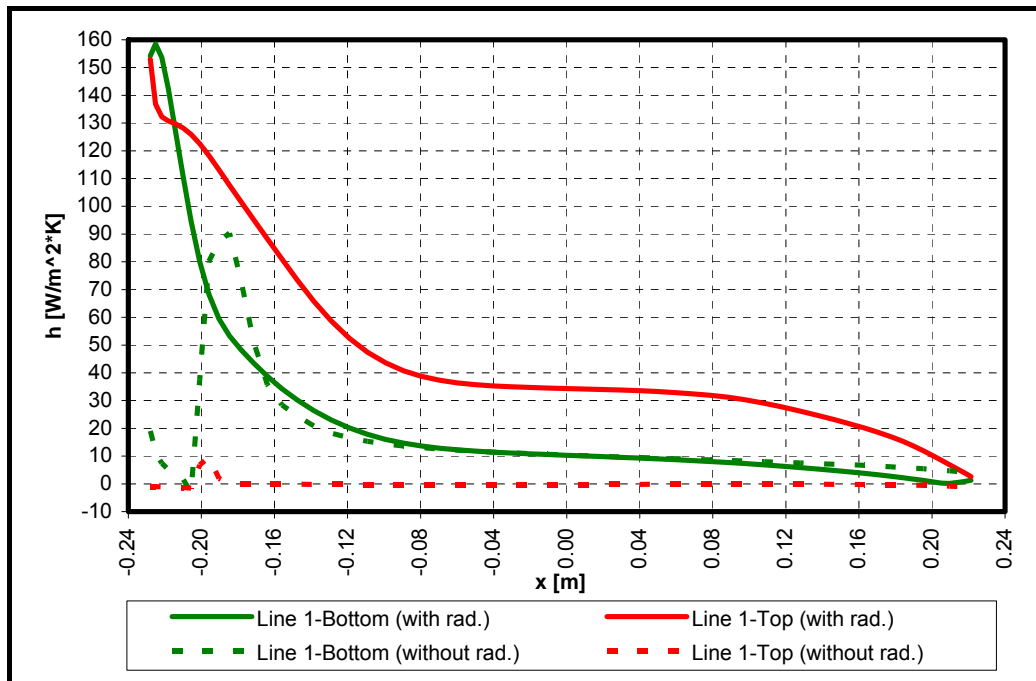
Figure 4.50. Steady state effective heat transfer coefficient values at the bottom and the top walls for the single compartment analysis

Although the total heat flux value for the line 1 on the bottom is greater than the corresponding line 1 on the top wall in Figure 4.49, effective heat transfer coefficient for reference line on bottom wall is smaller than the other one in Figure 4.50 since temperature difference between the top wall and the reference point is much smaller than that of the difference between the bottom wall and the reference point.

The last step for the heat transfer analysis of single compartment study is the determination of the heat transfer rate from the system at the time t=3600 s. In Table 4.7, the total and radiative heat transfer rates obtained from the numerical analyses of the single compartment by applying radiation model or neglecting it are tabulated. It is shown that 3600 seconds is a very good prediction of the time to reach steady state. In Table 4.7, it is also presented that including radiation into the analysis by applying radiation model makes the value of the residuals of the energy balance of the system very close to zero which is the indication of the

convergence of the analysis. Moreover, it can be determined that radiative heat transfer is a significant portion of the total heat transfer rates from or to the walls. For instance, radiative heat transfer rate is about 55 % of the total heat transfer rate for the evaporator.

Table 4.7. Radiative and total heat transfer rates (in Watts) for the single compartment analysis, t=3600 s

	With Rad. Model		Without Rad. Model
	Rad. Heat Tr. Rate	Tot. Heat Tr. Rate	Tot. Heat Tr. Rate
Front Wall	0.67	1.15	0.49
Rear Wall	0.37	0.73	0.37
Top Wall	1.59	1.38	-0.14
Bottom Wall	0.22	2.27	2.05
Left Side Wall	0.68	1.08	0.41
Right Side Wall	0.68	1.08	0.41
Evaporator	-4.18	-7.67	-3.59
Residual of the Energy Balance	*0.02*	*2.32E-06*	*-1.53E-04*

4.4.3. Verification of Radiation Heat Transfer Rates

Although the radiation heat transfer mode does not affect the steady state temperature and velocity distributions inside the compartment, the radiative heat transfer rate is comparable to the convection heat transfer rate. That is why; it is worthwhile to calculate the radiative heat transfer rate analytically at steady state.

Considering the compartment model in Figure 3.2, view factors for the walls can be found easily since the surfaces are parallel or perpendicular to each other. If evaporator is named as the surface 1 and top, bottom, left and right side, front

and rear walls at two sides of the evaporator as surfaces 2, 3, 4, 5, 6, 7 and 8 respectively then available view factor equations are:

$$2F_{1\rightarrow 2} + 2F_{1\rightarrow 4} + F_{1\rightarrow 6} = 1 \tag{4.1}$$

$$F_{2\rightarrow 1} + F_{2\rightarrow 3} + 2F_{2\rightarrow 4} + F_{2\rightarrow 6} + 2F_{2\rightarrow 7} = 1 \tag{4.2}$$

$$F_{4\rightarrow 1} + 2F_{4\rightarrow 2} + F_{4\rightarrow 5} + F_{4\rightarrow 6} + F_{4\rightarrow 7} + F_{4\rightarrow 8} = 1 \tag{4.3}$$

$$F_{6\rightarrow 1} + 2F_{6\rightarrow 2} + 2F_{6\rightarrow 4} + 2F_{6\rightarrow 7} = 1 \tag{4.4}$$

$$2F_{7\rightarrow 2} + 2F_{7\rightarrow 4} + F_{7\rightarrow 6} = 1 \tag{4.5}$$

Applying the reciprocity law and using proper relations for the parallel and perpendicular surfaces in literature [71], view factors are to be determined as; $F_{1\rightarrow 2} = 0.346$, $F_{1\rightarrow 4} = 0.087$, $F_{1\rightarrow 6} = 0.135$, $F_{2\rightarrow 3} = 0.487$, $F_{2\rightarrow 4} = 0.109$, $F_{2\rightarrow 6} = 0.147$, $F_{2\rightarrow 7} = 0.019$, $F_{4\rightarrow 5} = 0.069$, $F_{4\rightarrow 6} = 0.151$, $F_{4\rightarrow 7} = 0.068$, $F_{6\rightarrow 7} = 0.018$.

As a sample wall, the radiative heat gain of the evaporator will then be:

$$Q_{evap} = \sigma \varepsilon A_1 \begin{bmatrix} 2F_{1\rightarrow 4}(T_4^4 - T_1^4) + F_{1\rightarrow 6}(T_6^4 - T_1^4) + \\ F_{1\rightarrow 2}(T_2^4 - T_1^4) + F_{1\rightarrow 3}(T_3^4 - T_1^4) \end{bmatrix} \tag{4.6}$$

where;

σ : Stefan-Boltzman constant ($5.67*10^{-8}$ W/m^{2}K^4),

ε : emissivity of the surface (0.9 in this analysis),

A_1 : surface area of evaporator.

Substituting the values in Equation 4.6, radiative heat gain of the evaporator is found as *4.19 W* which is very close to the value of 4.18 in Table 4.7. Using Equation 4.6, radiative heat transfer for all walls are calculated and presented in Table 4.8. The results in Table 4.8 show that the radiation model used and

corresponding radiative heat transfer rates calculated in numerical analysis are proper.

Table 4.8. Radiative heat transfer rates (in Watts) calculated analytically for the walls of the single compartment

Front Wall	0.67
Rear Wall	0.35
Top Wall	1.58
Bottom Wall	0.20
Left Side Wall	0.69
Right Side Wall	0.69
Evaporator	-4.19

4.4.4. Comparison of Temperature Values Obtained from the Single Compartment Analysis and the Experimental Work

In this section, temperature distribution obtained for the reference lines on symmetry plane in numerical analysis will be compared with the temperature values measured in experimental study of the same compartment. The reference lines selected in numerical analysis shown in Figure 4.51 are the vertical lines on which the thermocouples are located in experimental work. The exact coordinates of the thermocouples were shown in Figure 3.7. In Figure 4.52, experimental temperature values measured on three vertical lines away from the evaporator on the symmetry plane with the numerical simulations performed including radiation or omitting it are compared. It can be said that numerical analyses performed with or without radiation model give very close temperature values on the same vertical lines.
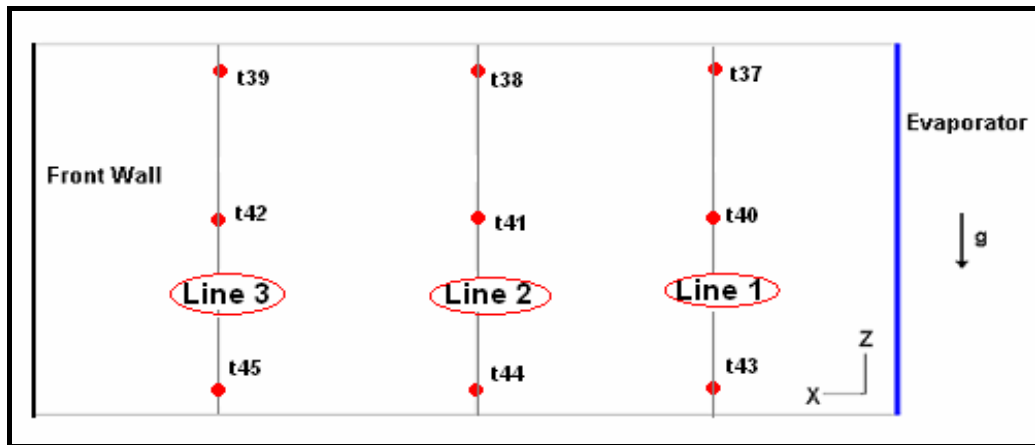
Figure 4.51. Configuration of reference lines on the symmetry plane for the single compartment analysis
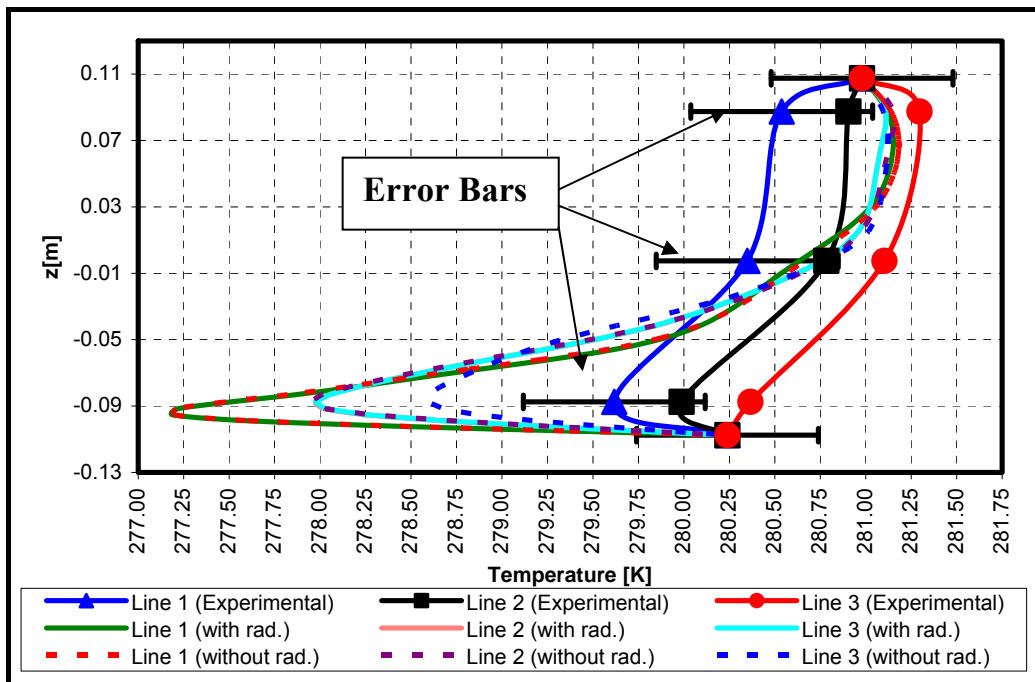

Figure 4.52. Comparison of temperature values on the symmetry plane obtained from the numerical analysis and the experimental work

On the other hand; experimental temperature values are not overlap the numerically obtained results but they are in a good agreement especially on the

upper half of the symmetry plane. The frame used to locate the thermocouples on the symmetry plane in the experimental study may disturb the boundary layer at the lower part close to the bottom wall and there is a conduction heat transfer through the solid frame. Therefore, experimental temperature values at the bottom level of all three vertical reference lines deviate from the values obtained in theoretical numerical analysis but numerical results still remain in the uncertainty range (error bar range is 1 $^{\circ}$C in Figure 4.52) of the experimental temperature values.

4.5. Results of Numerical Analysis of the Total Refrigerator

There are lots of natural convection cavity analyses but for the total refrigerator as an application the literature study is limited [37, 38, 72]. For this reason the final numerical work in the present study is focused on the actual dimensions of the total refrigerator cabinet used in experimental work.

4.5.1. Temperature and Velocity Profiles

The analysis of the total refrigerator is again time dependent. Natural convection analysis is done for either including or omitting the radiation and corresponding temperature and velocity profiles are presented at the midplanes.

Temperature and velocity profiles are searched and visualized at two different planes; x-z midplane which is the symmetry plane orthogonal to the evaporator and front wall and y-z midplane of the cavity. Results obtained for the y-z midplane are shifted behind to make the distributions comprehensible.

In Figures 4.53 and 4.54, at t=150 seconds, temperature profile in the compartment is nearly the same for the cases, radiation included or omitted. Moreover, a stratified temperature distribution is observed on the midplanes.

Natural convection characteristics are dominant in the enclosure. Boundary layers developing on the evaporator and bottom wall are observed. Although the maximum temperature is the same in Figures 4.53 and 4.54, when Figures 4.55 and 4.56 are analyzed, maximum velocity value in the domain is 0.162 m/s for the radiation included analysis and it is 0.159 m/s for the analysis where radiation is not taken into account.
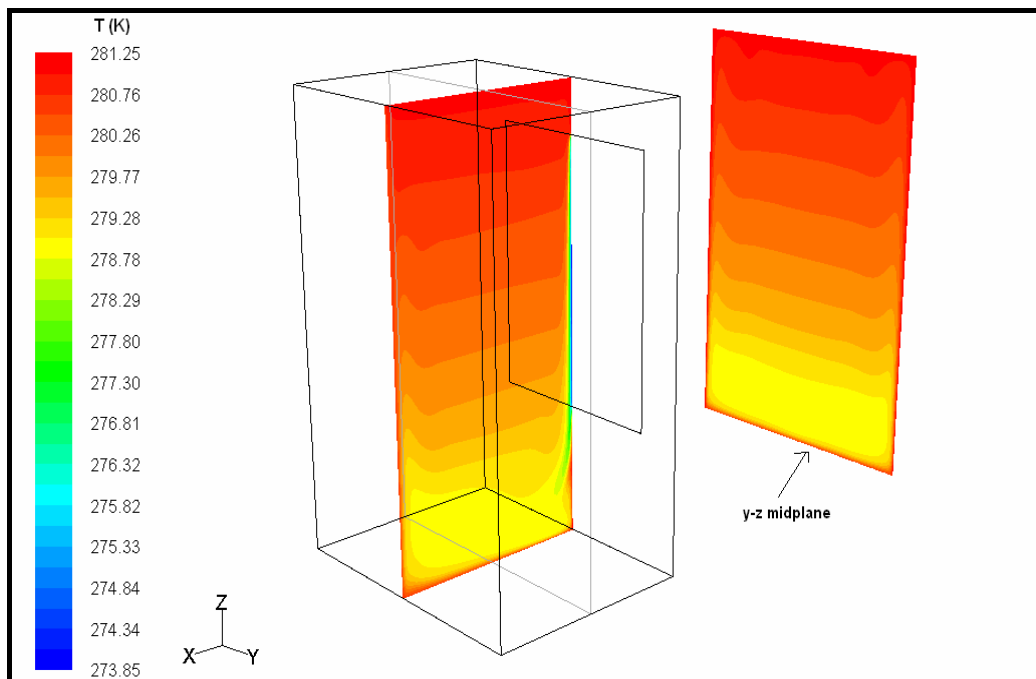

Figure 4.53. Temperature profile for the total refrigerator analysis, t=150 s (with radiation)
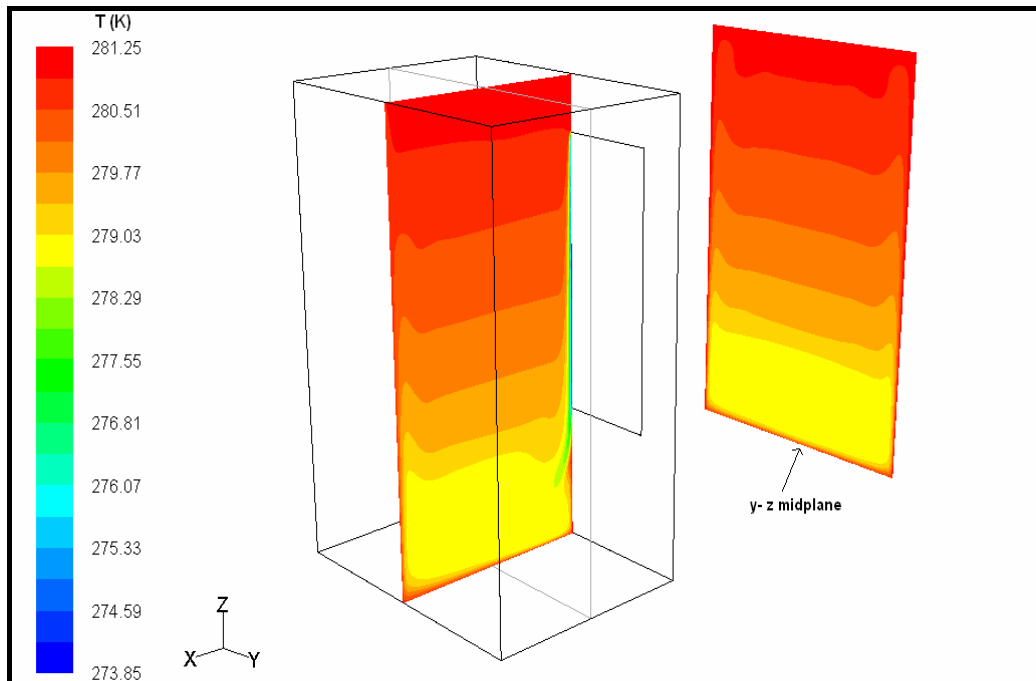
Figure 4.54. Temperature profile for the total refrigerator analysis, t=150 s
(without radiation)
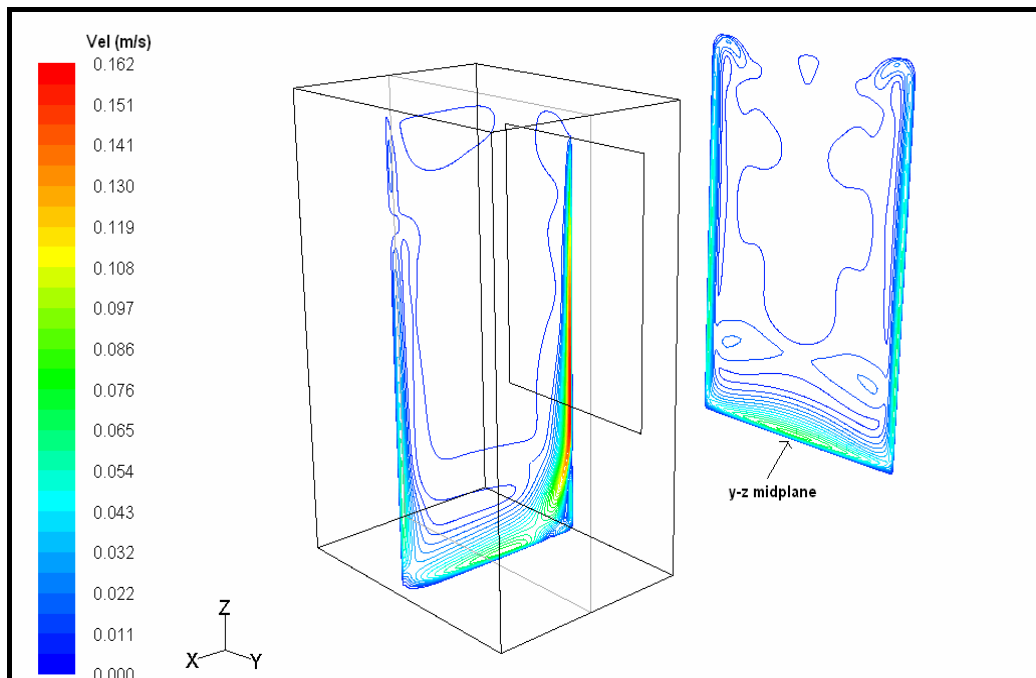
Figure 4.55. Velocity profile for the total refrigerator analysis, t=150 s
(with radiation)
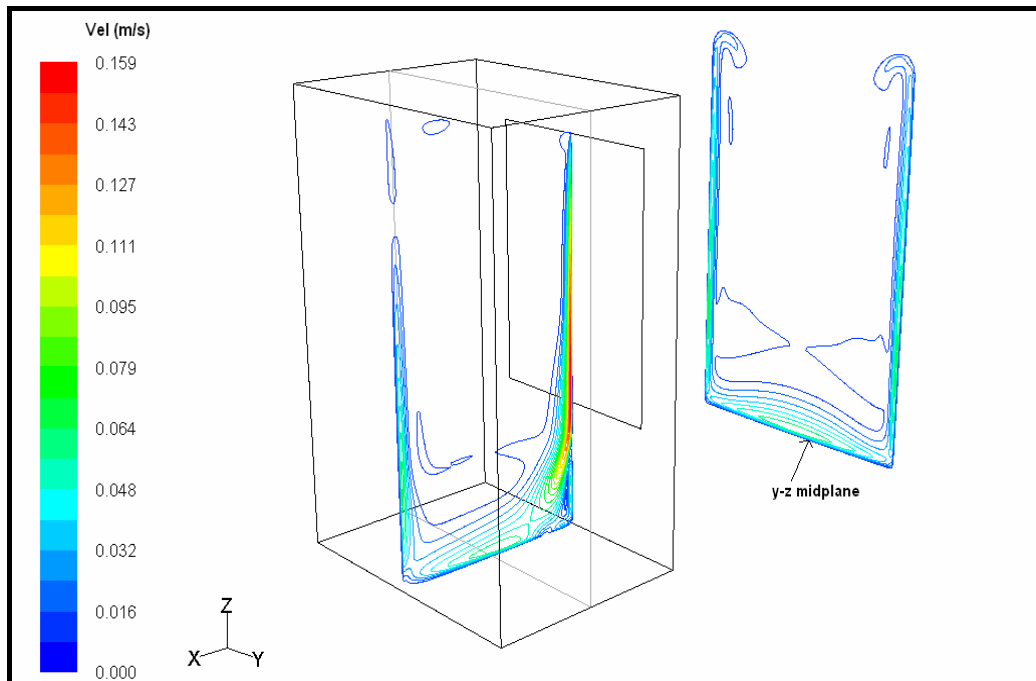
Figure 4.56. Velocity profile for the total refrigerator analysis, t=150 s
(without radiation)

In Figures 4.57 and 4.58, it is presented that the air at the lower part of the refrigerator cabinet gets warmer so the air temperature inside the cabinet is between 279 K and 281 K at the time of 5 minutes. Additionally, stratification of air inside the refrigerator cabinet is still observed.

Velocity contours for the time instant of 300 seconds are shown in Figures 4.59 and 4.60. In these figures, velocity profiles are not changing so much but a separation from the boundary layer on the evaporator is observed in the results of the numerical analysis taking the radiation into account. The maximum velocity values are the same and equal to 0.166 m/s for both of the analyses including radiation or neglecting it.
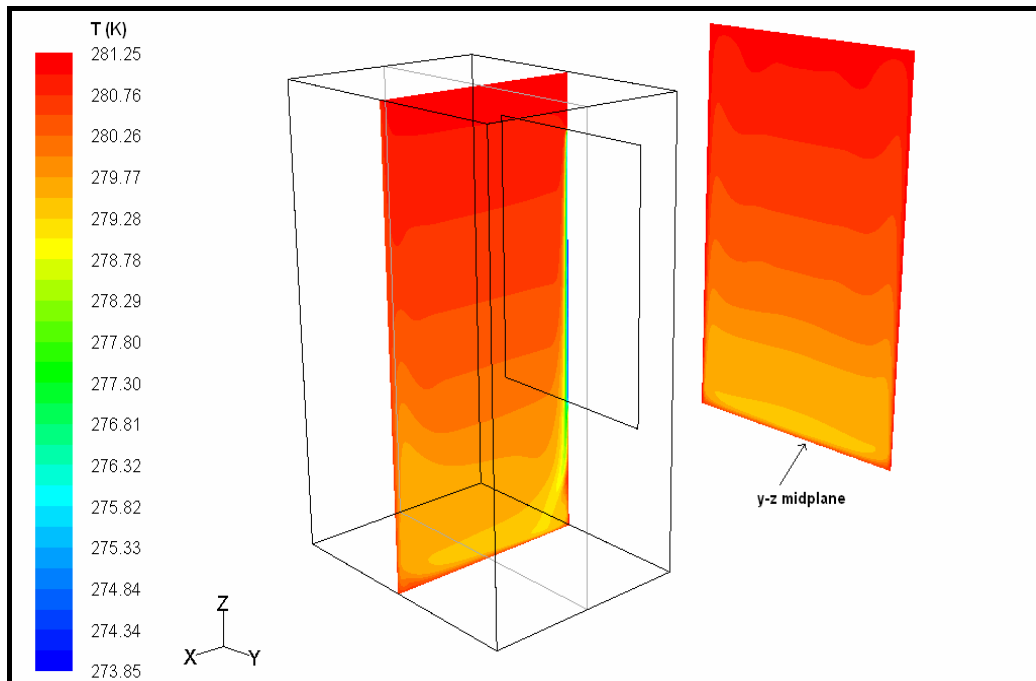
Figure 4.57. Temperature profile for the total refrigerator analysis, t=300 s
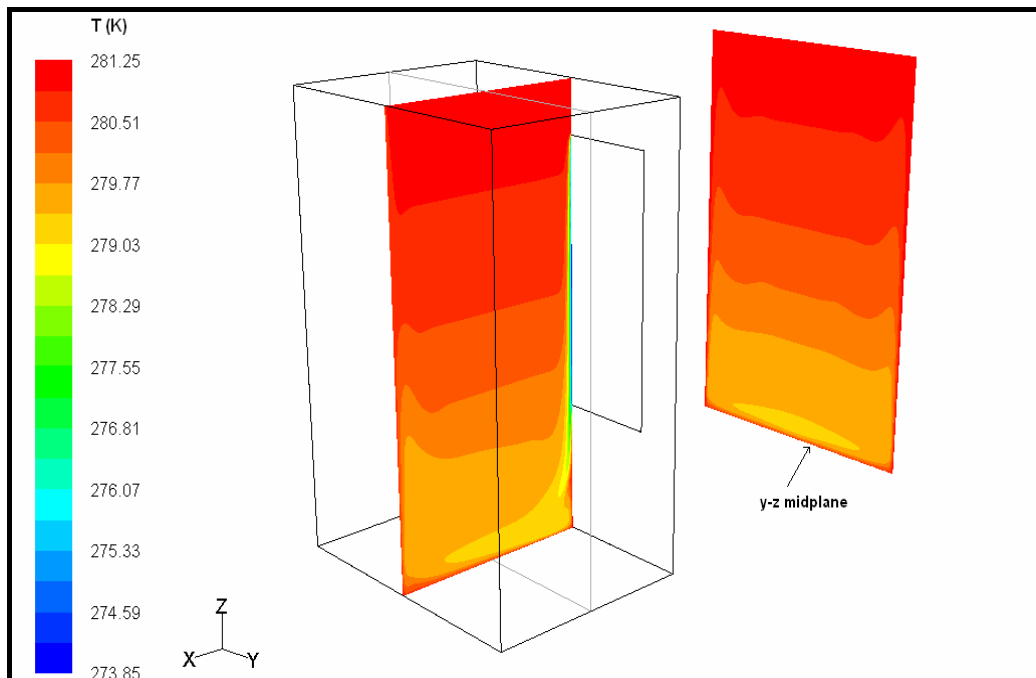
(with radiation)

Figure 4.58. Temperature profile for the total refrigerator analysis, t=300 s
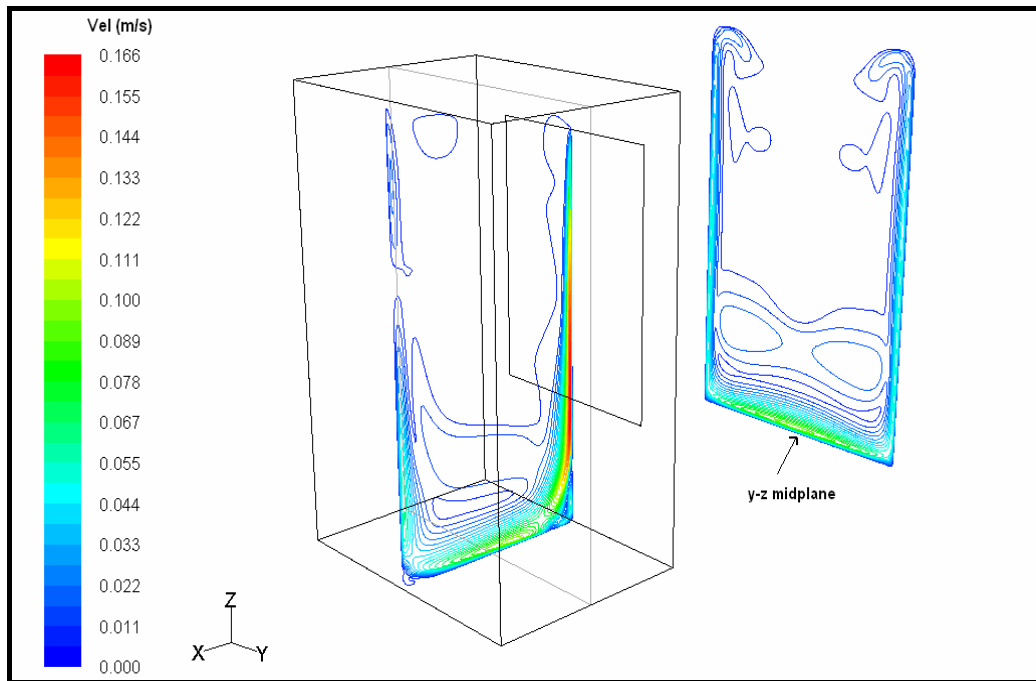
(without radiation)

Figure 4.59. Velocity profile for the total refrigerator analysis, t=300 s
(with radiation)
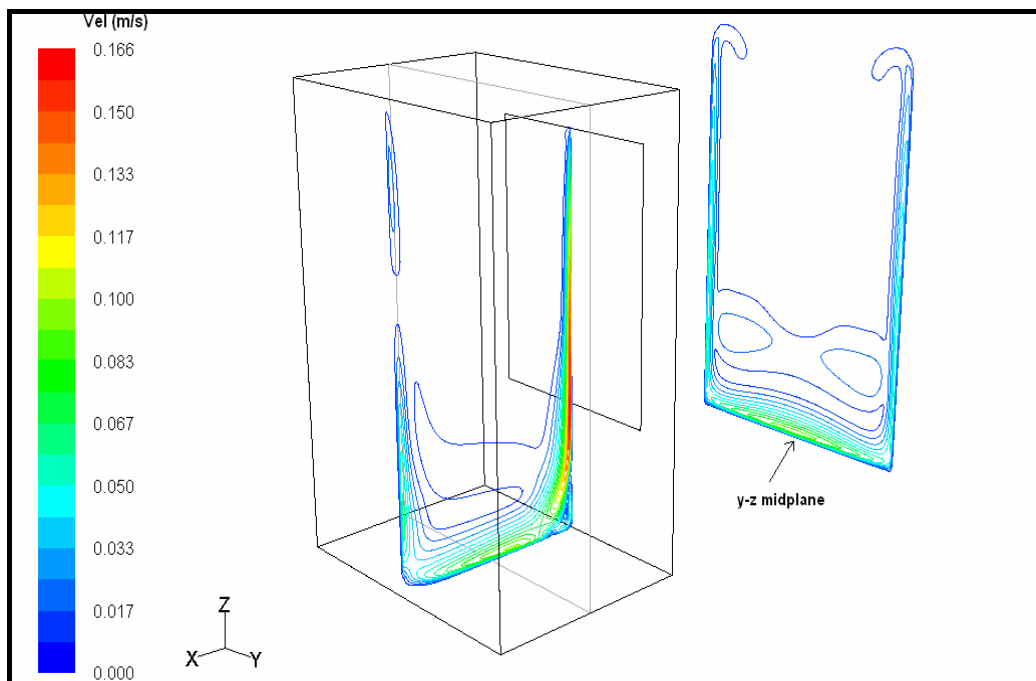
Figure 4.60. Velocity profile for the total refrigerator analysis, t=300 s
(without radiation)
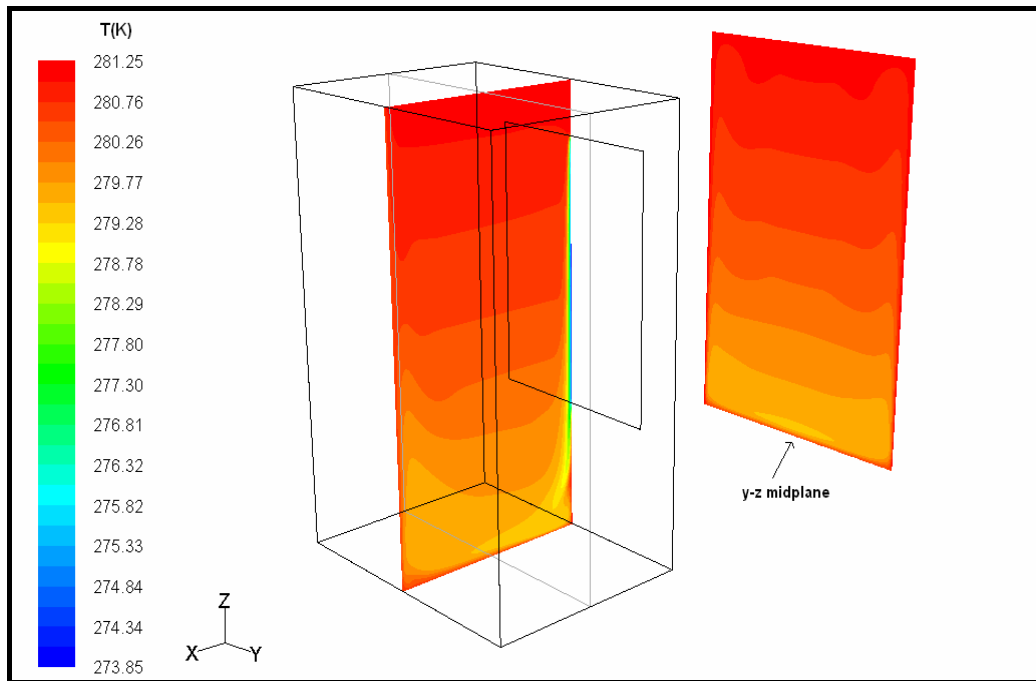
Figure 4.61. Temperature profile for the total refrigerator analysis, t=600 s
(with radiation)
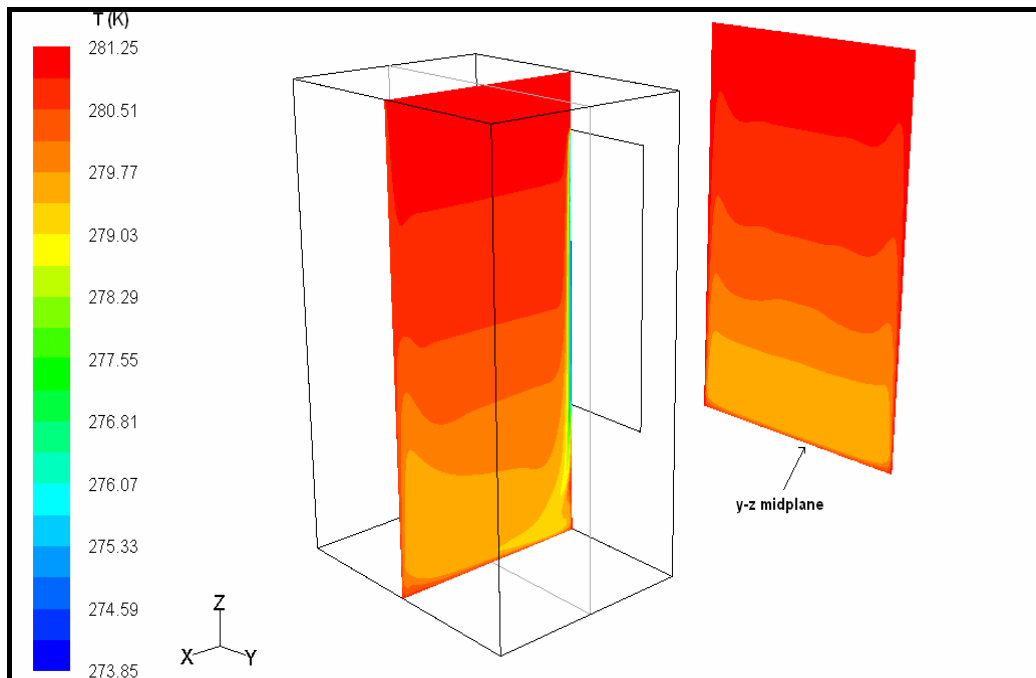
Figure 4.62. Temperature profile for the total refrigerator analysis, t=600 s
(without radiation)

At the time instants of 600 to 3600 seconds, profiles are not changing for both radiation included or omitted cases. The only difference is that an occurrence of the boundary layer separation on evaporator for the analysis including the radiation model.

When the results presented in Figures 4.63 and 4.64 or 4.67 and 4.68 are compared, radiation affects the flow on the evaporator. A boundary layer separation is still observed on evaporator when the analysis including radiation is considered. Moreover a flow of air on y-z midplane from the side walls to the central zone is determined for the analysis with radiation. On the other hand, cellular zone at the lower part of the y-z midplane is observed in the analysis where radiation is not taken into account.
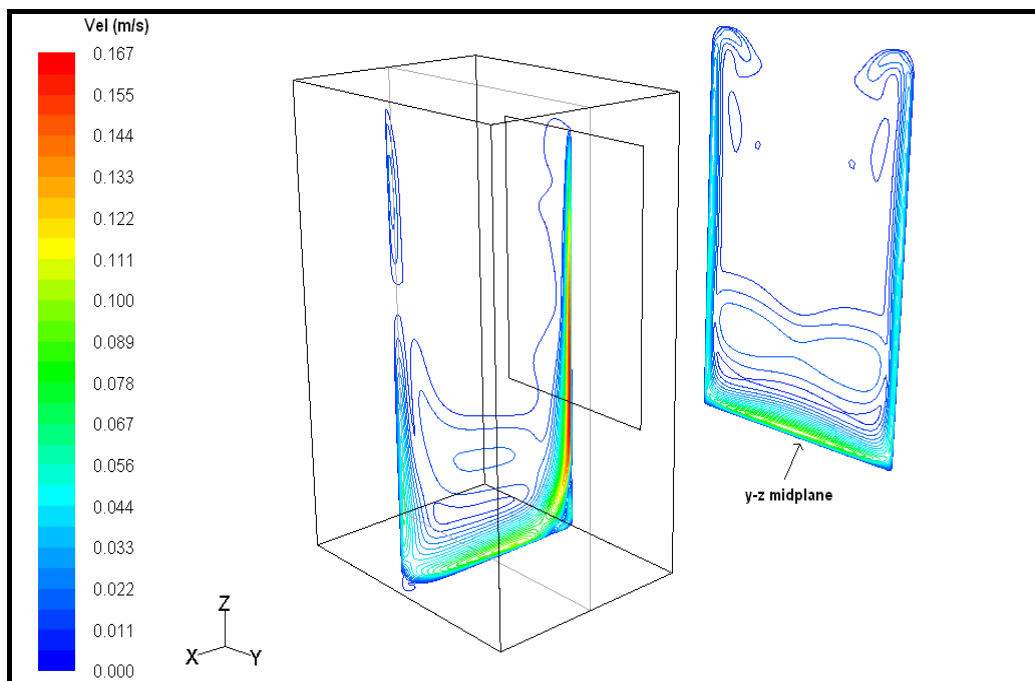
Figure 4.63. Velocity profile for the total refrigerator analysis, t=600 s
(with radiation)
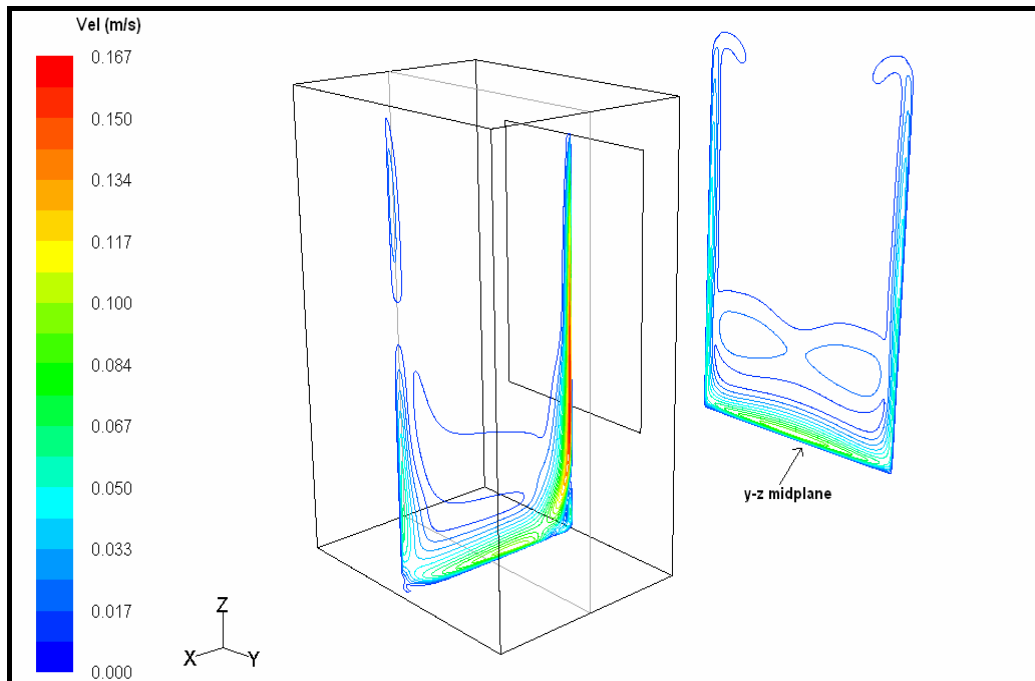
Figure 4.64. Velocity profile for the total refrigerator analysis, t=600 s
(without radiation)
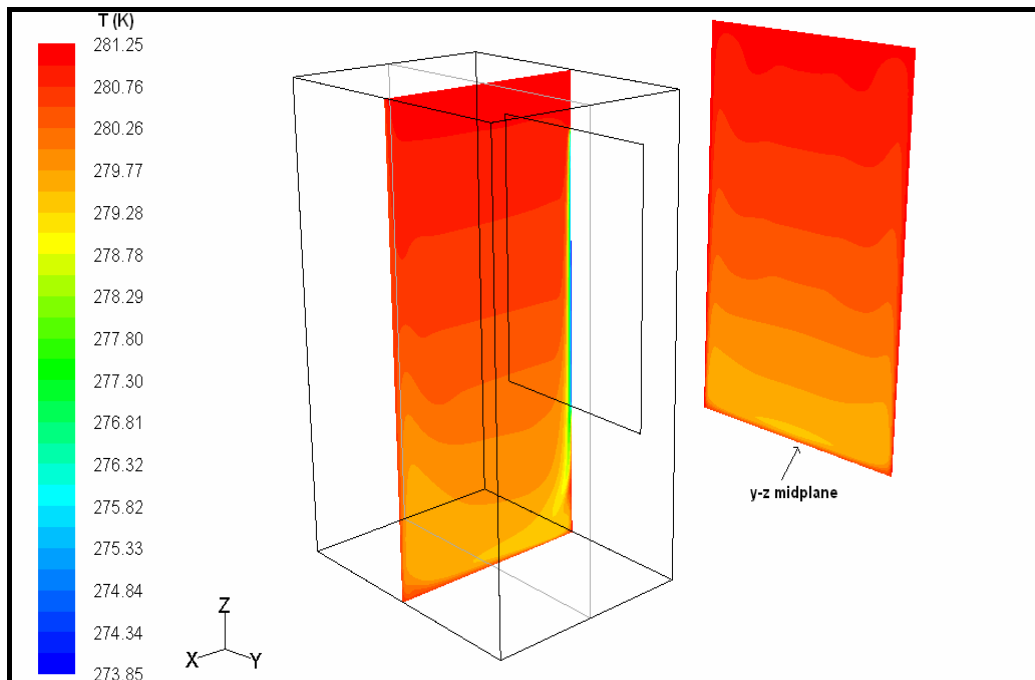
Figure 4.65. Temperature profile for the total refrigerator analysis, t=3600 s
(with radiation)
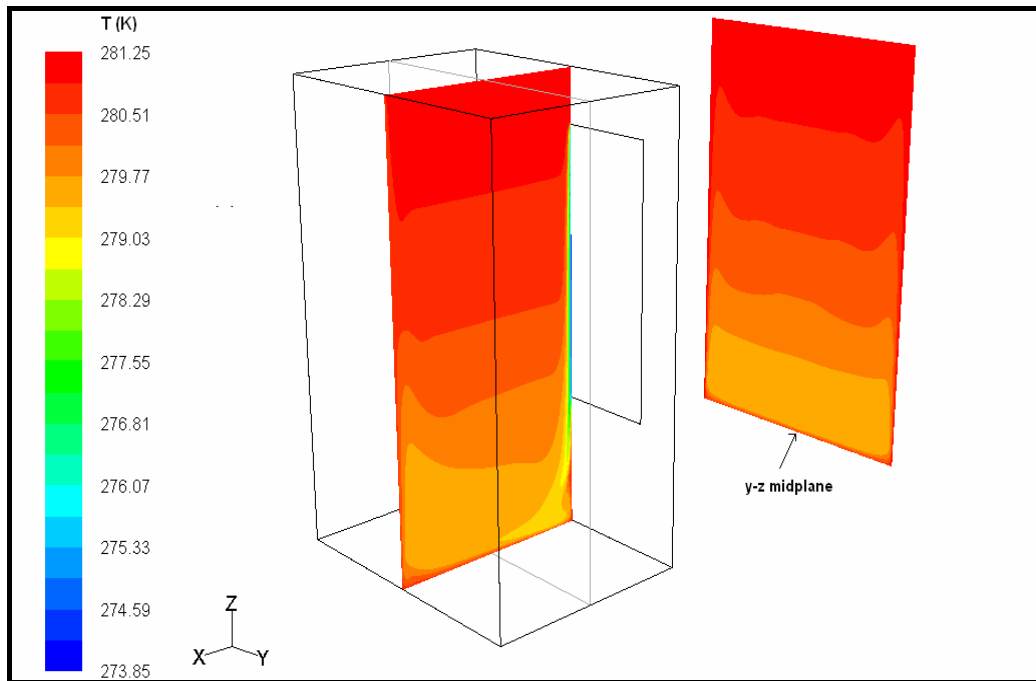
Figure 4.66. Temperature profile for the total refrigerator analysis, t=3600 s
(without radiation)
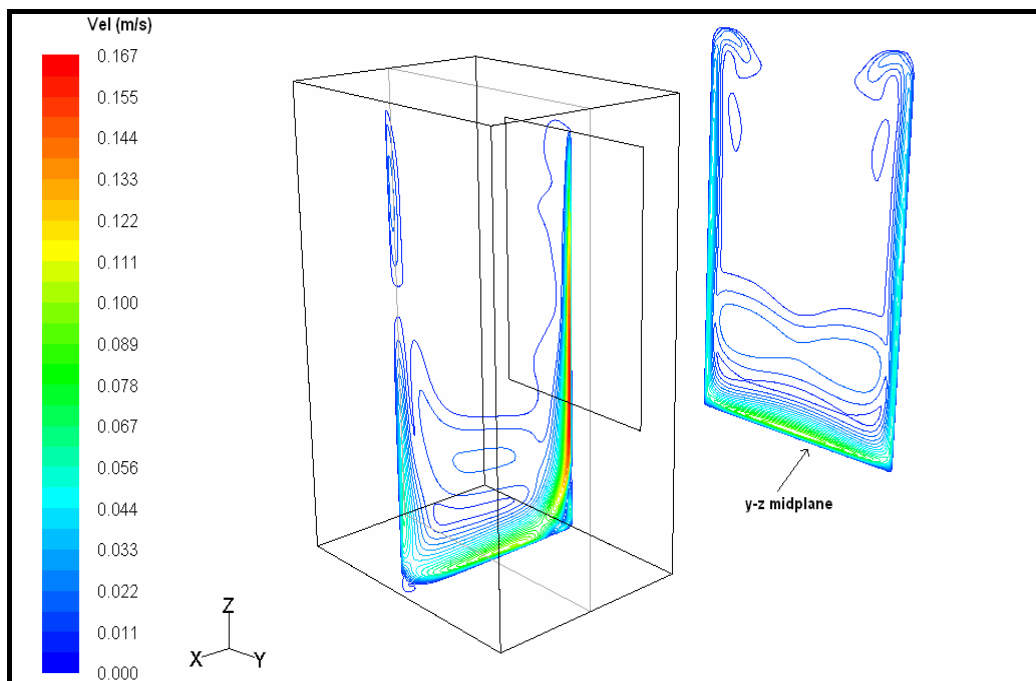
Figure 4.67. Velocity profile for the total refrigerator analysis, t=3600 s
(with radiation)
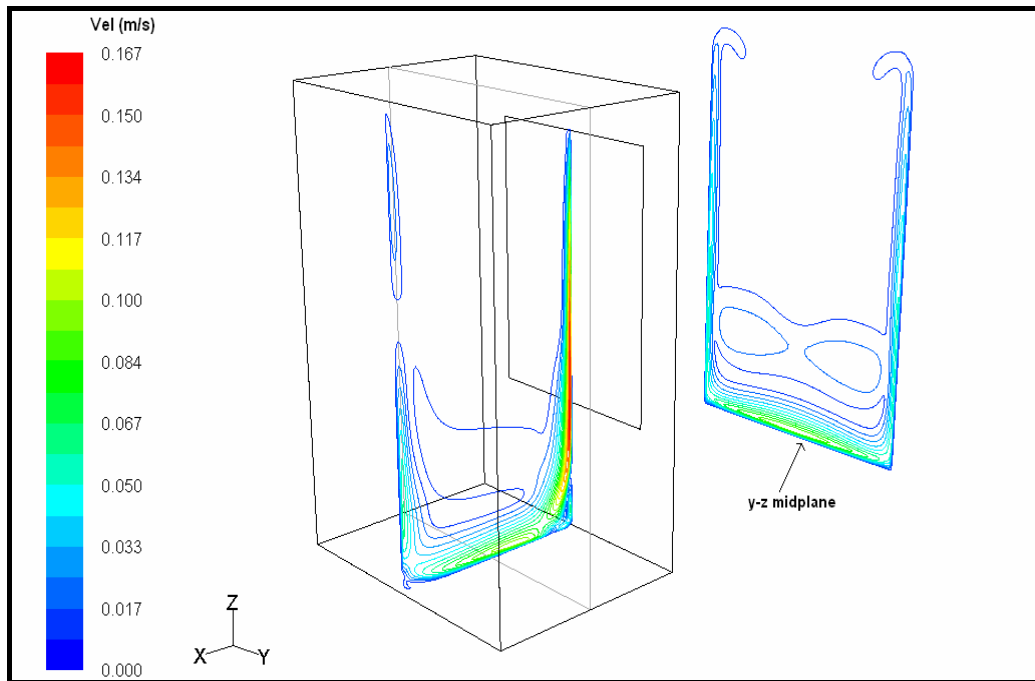
Figure 4.68. Velocity profile for the total refrigerator analysis, t=3600 s (without radiation)

The time to reach the steady state for the total refrigerator analysis is shorter when the radiation is considered. The time to reach steady state is about 10 minutes and 7 minutes for the analysis without radiation and with radiation respectively. Using Celeron two core dual T7400 processor, 2.3 GHz, 12 GB ram computer run time of the total refrigerator model analysis with radiation is one week, whereas it is four days for the analysis with no radiation.

The velocity boundary layers at the walls and the flow directions are presented in Figures 4.69 and 4.70 for the symmetry plane of the cavity (x-z midplane) at steady state for radiation included or neglected models respectively. The velocity vectors are not plotted proportional to their magnitudes since they are not visualized in that case. In Figures 4.69 and 4.70, the inclination of stagnant air inside towards the boundary layers formed on the evaporator and bottom wall is shown.
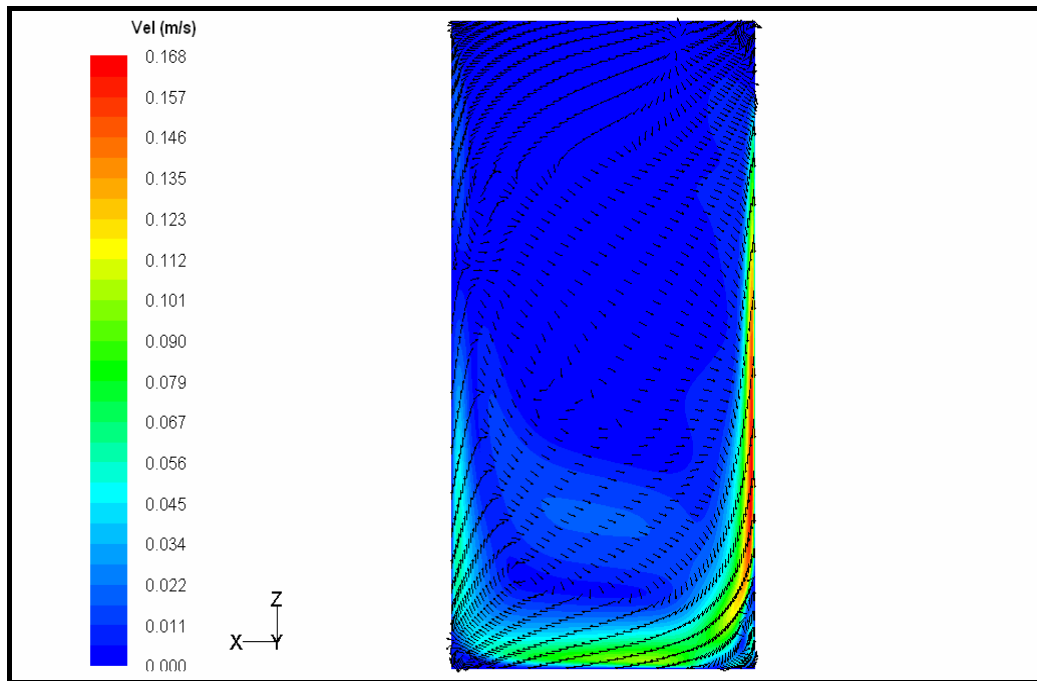
Figure 4.69. Velocity vectors at the symmetry plane for the total refrigerator analysis, t=3600 s (with radiation)
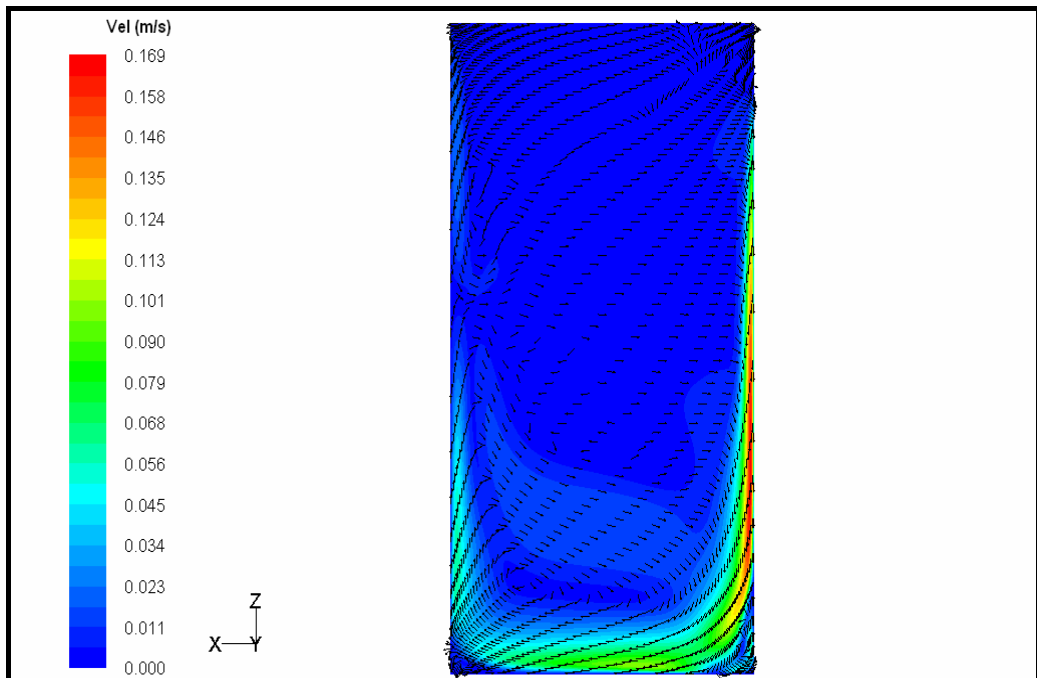
Figure 4.70. Velocity vectors at the symmetry plane for the total refrigerator analysis, t=3600 s (without radiation)

4.5.2. Heat Transfer Analysis

Including or omitting radiation, heat transfer analysis formulated in the previous chapter is performed for the total refrigerator model also. The variation of the heat transfer parameters with time or spatial coordinates those have been investigated in the single compartment analysis is repeated and same graphs for larger scale domain of refrigerator cabinet are plotted. Since the total refrigerator analysis is also performed up to 3600 seconds, heat flux and effective heat transfer coefficient variations with time are presented till this time instant. Area weighted average of the flux values at each face of the corresponding wall are used to determine the total heat flux on that surface. Reference temperature necessary for the calculation of effective heat transfer coefficient is again selected as the geometric center (origin of the coordinate system) temperature of the domain.
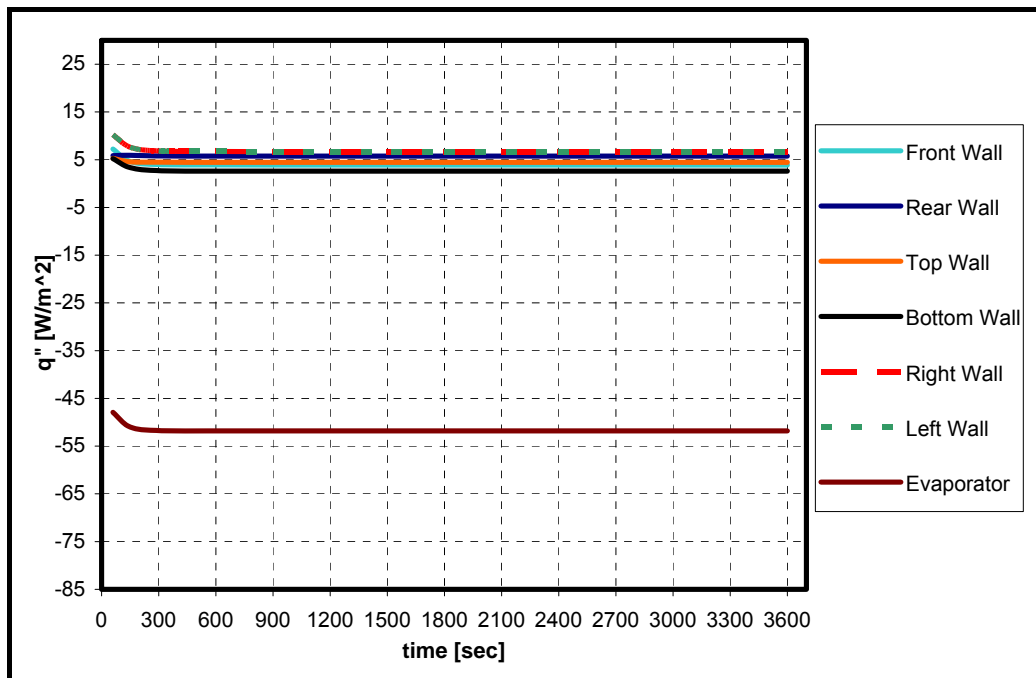
Figure 4.71. Time dependent heat flux values for the total refrigerator analysis (with radiation)
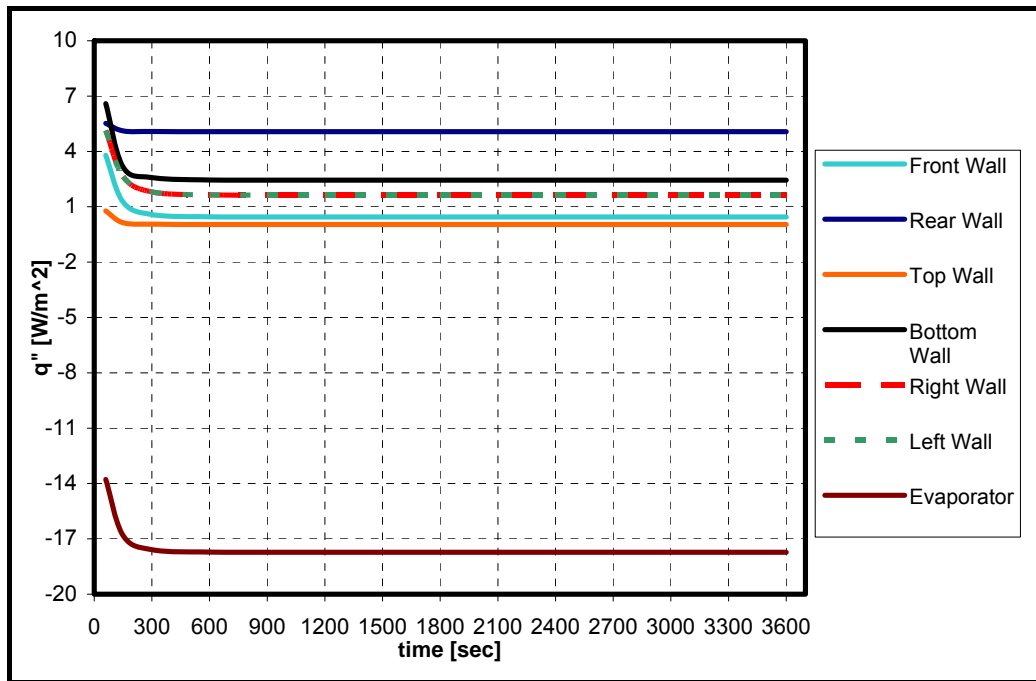
Figure 4.72. Time dependent heat flux values for the total refrigerator analysis
(without radiation)

In Figures 4.71 and 4.72, heat flux values from or to the walls are constant after 300 seconds and radiative heat flux value is about two times the convective heat flux at all time instances for all walls. In addition; absolute heat flux value at the evaporator is much more than the other walls due to a radiative gain from the other walls of the refrigerator.

Time dependent effective heat transfer coefficients for all walls are plotted in Figures 4.73 and 4.74. Effective heat transfer coefficient values are not changing with time after 900 seconds for radiation or without radiation cases. Due to small temperature difference between the front wall and center of the domain effective heat transfer coefficient on this wall is greater than the others. When focused on evaporator, it is observed that effective heat transfer coefficient value is about 8 W/m²K for radiation included analysis. As remembered, this value was about 10 W/m²K for single compartment numerical analysis with radiation.
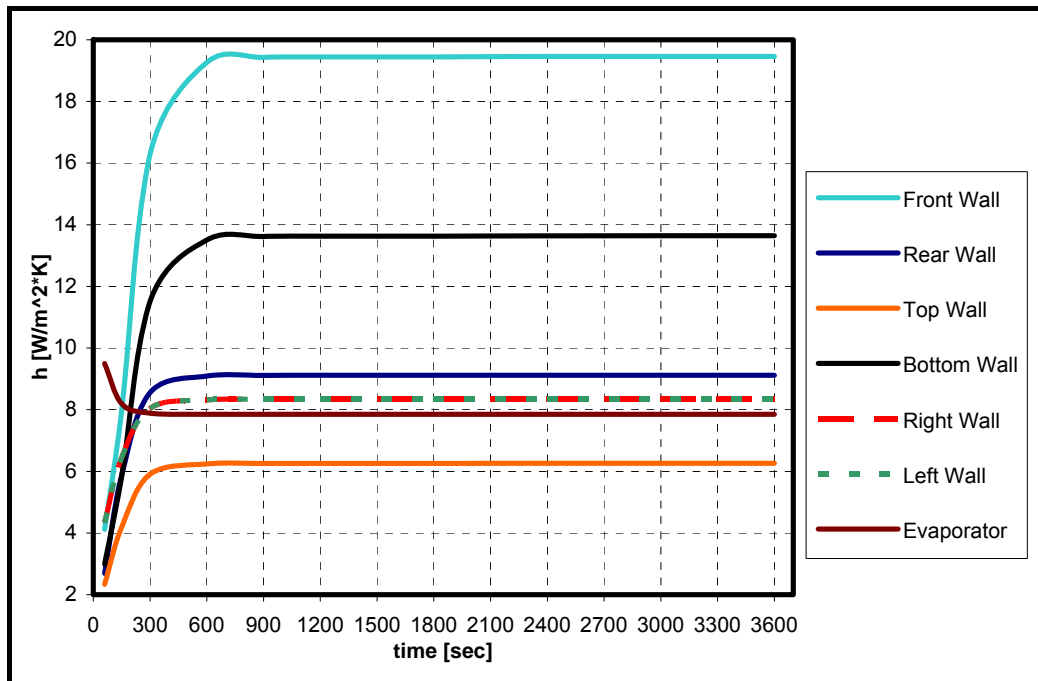
Figure 4.73. Time dependent effective heat transfer coefficient values for the
total refrigerator analysis (with radiation)
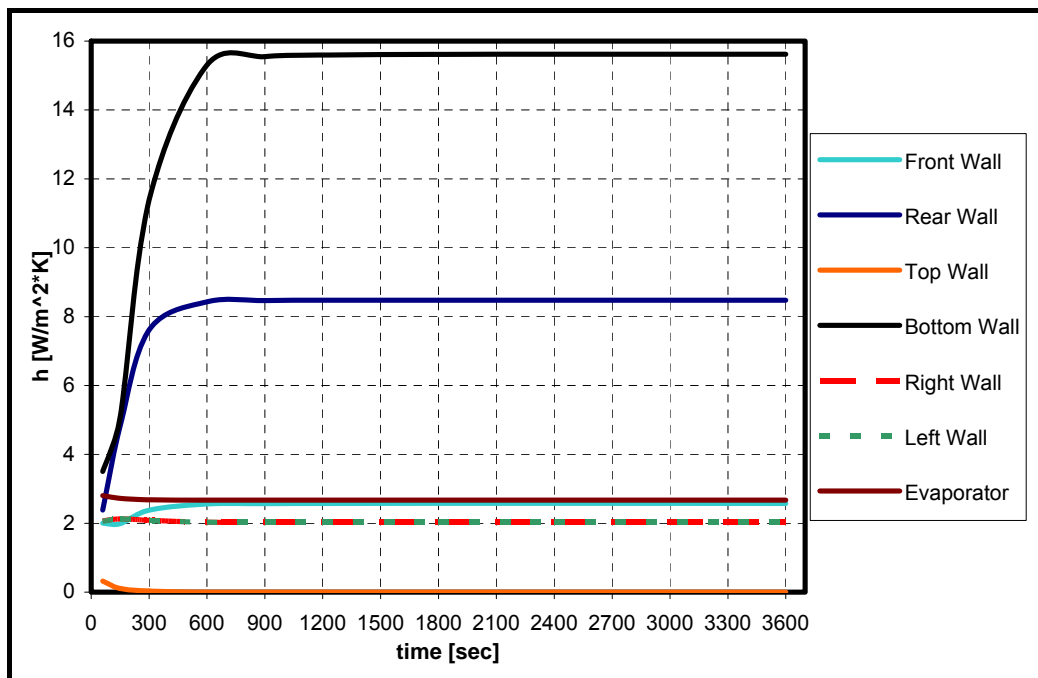
Figure 4.74. Time dependent effective (convective) heat transfer coefficient
values for the total refrigerator analysis (without radiation)

Inserting the radiation model into the analysis or neglecting it; at the time of 3600 seconds, q" and h variations with spatial coordinates are obtained for the reference lines shown with the evaporator region in Figure 4.75. As in the single compartment analysis, heat flux and effective heat transfer coefficient parameters are calculated for three and four vertical equidistance lines (9 cm between each) on evaporator and front wall respectively. Then, heat flux and effective heat transfer coefficient parameters are calculated only only for the lines, Line 1 (top wall) and Line 1 (bottom wall), on top and bottom walls. In Figure 4.76, heat flux values are the same for three vertical reference lines located in parallel on the evaporator for both radiation and without radiation cases. Total heat flux values of both radiation included or omitted analyses decrease from top to bottom since convective heat flux is larger at the upper region of the evaporator. Radiative heat flux is not changing with z because it is only the function of temperature of the walls and the evaporator.
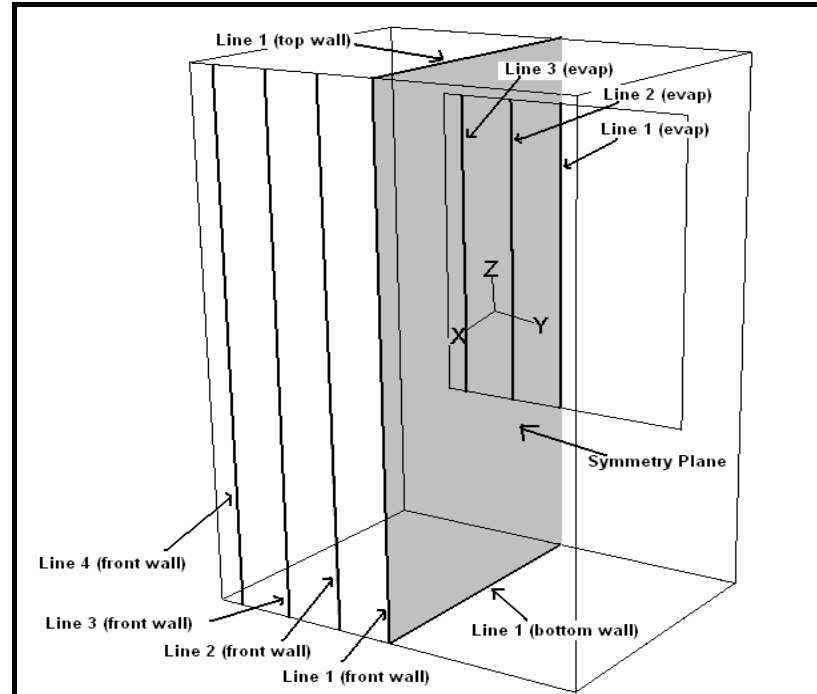
Figure 4.75. Configuration of reference lines used for s.s. heat transfer analysis in the total refrigerator analysis
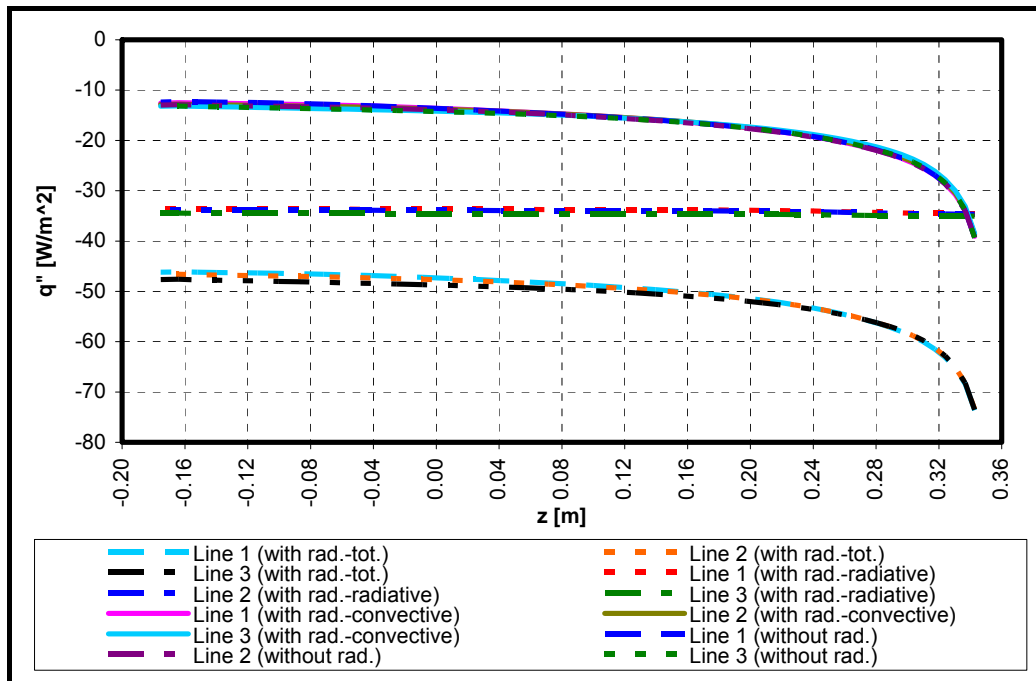
Figure 4.76. Steady state heat flux values at the evaporator for the total refrigerator analysis
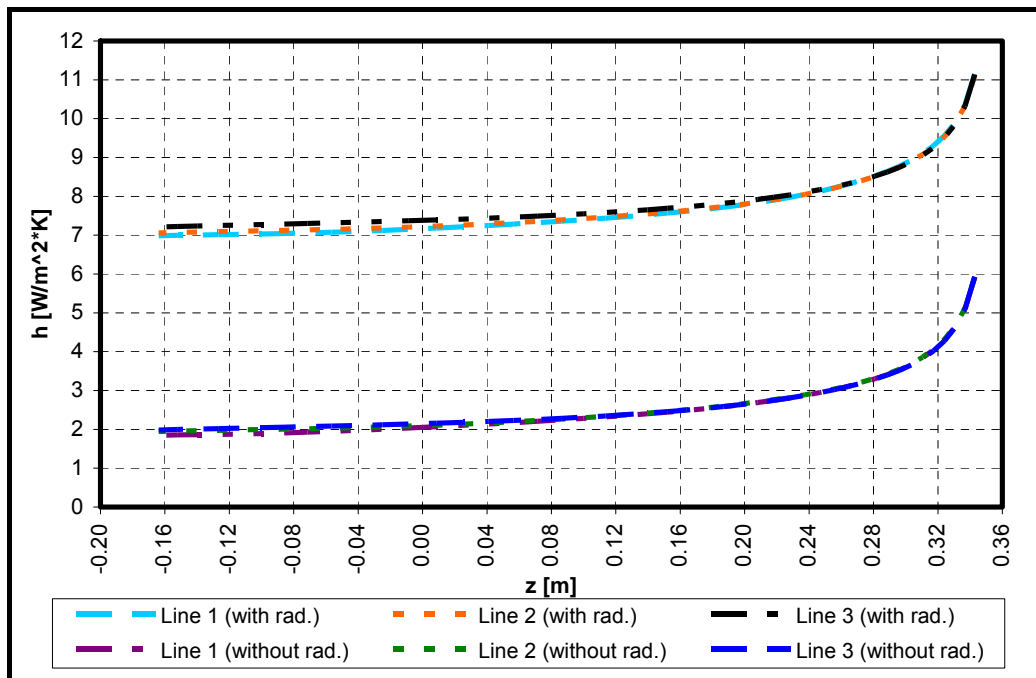
Figure 4.77. Steady state effective heat transfer coefficient values at the evaporator for the total refrigerator analysis

Reflecting the total heat flux behavior; effective heat transfer coefficient values increase from bottom to top at the evaporator wall as presented in Figure 4.77. Effective heat transfer coefficient values are close to the ones obtained in the single compartment analysis but they are slightly greater in total compartment numerical analysis. In Figure 4.78 it is shown that total heat flux is from the front wall to the air inside and it is fluctuating from bottom to top. There is an increase in the total heat flux at the bottom region of the front wall and then a slight decrease is observed, but after z=-0.08 m, a significant increase is seen. This level is nearly aligned with the bottom of the evaporator facing the front wall. After z=0.08 m, again a drop appeared. The radiative heat flux has also the same trend. Additionally, total and radiative heat flux values are decreasing from line 1 to line 4 on the wall. Convective heat fluxes are not changing with y, instead they are decreasing from bottom to the top on the wall which is an expected characteristic of natural convection problem for the wall representing the door of the refrigerator.
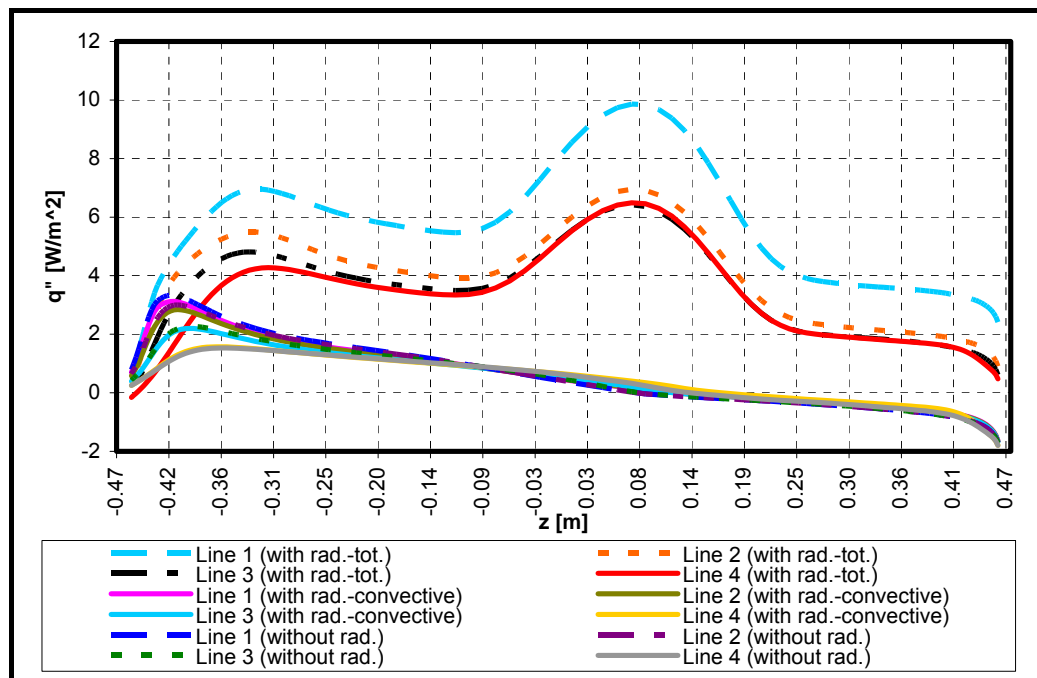
Figure 4.78. Steady state heat flux values at the front wall for the total refrigerator analysis
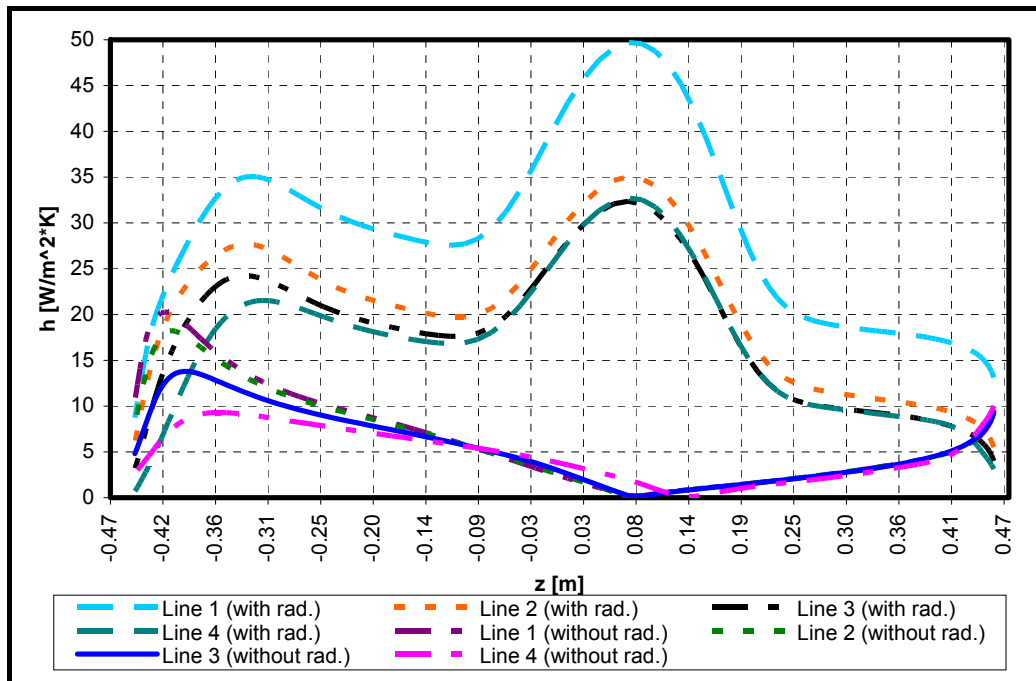
Figure 4.79. Steady state effective heat transfer coefficient values at the front wall for the total refrigerator analysis

In Figure 4.79, the behavior of the effective heat transfer coefficient for the reference lines is exactly the same with the radiative or total heat flux values presented in Figure 4.78. For this reason, the ratio of the magnitude of the effective heat transfer to the magnitude of the convective heat transfer coefficient for any reference line is varying.

In Figures 4.80 and 4.81, q"(x) and h(x) are presented respectively only for Line 1 (top wall) and Line 1 (bottom wall), shown in Figure 4.75. In Figure 4.80, total heat fluxes for top and bottom walls are high at the region close to the back wall but they decrease very rapidly. After x=-0.06 m, an increase in total and radiative heat fluxes on the top wall is evident but due to a drop in convective heat flux total heat flux from the bottom wall continues to decrease. On the other hand; convective heat flux value for the top wall is nearly zero throughout the line.
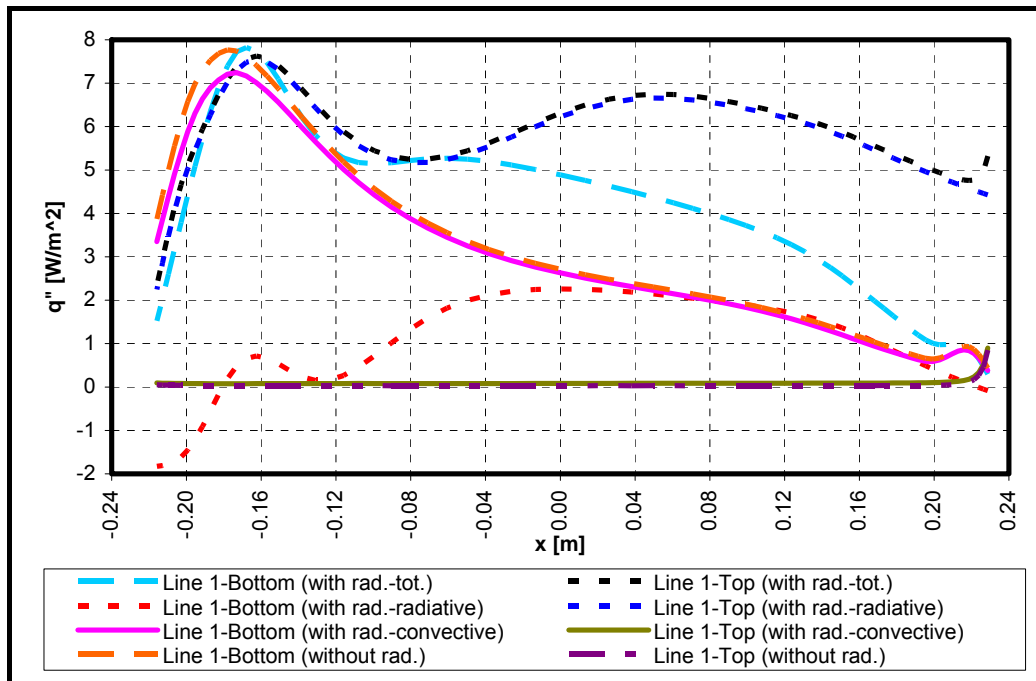
Figure 4.80. Steady state heat flux values at the bottom and the top walls for the
total refrigerator analysis
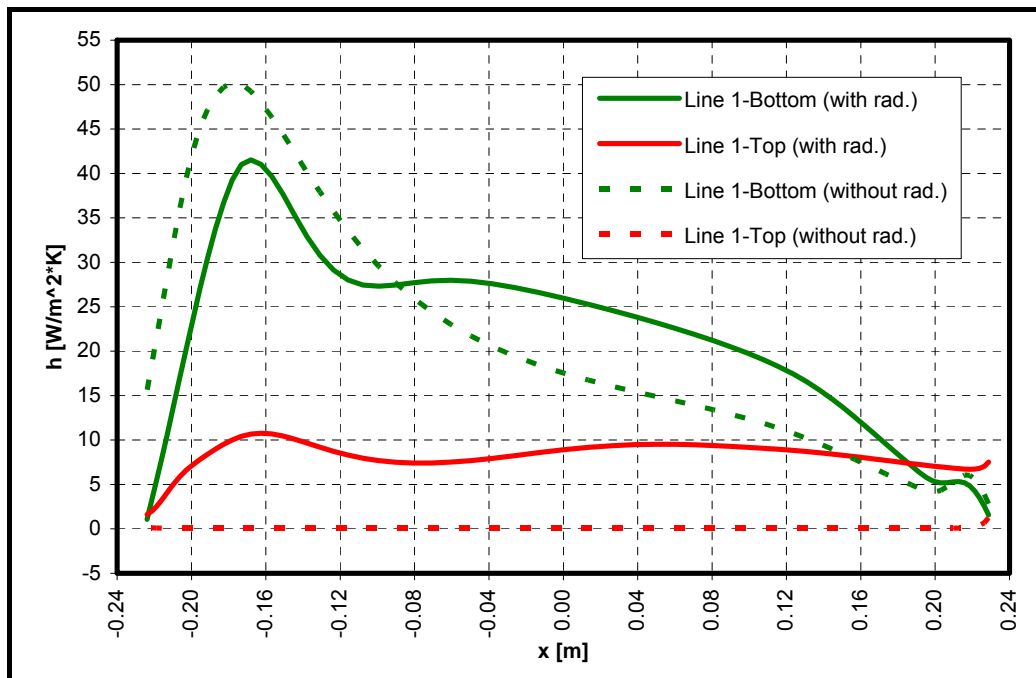
Figure 4.81. Steady state effective heat transfer coefficient values at the bottom
and the top walls for the total refrigerator analysis

- 113 -

Since the convective heat flux and total heat flux values are close to each other at the back part of the bottom wall, convective heat transfer coefficient value is greater than the effective one up to x=-0.08 m for the bottom wall in Figure 4.81. Moreover, the effective heat transfer coefficient value for the reference line on the top wall is smaller than that of the bottom wall since the reference temperature is close to the temperature of the bottom wall. It is an expected situation because bottom wall and evaporator temperature boundary conditions are effective on the temperature distribution inside the domain.

Heat transfer analysis ends with the determination of heat transfer rate from the system at the time t=3600 s. The total and radiative heat transfer rates obtained from the numerical analyses of total refrigerator are tabulated in Table 4.9. Results in Table 4.9 indicate that 3600 seconds is a perfect prediction of steady state time. Values in Table 4.9 also show the impact of radiative heat transfer on the analysis. A significant share of the total heat transfer rates from or to the walls is due to radiation. About 55 % of the total heat transfer rate to the evaporator was radiative heat transfer rate for single compartment analysis, but the percentage reaches to 66 % for the total refrigerator analysis.

Table 4.9. Radiative and total heat transfer rates (in Watts) for the total refrigerator analysis, t=3600 s

	With Rad. Model		Without Rad. Model
	Rad. Heat Tr. Rate	Tot. Heat Tr. Rate	Tot. Heat Tr. Rate
Front Wall	1.95	2.21	0.22
Rear Wall	0.22	1.97	1.73
Top Wall	1.28	1.31	0.02
Bottom Wall	0.05	0.73	0.69
Left Side Wall	2.25	2.96	0.74
Right Side Wall	2.25	2.96	0.74
Evaporator	-8.03	-12.15	-4.16
Residual of the Energy Balance	*-0.04*	*-0.01*	*-0.01*

4.5.3. Verification of Radiation Heat Transfer Rates

The same analytical study performed to determine the view factors and radiative heat transfer rates from or to the walls for the single compartment is done for the total refrigerator also. Considering the total refrigerator model in Figure 3.3, view factors for the walls are found. If evaporator is named as the surface 1 and top, bottom, left and right side, front and rear wall as surfaces 2, 3, 4, 5, 6 and 7 respectively then available view factor equations of 4.1 to 4.5 are used and applying the reciprocity law and using proper relations for the parallel and perpendicular surfaces in literature [71, 73-77], view factors are to be determined as; $F_{1\to2} = 0.138$, $F_{1\to3} = 0.076$, $F_{1\to4} = 0.198$, $F_{1\to6} = 0.39$, $F_{2\to3} = 0.088$, $F_{2\to4} = 0.198$, $F_{2\to6} = 0.258$, $F_{3\to4} = 0.198$, $F_{3\to6} = 0.258$, $F_{4\to5} = 0.207$, $F_{4\to6} = 0.265$.

Applying Equation 4.6 for all walls of the total refrigerator the radiative heat transfer for the walls are determined and tabulated in Table 4.10. The results in Table 4.10 are very close to the radiative heat transfer rate results obtained from numerical analysis.

Table 4.10. Radiative heat transfer rates (in Watts) calculated analytically for the walls of the total refrigerator

Front Wall	1.90
Rear Wall	0.23
Top Wall	1.28
Bottom Wall	0.02
Left Side Wall	2.27
Right Side Wall	2.27
Evaporator	-7.96

4.5.4. Comparison of Temperature Values Obtained from the Total Refrigerator Analysis and the Experimental Work

In this section, temperature distribution obtained for the reference lines on symmetry plane (Figure 4.75) in numerical analysis of total refrigerator is compared with the temperature values measured in the experimental study. The vertical reference lines presented in Figure 4.82 are coinciding with the wires of the grill on which the thermocouples are located in experimental work. The exact coordinates of the thermocouples were explained in Figure 3.7.

In Figure 4.83, experimental temperature values measured on three vertical lines away from the evaporator on the symmetry plane with the numerical simulations performed are compared. First observation is that the temperature distributions obtained from numerical analyses performed with or without radiation model give very close results on the same vertical lines.
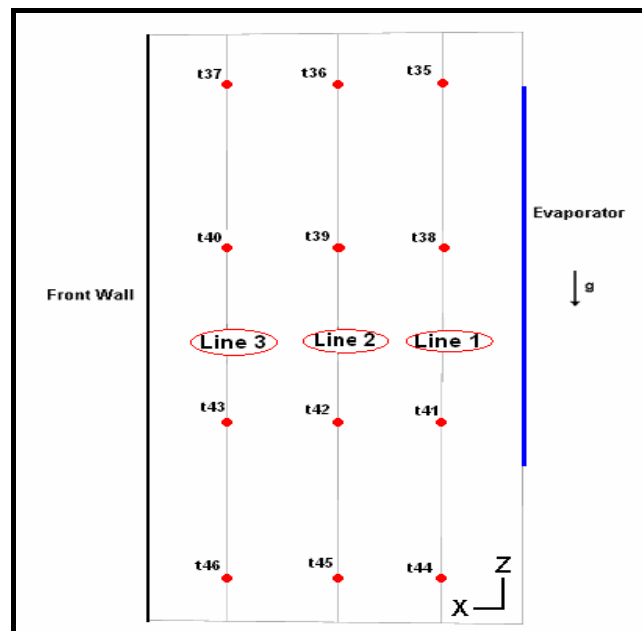
Figure 4.82. Configuration of reference lines on the symmetry plane for the total refrigerator analysis
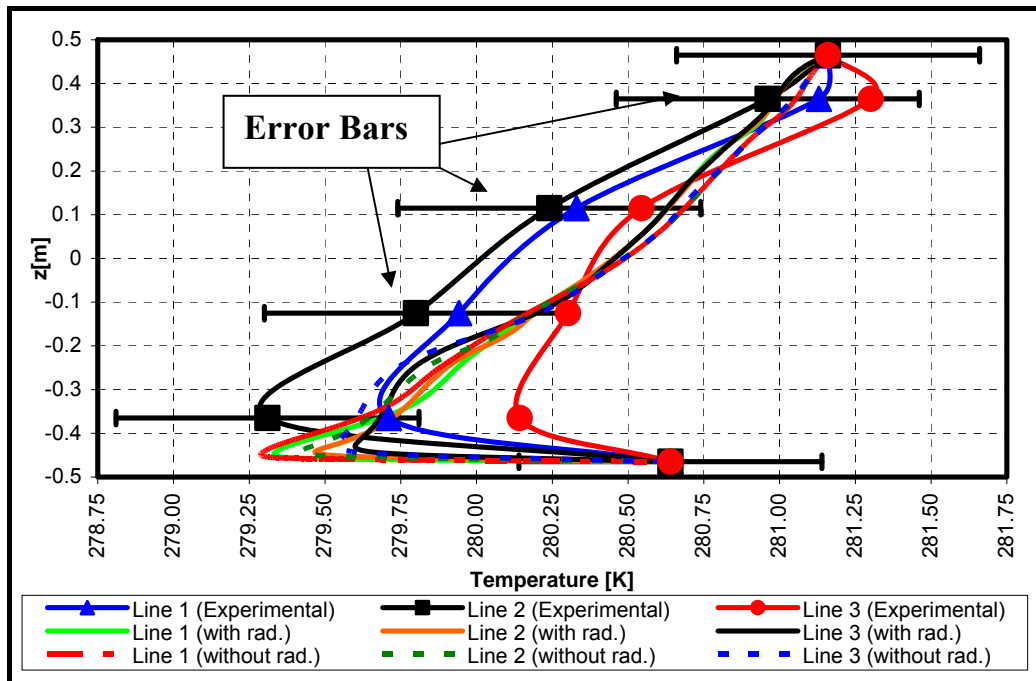
Figure 4.83. Comparison of temperature values on the symmetry plane obtained from the numerical analysis and the experimental work

However; experimental temperature values do not exactly overlap the numerical ones especially at the lower portion but the discrepancy is better with respect to the single compartment case. The reason for this is the distance of the thermocouples from the bottom wall. Thermocouples 44, 45 and 46 in Figure 4.82 are 10 cm away from the bottom wall of the refrigerator but the corresponding thermocouples 43, 44 and 45 in Figure 4.51 were 2 cm away from the bottom wall of the compartment. On the contrary, experimental and numerical temperature values are in a good agreement on the upper half of the symmetry plane. Finally it can be pointed out that numerically obtained temperature results still remain in the uncertainty range (error bar range is 1 $^{\circ}$C in Figure 4.83) of the experimental temperature values.

CHAPTER 5

SUMMARY AND CONCLUSION

In this study, numerical simulation of natural convection problem in an empty cavity using package program Fluent 6.3.26 is investigated and comprehensive heat transfer analyses are also performed using the results of numerical studies. While executing this task, experimental study on a real refrigerator cabinet and one of its compartments for the determination of temperature on the walls and symmetry plane of the volume, evaluation of radiation effect by comparing the numerical model with a similar one in literature and verification of the radiation heat transfer results are also covered.

Since free convection in refrigerator applications is evaluated as a 3-D, mostly turbulent, transient and coupled non-linear flow problem, detailed analyses are necessary to solve momentum, energy and continuity equations and to realize the objective.

First a preliminary study was done to determine the parameters affecting the natural convection analyses in cavities and a resultant numerical CFD model based on finite volume method was settled. Influences of mesh size or number of cells in the domain, temperature difference between vertical walls and initial z velocity definition were searched to form the final preliminary model mentioned above.

Forming the first stage of the present work, preliminary numerical analysis was performed to simulate the fluid flow and temperature distributions inside the

domain. It was also aimed to present the general characteristics of natural convection problem with specified boundary conditions and dimensions of the cavity. In the preliminary numerical analysis, radiation was not considered.

Next; evaluation of radiation effect by comparing the radiation included numerical model in the present study and the one in literature was done. The analyses in this stage were performed for the whole refrigerator cabinet when it was empty.

Then, an experimental study was made in Arçelik, Çayırova factory research department to define the constant temperature boundary conditions for the following numerical analyses of a single compartment and total refrigerator.

Creating the domains using the real dimensions of the single compartment or total refrigerator cabinet in the experimental work, two additional numerical analyses were performed in order to apply the natural convection problem to the refrigerator. Radiation model evaluated before was implemented on the numerical models for the two cases above and analyses were repeated for both including and omitting the radiation.

After determination of temperature and velocity distributions inside the domains, heat transfer analyses were performed for each numerical model to calculate time dependent heat fluxes and effective heat transfer coefficients, to clarify variation of these parameters with spatial coordinates at specified locations and to obtain the values of total, radiative and convective heat transfer rates from the surfaces at steady state time. The total refrigerator and compartment volumes are empty.

The k-ε and discrete ordinate (DO) models were used for turbulence and radiation respectively. Moreover, PISO pressure-velocity coupling algorithm with PRESTO discretization method was applied. Information about preliminary

numerical analysis, experimental work and final numerical studies consisting of single compartment and total refrigerator analyses is given in Chapter 3 extensively.

The results of all analyses have been discussed in Chapter 4 in detail, but here some highlights will be summarized.

Preliminary analysis clearly describes the natural convection phenomena inside a cavity heated from front and cooled from rear walls. This condition is parallel to the real application of refrigerator cabinet or compartment. The steady state time for the analysis is about 800 seconds. Maximum values of the temperature and velocity for the air inside the cavity are 279.85 K and 0.081 m/s respectively. Boundary layers develop at the rear, bottom and front walls indicating the flow direction of air and stagnant regions inside the domain.

Steady state heat fluxes for the walls are achieved after t=600 seconds and their magnitudes are in the range of 0 to 17 W/m^2 with the maximum heat flux value for the rear wall. Since radiation is not considered in preliminary numerical analysis, heat fluxes mentioned above are convective.

Convective heat transfer coefficients are calculated and the reference temperature is taken as the geometric center temperature of the domain in these calculations. The greatest heat transfer coefficient value is obtained at the bottom wall as 12 W/m^{2}K because the difference between the temperatures of the bottom wall and the reference point is smaller than the other walls.

Additionally it is observed that heat flux and convective heat transfer coefficient magnitudes are not changing from symmetry plane to the sides of the cavity for front and rear walls, and due to the formation of boundary layers at these walls, convective heat transfer coefficient values are greater at the upper region than the lower part of the rear wall in contrast to the front wall.

Steady state heat transfer rates from the walls at the time instant of 3600 seconds are varying between -2 to 1.3 Watts.

Next item is the evaluation of radiation effect and for this; a comparison study performed for a whole refrigerator is performed with selected turbulence model (k-ε), emissivity values for the walls (0.9) and PISO algorithm in the present work. The results show a good agreement and it is observed that the temperature distribution on a line selected away from the evaporator at the symmetry plane is harmonious with the experimental data when discrete ordinate (DO) radiation model is applied.

In this comparative work, for the time instant of 6000 seconds, radiative heat transfer rate values from or to the rear and front walls are found to be the nearly 72 % of the total heat transfer rates on the corresponding walls. That is why, a necessity for further detailed numerical analyses including radiation model arises.

Before further numerical analyses, an experimental study is done for the determination of wall and symmetry plane temperatures of a real refrigerator cabinet and a single compartment at Arçelik Çayırova factory research department. Measurements are made using thermocouples as explained in the preceding chapters and arithmetic average of the temperature values at the locations of the thermocouples belonging to a wall are evaluated as the corresponding constant temperature wall boundary condition of the numerical analyses performed for the single compartment cavity and total refrigerator cabinet.

It can be concluded from two-hour temperature distribution presented in Figure 3.7.a for the side wall of the compartment that temperature values measured by thermocouples t12, t15 and t18 located on the same vertical line which is nearest to the front wall (door) of the refrigerator are higher than the others.

Temperature values measured by the thermocouples, t10, t13 and t16 are lower than the first three. These thermocouples are also positioned on a vertical line close to the relatively hot rear side walls. On the other hand; t11, t14 and t17 which are located on the vertical line at the middle of the side wall measure the lowest temperatures. Fluctuation in the temperature measurements decreases from back to front because of the vanishing effect of the compressor.

On the side wall of the total refrigerator cabinet shown in Figure 3.7.b, highest temperature values are measured by thermocouples, t11, t6 and t8 and t7 which are in the hot air zone very close to the top wall. Slightly smaller temperature values are measured by the thermocouples, t12 and t15 which are affected from hot rear wall. Relatively cold air results in a small decrease in the temperature values of t14, t17 and t16. Temperatures of the points of thermocouples, t13 and t10 are lower than the others but still higher than the temperature value indicated by t9. The lowest temperature is measured by t9 because it is very close to the evaporator.

The insulation characteristics of the static refrigerator used in experiments is poor. This can be understood from the on and off times of the compressor. If related graphs are examined, compressor seems to run about 15 minutes and then it stops nearly 15 minutes again. If the insulation were better, off time of the compressor would be longer.

The further numerical analyses of single compartment and total refrigerator are done. Domains of these two analyses have the same dimensions of the compartment and the refrigerator cabinet in experiments.

Temperature and velocity profiles obtained at some instances for single compartment analysis reveal that radiation model does not affect the temperature and velocity profiles inside the domain since the medium is non-participating and radiation heat exchange is between the walls with constant

temperatures. But analysis including radiation model reaches to steady state faster than the analysis performed without radiation.

The maximum temperature and velocity values are 282.82 K and 0.124 m/s in the domain for single compartment analysis. Velocity vectors plotted at steady state indicate a downward air flow on evaporator which is then followed by a flow on bottom wall from back to front. In most of the regions, very small velocity magnitudes are obtained.

Radiation included analysis gives much higher heat flux and effective heat transfer coefficient values especially for evaporator with respect to the analysis where radiation model is omitted. This is an expected situation because radiation heat transfer to the evaporator is very dominant due to the temperature difference between the evaporator and other walls.

Similar to the case in preliminary numerical analysis, the heat flux and effective heat transfer coefficient values are not changing with y coordinate at evaporator, but when the front wall is considered these parameters are sensitive to the location of reference lines. Closer the line to the symmetry plane of the problem greater the total heat fluxes and corresponding effective heat transfer coefficients.

When the total heat transfer rates from the walls and to the evaporator are calculated at steady state (t=3600 s) it is explored that more than half of the total heat transfer rate is due to radiation exchange between the walls.

This surprising result leads the researcher to evaluate the radiative heat transfer rate on the evaporator by view factor algebra. After determination of view factors of surfaces it is found that radiative heat transfer rate calculated numerically is nearly the same with the algebraically determined one. Results

imply that discrete ordinate method (DO) for radiation model is a good selection.

Next, symmetry plane temperature distributions obtained from numerical work are compared with the experimental study. Experimental temperature values are deviating from numerical ones at the lower region of the symmetry plane. This may be due to the frame used on the symmetry plane of the compartment in experiments. The frame as a solid conducting body might result in a disturbance of the boundary layer on the bottom wall and axial conduction on the frame from upper hot region to the cold bottom region may occur.

Single compartment numerical analysis is repeated for a larger scale total refrigerator cabinet. Temperature and velocity profiles are simulated and presented at the midplanes once more. Stratification is clearly seen from temperature profiles. Although the maximum temperature and velocity values were 282.82 K and 0.124 m/s in the domain for single compartment analysis, these are 281.25 K and 0.167 m/s respectively for total refrigerator analysis. The significant difference between velocity magnitudes comes from the position of the compartment in the experimental study. The compartment in experimentation was nearly at the middle of the refrigerator cabinet so high velocity region at the bottom edge of the evaporator and a region below evaporator are not included by the single compartment analysis.

Same heat transfer analyses are also performed for total refrigerator. Effective heat transfer coefficient value at steady state is about 8 W/m²K for radiation included analysis whereas this value was about 10 W/m²K for single compartment numerical analysis with radiation.

General trends in time dependent total heat flux, effective heat transfer coefficient and steady state characteristics of these parameters are the same with single compartment analysis. The only difference is observed in the steady state

heat flux values versus z graph on the reference lines at the front wall. The fluctuations in Figures 4.78 and 4.79 may be due to the dominant radiation exchange between surfaces. Total and radiative heat flux values are starting to increase at a level corresponds to the bottom edge of the evaporator opposing to the front wall, and then after a peak these quantities decrease to constant values at a position whose projection is nearly coinciding with the upper edge of the evaporator.

Although 55 % of total heat transfer rate was radiative for the evaporator of the single compartment analysis, this ratio increases up to 66 % for the evaporator in the total refrigerator study.

Comparison of the experimental and numerical temperature distributions are also done for total refrigerator. Experimental values are not overlapping the numerical results but differences between the results are smaller with respect to single compartment analysis. This may be due to the location of the thermocouples at the bottom level. They are 10 cm above the bottom wall and are not affected from the solid frame used. Finally it should be noted that numerically obtained temperature results still remain in the uncertainty range of the experimental values.

As the future work of this PhD study some items can be investigated. The first point is putting the separators of the compartments and then analyzing the total refrigerator cabinet with shelves using the same boundary conditions and domain of the total refrigerator numerical analysis performed in this PhD work. Assuming the compartments as small cavities, the temperature and velocity profiles inside each cavity can be examined and compared. While performing analysis, conduction inside the separators (glass etc.) of the compartments may also be included.

Next, inserting fans or blowers at specified locations, the total refrigerator analysis may be repeated and effect of forced convection on the whole domain can be visualized.

CFD analyses mentioned above should investigate the significance of radiation and compare with the results of the presented studies.

The other point is the conjugate heat transfer analysis inside the refrigerator. Putting a heat source at different locations inside which stands for a relatively hot food, the analyses can be done [10, 17-20, 29, 30, 36, 37]. Since the problem will be the application of loaded refrigerator, the heat transfer analyses should be performed and obtained results of heat transfer rate or heat transfer coefficient must be compared with the corresponding studies in this report.

As the extension of the experimental work done, temperature measurements of air on the symmetry plane and at other locations can be done using very thin wires such as fishing line instead of frame used [36-38]. Additionally, the thermocouples can be located in a dense fashion close to the boundaries since the flow is dominant on the surfaces. At the end of such an experiment one can have a chance to compare the numerical and experimental air temperature values at different locations from the symmetry plane inside the volume.

The second development in experimentation will be the measurement of air velocity inside. Since inserting a probe at the flow zones will easily disturb the boundary layer formation and result in an error, techniques such as PIV (particle image velocimetry) may be used to visualize the velocity distribution of the domain [38, 39, 78, 79].

Total refrigerator analysis may be repeated by considering the inside volume, walls of the refrigerator and the surroundings as a whole as in the literature study [37]. Instead of constant temperature wall boundary condition overall heat

transfer coefficient between the ambient room air and interior of the wall and constant room air temperature are defined and given as the convection thermal boundary condition with the free stream temperature as the external air temperature in Fluent. The analysis will then be more realistic because the room with constant temperature is also included and conservation of energy will determine the wall temperatures of the refrigerator. An experimental study of this numerical case may also be carried out in a temperature-controlled room in laboratory.

A future work may be the optimization procedure of the refrigerator keeping the outer dimensions constant in the light of the above offered studies as well as the numerical and experimental analyses performed in this PhD work.

REFERENCES

[1]   S. Ostrach, W.J. Austin, "Natural convection in enclosures", Journal of Heat Transfer, Vol. 110, (1988).

[2]   I. Catton, "Natural convection in enclosures", Journal of Heat Transfer, Vol. 6, (1978).

[3]   J. Patterson, J. Imberger, "Unsteady natural convection in rectangular cavity", Journal of Fluid Mechanics, Vol. 100, part 1, (1980).

[4]   M. Corcione, "Effects of the thermal boundary conditions at the sidewalls upon natural convection in rectangular enclosures heated from below and cooled from above", Int. Journal of Thermal Sciences, Vol. 42, (2003).

[5]   G. de Vahl Davis, "Natural convection of air in a square cavity: A benchmark numerical solution", Int. Journal of Numerical Meth. Fluids, Vol. 3, (1983).

[6]   N.C. Markatos, K.A. Pericleous, "Laminar and turbulent natural convection in an enclosed cavity", Int. Journal of Heat Mass Transfer, Vol. 27, (1984).

[7]   G. de Vahl Davis, "Natural convection in a square cavity: A comparison exercise", Int. Journal for Numerical Meth. in Fluids, Vol. 3, (1983).

[8]   J.M. Hyun, J.W. Lee, "Numerical solution for transient natural convection in a square cavity with different sidewall temperatures", Int. Journal Heat and Fluid Flow, Vol. 10, (1989).

[9]   Y.S. Tian, T.G. Karayiannis, "Low turbulence natural convection in an air filled square cavity Part I: the thermal and fluid flow fields", Int. Journal of Heat and Mass Transfer, Vol. 43, (2000).

[10]   F. Ampofo, T.G. Karayiannis, "Experimental benchmark data for turbulent natural convection in an air filled square cavity", Int. Journal of Heat and Mass Transfer, Vol. 46, (2003).

[11]   F. Ampofo, "Turbulent natural convection in an air filled partitioned square cavity", Int. Journal of Heat and Fluid Flow, Vol. 25, (2004).

[12]   F. Ampofo, "Turbulent natural convection in a non-partitioned or partitioned cavity with differentially heated vertical and conducting horizontal walls", Exp. Thermal and Fluid Science, Vol. 29, (2005).

[13]   F. Penot, A. N'Dame, "Successive bifurcations of natural convection in a vertical enclosure heated from the side", Heat Transfer, 3rd UK N. Conf., Vol. 1, (1992).

[14]   S.P. Das, S. Chakraborty, P. Dutta, "Natural convection in a two-dimensional enclosure heated symmetrically from both sides", Int. Comm. Heat Mass Transfer, Vol. 29, (2002).

[15]   M.W. Nansteel, R. Greif, "An investigation of natural convection in enclosures with two and three dimensional partitions", Int. Journal of Heat and Mass Transfer, Vol. 27, (1984).

[16]   N. Wansophark, P. Dechaumphai, "Combined adaptive meshing technique and segregated finite element algorithm for analysis of free and forced convection heat transfer", Finite Element in Analysis and Design, Vol. 40, (2004).

[17]   Q-H. Deng, G-F. Tang, "Numerical visualization of mass and heat transport for conjugate natural convection/heat conduction by streamline and heatline", Int. Journal of Heat and Mass Transfer, Vol. 45, (2002).

[18]   S-F. Dong, Y-T. Li, "Conjugate of natural convection and conduction in a complicated enclosure", Int. Journal of Heat and Mass Transfer, Vol. 47, (2004).

[19]   A. Liaqat, A.C. Baytas, "Conjugate natural convection in a square enclosure containing volumetric sources", Int. Journal of Heat and Mass Transfer, Vol. 44, (2001).

[20]   J.R. Lee, M.Y. Ha, "Numerical simulation of natural convection in a horizontal enclosure with heat-generating conducting body", Int. Journal of Heat and Mass Transfer, Vol. 49, (2006).

[21]   S. Wakashima, T.S. Saitoh, "Benchmark solutions for natural convection in a cubic cavity using the high order time-space method", Int. Journal of Heat and Mass Transfer, Vol. 47, (2004).

[22]   R.J.A. Janssen, R.A.W.M. Henkes, C.J. Hoogendoorn, "Transition to time-periodicity of a natural-convection flow in a 3D differentially heated cavity", Int. Journal Heat Mass Transfer, Vol. 36, (1993).

[23]   T. Fusegi, J.M. Hyun, K. Kuwahara, B. Farouk, "A numerical study of three-dimensional natural convection in a differentially heated cubical enclosure", Int. Journal Heat Mass Transfer, Vol. 34, (1991).

[24]   W. H. Leong, K. G. T. Hollands, A. P. Brunger, "On a physically-realizable benchmark problem in internal natural convection", Int. J. Heat Mass Transfer, Vol. 41, (1998).

[25]   W. H. Leong, K. G. T. Hollands, A. P. Brunger, "Experimental Nusselt numbers for a cubical-cavity benchmark problem in natural convection", Int. J. Heat Mass Transfer, Vol. 42, (1999).

[26]   M.A.H. Mamun, W.H. Leong, K.G.T. Hollands, D.A. Johnson, "Cubical-cavity natural-convection benchmark experiments: an extension", Int. Journal of Heat and Mass Transfer, Vol. 46, (2003).

[27]   D.W. Pepper, K.G.T. Hollands, "Summary of benchmark numerical studies for 3-D natural convection in an air-filled enclosure", Numerical Heat Transfer, Part A, Vol. 42, (2002).

[28]   S.S. Hsieh, S.S. Yang, "Transient three-dimensional natural convection in a rectangular enclosure", Int. J. Heat Mass Transfer, Vol. 39, (1996).

[29]   M.Y. Ha, M.J. Jung, "A numerical study on three-dimensional conjugate heat transfer of natural convection and conduction in a differentially heated cubic enclosure with a heat-generating cubic conducting body", Int. Journal of Heat and Mass Transfer, Vol. 43, (2000).

[30]   S.B. Amara, O. Laguerre, D. Flick, "Experimental study convective heat transfer dooring cooling with low air velocity in a stack of objects", Int. Journal of Thermal Sciences, Vol. 43, (2004).

[31] G. Ding, C. Zhang, Z. Lu, "Dynamic simulation of natural convection bypass two-circuit cycle refrigerator-freezer and its application Part I: component models", Applied Thermal Engineering, Vol. 24, (2004).

[32] G. Ding, C. Zhang, Z. Lu, "Dynamic simulation of natural convection bypass two-circuit cycle refrigerator-freezer and its application Part II: system simulation and application", Applied Thermal Engineering, Vol. 24, (2004).

[33] J. Salat, S. Xin, P Joubert, A. Sergent, F. Penot, P. Le Quere, "Experimental and numerical investigation of turbulent natural convection in a large air filled cavity", Int. Journal of Heat and Fluid Flow, Vol. 25, (2004).

[34] G. Cortella, M. Manzan, G. Comini, "CFD simulation of refrigerated display cabinets", Int. Journal of Refrigeration, Vol. 24, (2001).

[35] O. Laguerre, D. Flick, "Heat transfer by natural convection in domestic refrigerators", Journal of Food Engineering, Vol. 62, (2004).

[36] O. Laguerrea, S. Ben Amara, D. Flick, "Experimental study of heat transfer by natural convection in a closed cavity: application in domestic refrigerator", Journal of Food Engineering, Vol. 70, (2005).

[37] O. Laguerre, S. Ben Amara, J. Moureh, D. Flick, "Numerical simulation of air flow and heat transfer in domestic refrigerators", Journal of Food Engineering, Vol. 81, (2007).

[38] O. Laguerre, S.B. Amara, M.C.C. Mojtabi, B. Lartigue, D. Flick, "Experimental study of air flow by natural convection in a closed cavity:

Application in domestic refrigerator", Journal of Food Engineering, Vol. 85, (2008).

[39]   S.B. Amara, O. Laguerre, M.C.C. Mojtabi, B. Lartigue, D. Flick, "PIV measurement of the flow field in a domestic refrigerator model: Comparison with 3D simuations", Int. Journal of Refrigeration, Vol. 31, (2008).

[40]   Fluent 6.2 User's Guide, Fluent Inc.

[41]   Y. Jaluria, Natural Convection, Pergamon Press, (1980).

[42]   A. Bejan, Convection Heat Transfer, John Wiley & Sons, (1995).

[43]   L.C. Burmeister, Convective Heat Transfer, John Wiley & Sons, (1993).

[44]   M. Pons, "Transition from single-to multi-cell natural convection of air in cavities with an aspect ratio of 20: A thermodynamic approach", Int. J. of Thermodynamics, Vol. 11, (2008).

[45]   M. Pons, P. Le Quere, "An example of entropy balance in natural convection, Part 1: the *usual* Boussinesq equations", C.R. Mecanique, Vol. 333, (2005).

[46]   M. Pons, P. Le Quere, "An example of entropy balance in natural convection, Part 1: the *thermodynamic* Boussinesq equations", C.R. Mecanique, Vol. 333, (2005).

[47]   M. Pons, P. Le Quere, "Modeling natural convection with the work of pressure-forces: a thermodynamic necessity", Int. Journal of Numerical Methods for Heat & Fluid Flow, Vol. 17, (2007).

[48]   H. Tennekes, J.L. Lumley, A First Course in Turbulence, MIT Press, (1972).

[49]   J.O. Hinze, Turbulence, McGraw-Hill, (1975).

[50]   S.B. Pope, Turbulent Flows, Cambridge University Press, (2000).

[51]   H. Schlichting, Boundary-Layer Theory, McGraw-Hill, (1960).

[52]   B.E. Launder, D.B. Spalding, Lectures in Mathematical Models of Turbulence, McGraw-Hill, (1972).

[53]   M. Akiyama, Q.P. Chong, "Numerical analysis of natural convection with surface radiation in a square enclosure", Numerical Heat Transfer, Part A, Vol. 31, (1997).

[54]   W.A. Fiveland, "Discrete-ordinates solutions of the radiative transport equation for rectangular enclosures", Journal of Heat Transfer, Vol. 106, (1984).

[55]   G. Colomer, M. Costa, R. Consul, A. Oliva, "Three-dimensional numerical simulation of convection and radiation in a differentially heated cavity using the discrete ordinates method", Int. Journal of Heat and Mass Transfer, Vol. 47, (2004).

[56]   A. Sanchez, T.F. Smith, "Surface Radiation Exchange for two-dimensional rectangular enclosures using the discrete-ordinates method", Journal of Heat Transfer, Vol. 114, (1992).

[57]   M. Mengüç, R. Viskanta, "Radiative transfer in three-dimensional rectangular enclosures containing inhomogeneous, anisotropically scattering media", J. Quant. Spectrosc. Radiat. Transfer, Vol. 33, (1985).

[58]   N. Selçuk, N. Kayakol, "Evaluation of discrete ordinates method for radiative transfer in rectangular furnaces", Int. J. Heat Mass Transfer, Vol. 40, (1997).

[59]   G.L. Ding, H-T Qiao, Z-L Lu, "Ways to improve thermal uniformity inside a refrigerator", Applied Thermal Engineering, Vol. 24, (2004).

[60]   O. Laguerre, E. Derens, B. Palagos, "Study of domestic refrigerator temperature and analysis of factors affecting temperature: a French survey", Int. Journal of Refrigeration, Vol. 25, (2002).

[61]   H.K. Versteeg, W. Malalasekera, An Introduction to Computational Fluid Dynamics The Finite Volume Method, John Wiley & Sons, (1995).

[62]   R.I. Issa, "Solution of implicitly discretized fluid flow equations by operator splitting", Journal of Computational Physics, Vol. 62, (1986).

[63]   S.V. Patankar, Numerical Heat Transfer and Fluid Flow, McGraw-Hill, (1980).

[64]   K. J. Hsieh, F. S. Lien, "Numerical modeling of buoyancy-driven turbulent flows in enclosures", Int. Journal of Heat and Fluid Flow, Vol. 25, (2004).

[64]   Agilent 34970A Data Acquisition/Switch Unit User's Guide, Agilent Technologies Inc., (2003).

[66]   Omega Engineering, Inc., www.omega.com/guides/thermocouples.html, 08/01/2009

[67]   J.P. Holman, Experimental Methods for Engineers, McGraw-Hill, (2001).

[68]   B.E. Launder, D.B. Spalding, "The numerical computations of turbulent flows", Computer Methods in Applied Mechanics and Engineering, Vol. 3, (1974).

[69]   C. Jayatilleke, "The influence of prandtl number and surface roughness on the resistance of the laminar sublayer to momentum and heat transfer", Prog. Heat Mass Transfer, Vol. 1, (1969).

[70]   M. Omri, N. Galanis, "Numerical analysis of turbulent buoyant flows in enclosures: Influence of grid and boundary conditions", Int. Journal of Thermal Sciences, Vol. 46, (2007).

[71]   M.F. Modest, Radiative Heat Transfer, McGraw-Hill, (1993).

[72]   C.J.L. Hermes, M.E. Marques, "A CFD model for buoyancy driven flow inside refrigerated cabinets and freezers", Purdue Conference Proceedings, Refrigeration Papers, (2002).

[73]   J.R. Ehlert, T.F. Smith, "View factors for perpendicular and parallel, rectangular plates", J. Thermophys. Heat Trans., Vol. 7, (1993).

[74]   U. Gross, K. Spindler, E. Hahne, "Shape factor equations for radiation heat transfer between plane rectangular surfaces of arbitrary position and size with rectangular boundaries", Lett. Heat Mass Transfer, Vol. 8, (1981).

[75] W. Boeke, L. Wall, "Radiative exchange factors in rectangular spaces for the determination of mean radiant temperatures", Build. Serv. Engrg., Vol. 43, (1976).

[76] I.R. Chekhovskii, V.V. Sirotkin, V. Yu, V.A. Chebanov, "Determination of radiative view factors for rectangles of different sizes", High Temp., Vol. 17, (1979).

[77] C.J. Hsu, "Shape factor equations for radiant heat transfer between two arbitrary sizes of rectangular planes", Can. J. Chem. Eng., Vol. 45, (1967).

[78] V.T. Lacerda, C. Melo, J.R. Barbosa, P.O.O. Duarte, "Measurements of the air flow field in the freezer compartment of a top-mount no-frost refrigerator: the effect of temperature", Int. Journal of Refrigeration, Vol. 28, (2005).

[79] I.S. Lee, S.J. Baek, M.K. Chung, D. Rhee, "A study of air flow characteristics in the refrigerator using PIV and computational simulation", J. of Flow Visualisation and Image Proces., Vol. 46, (1999).

APPENDIX A

SEGREGATED PRESSURE BASED SOLVER
ALGORITHM OF FLUENT PROGRAM
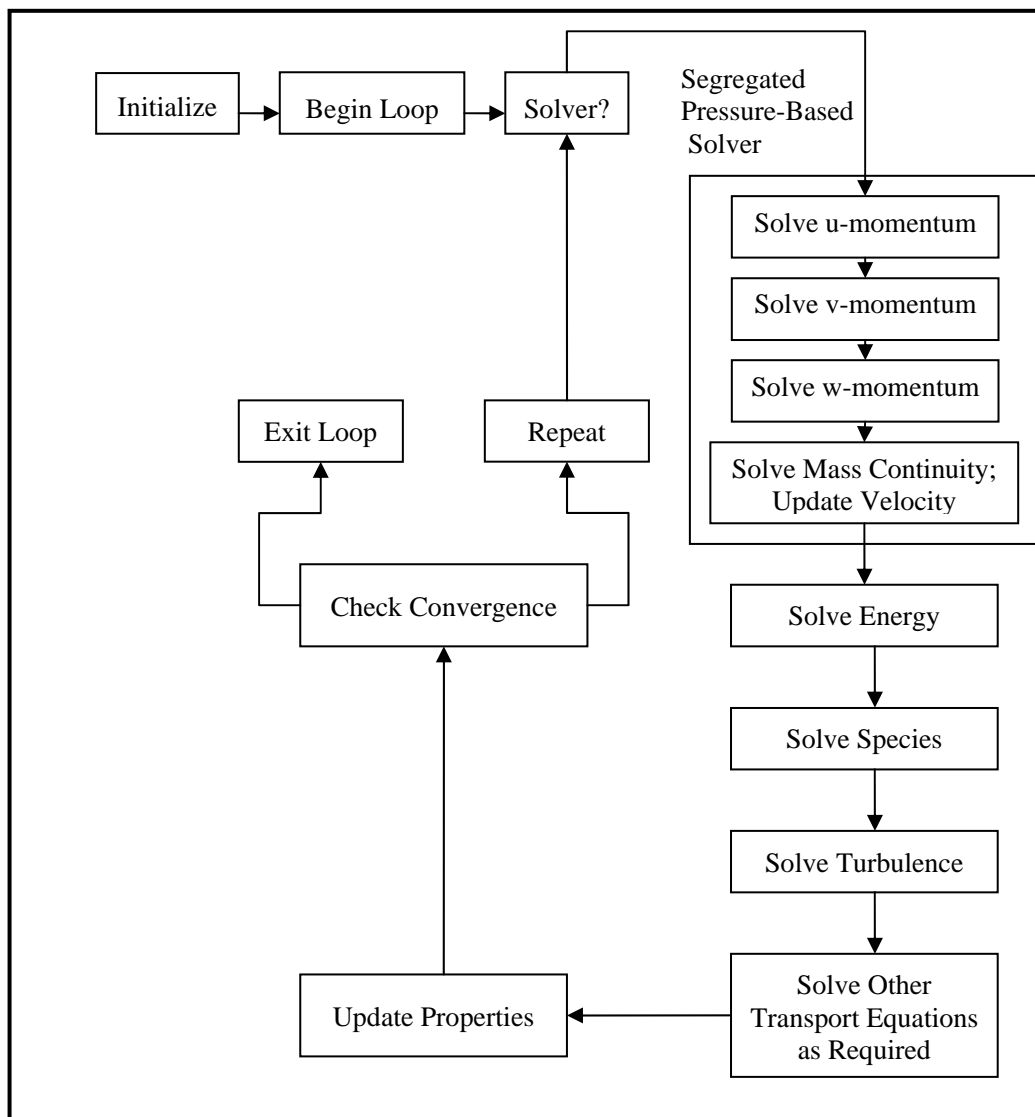
Figure A.1. Segregated pressure based solver algorithm of fluent program

APPENDIX B

SCREENSHOTS OF THE PANELS OF FLUENT PROGRAM SELECTED IN NUMERICAL ANALYSES
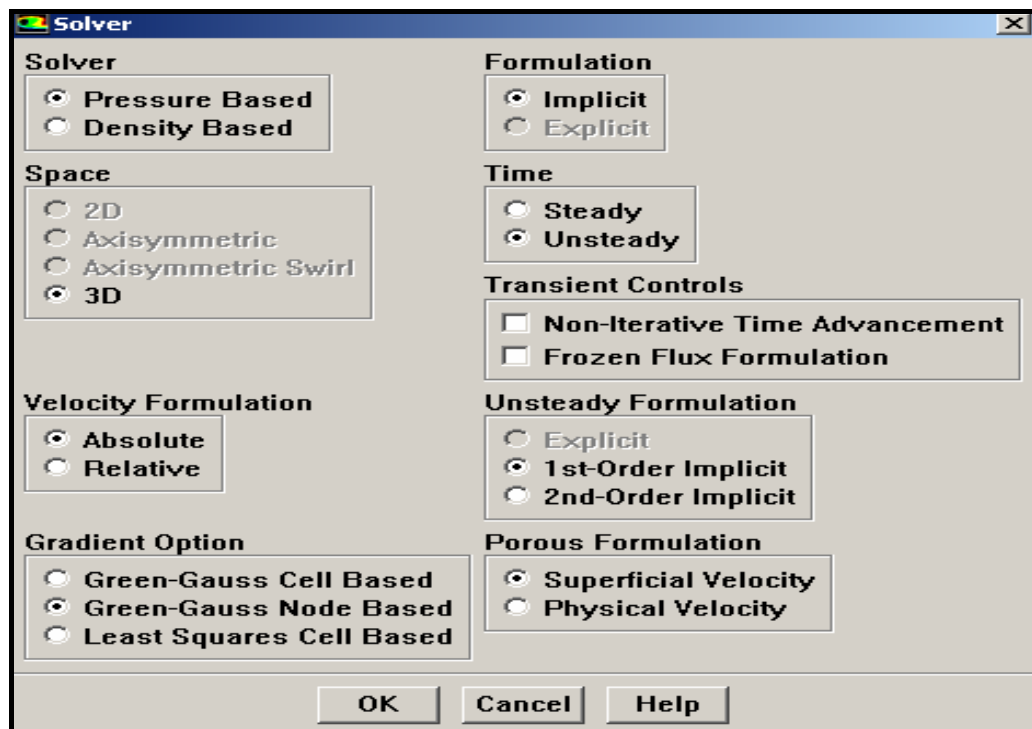
Figure B.1. Solver panel of fluent program
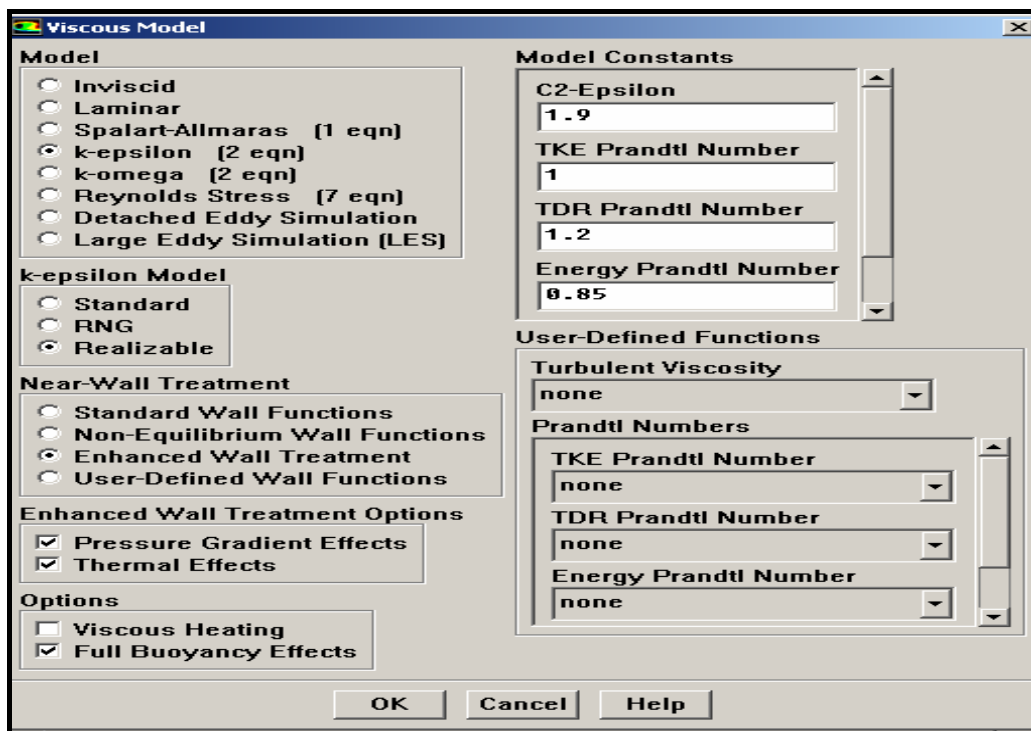
Figure B.2. Viscous model panel of fluent program
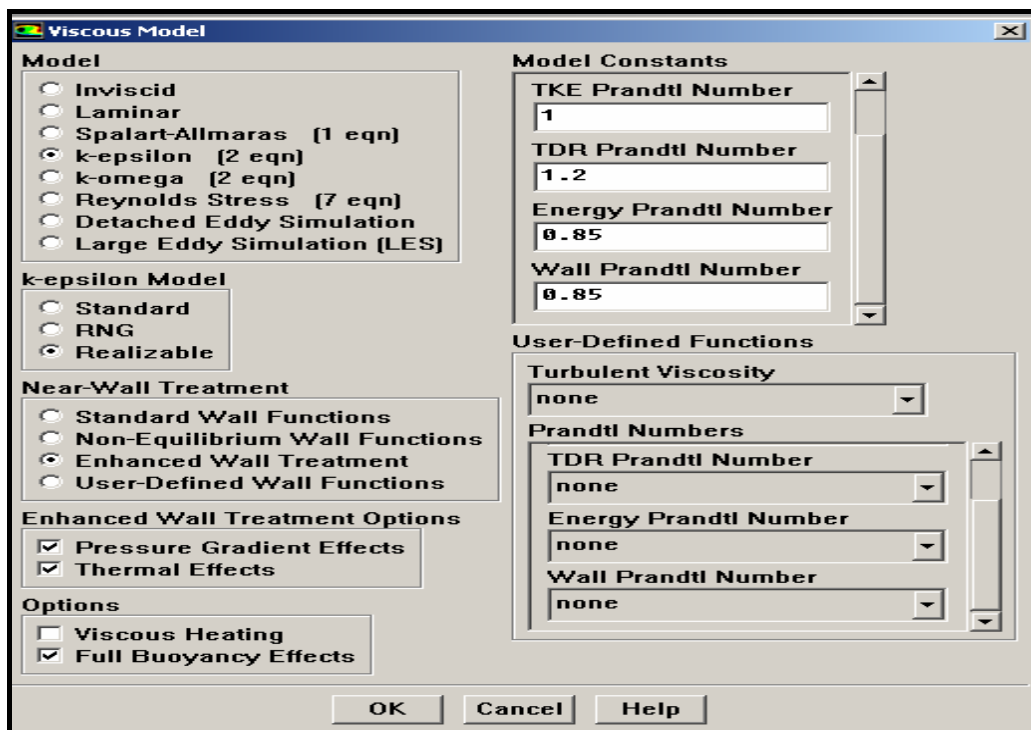
Figure B.2. Viscous model panel of fluent program
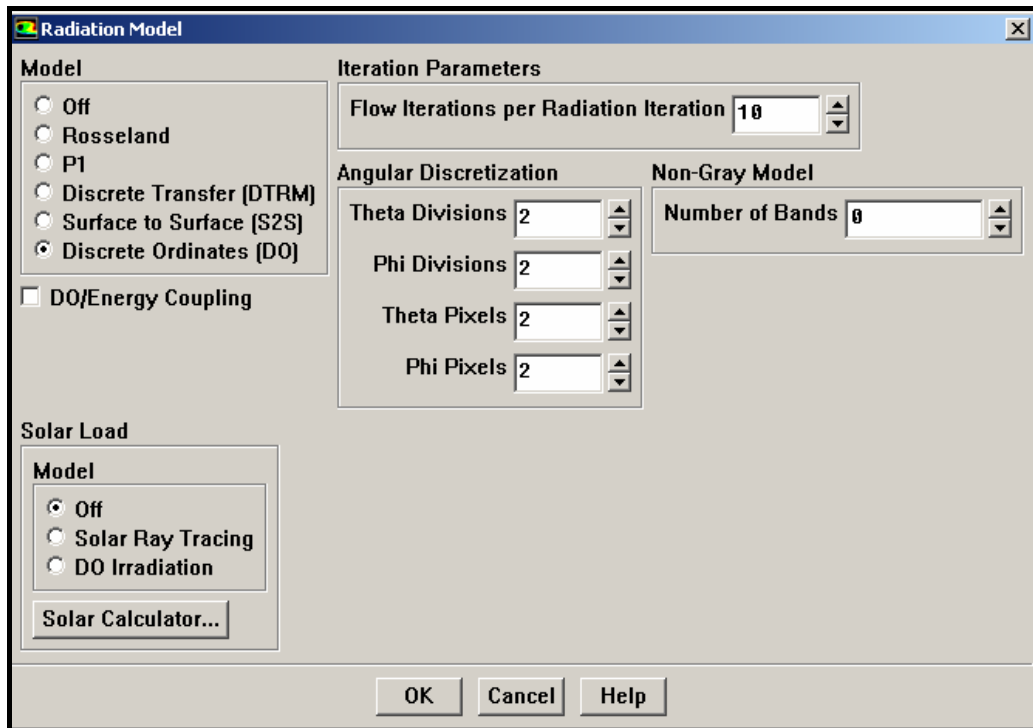
Figure B.3. Radiation model panel of fluent program
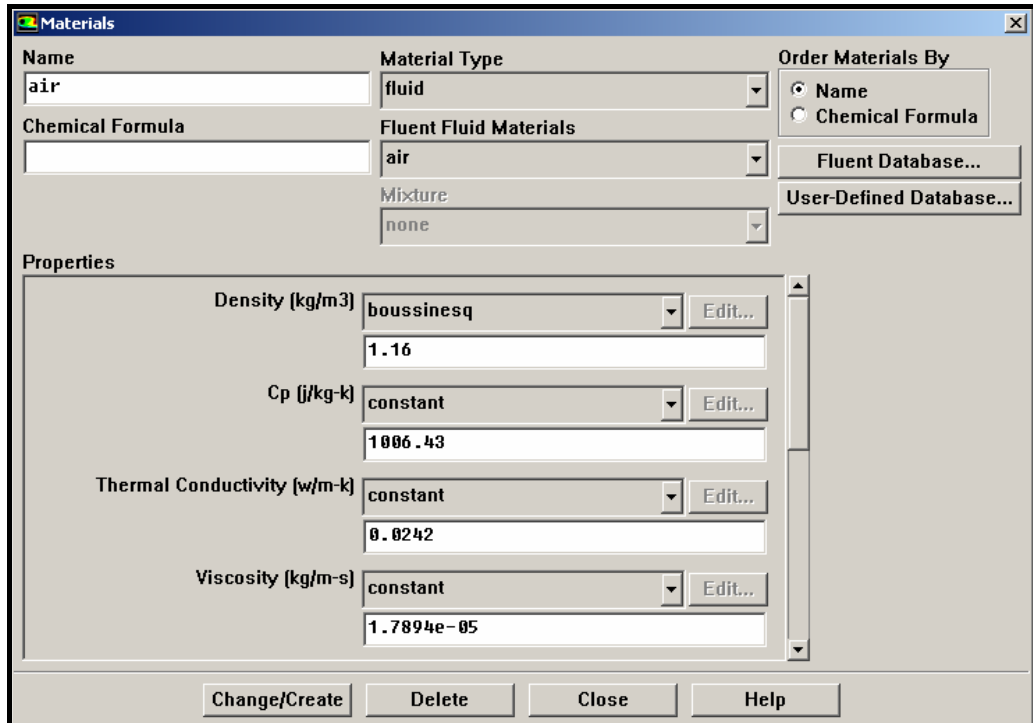
Figure B.4. Materials panel of fluent program
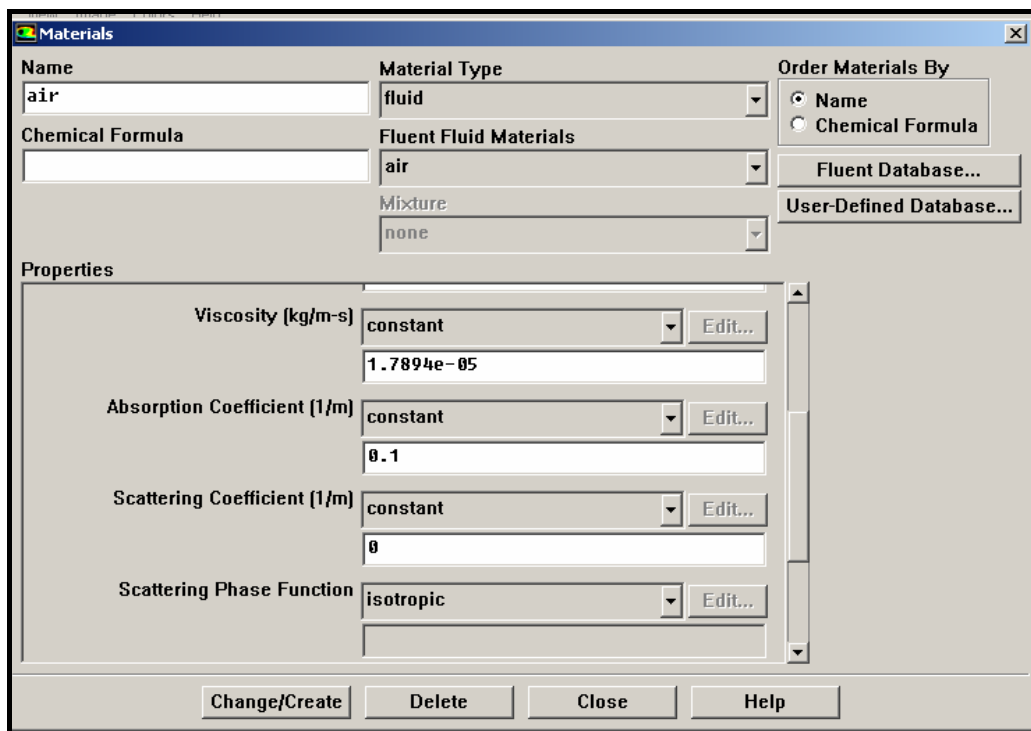
Figure B.4. *Continued,* Materials panel of fluent program
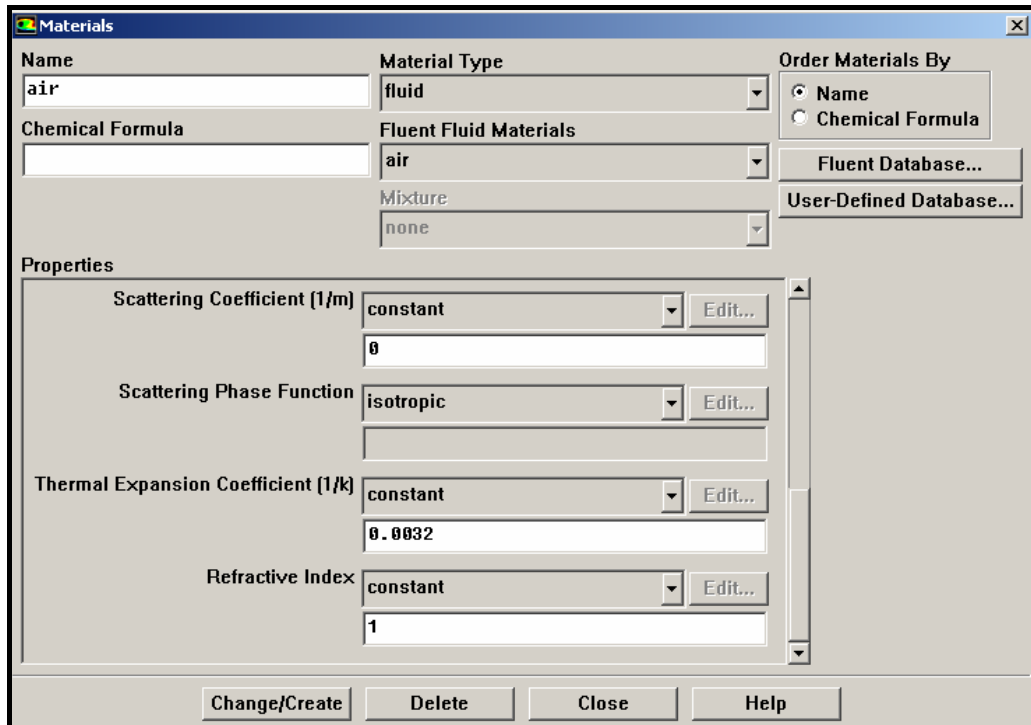
Figure B.4. *Continued,* Materials panel of fluent program
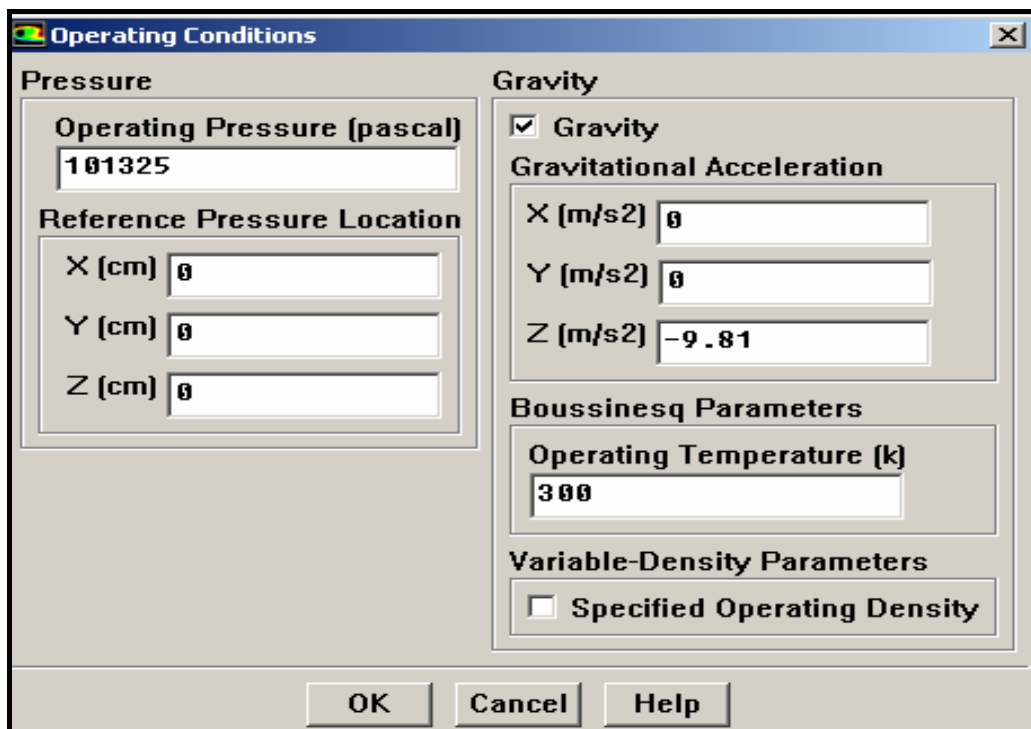
Figure B.5. Operating conditions panel of fluent program
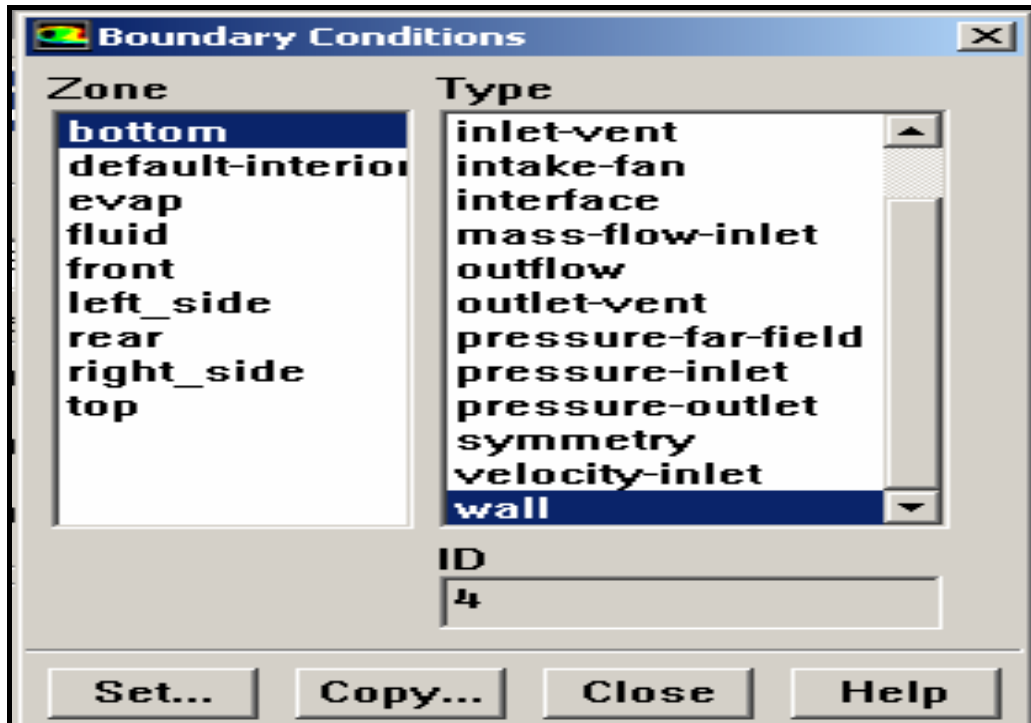
Figure B.6. Boundary conditions panel of fluent program
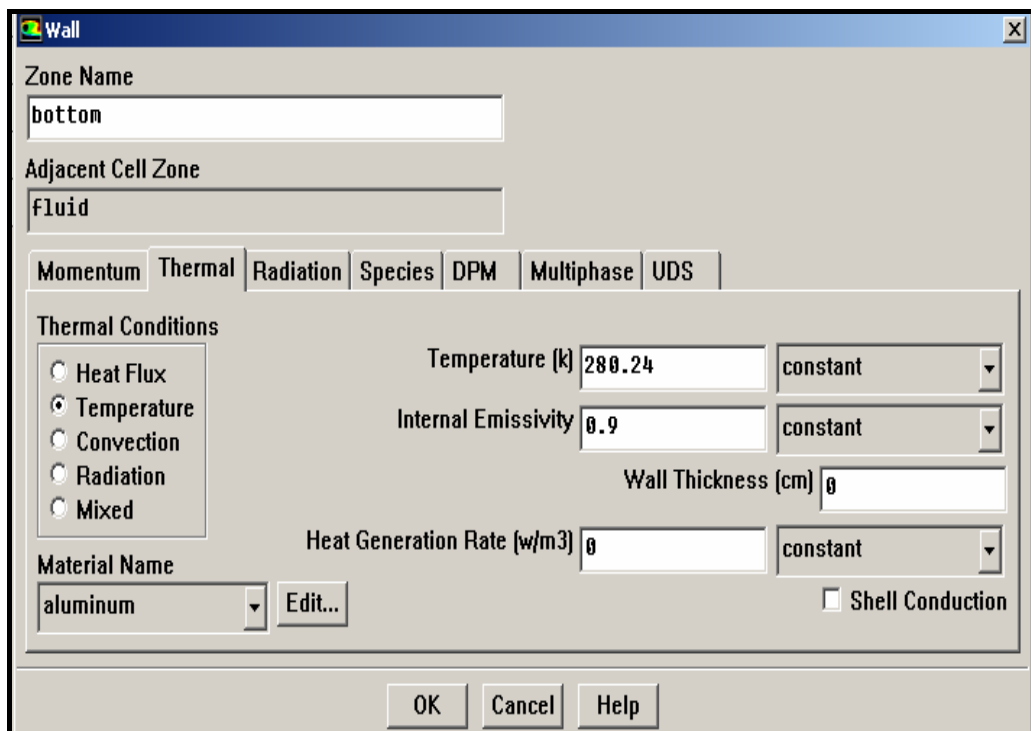
Figure B.6. *Continued,* Boundary conditions panel of fluent program
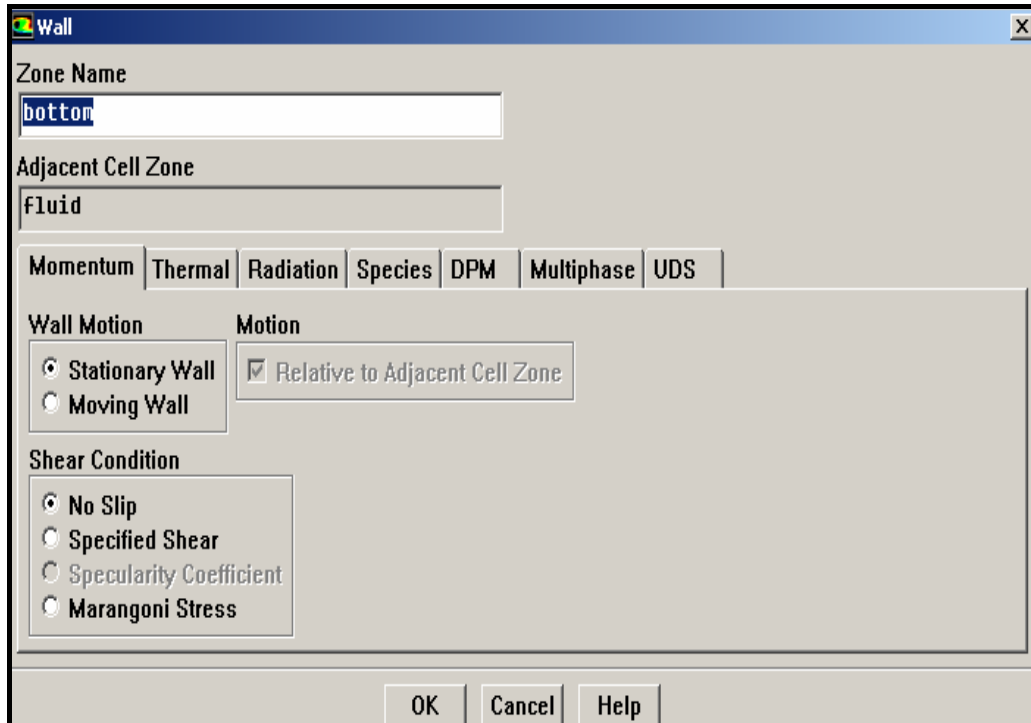
Figure B.6. *Continued,* Boundary conditions panel of fluent program
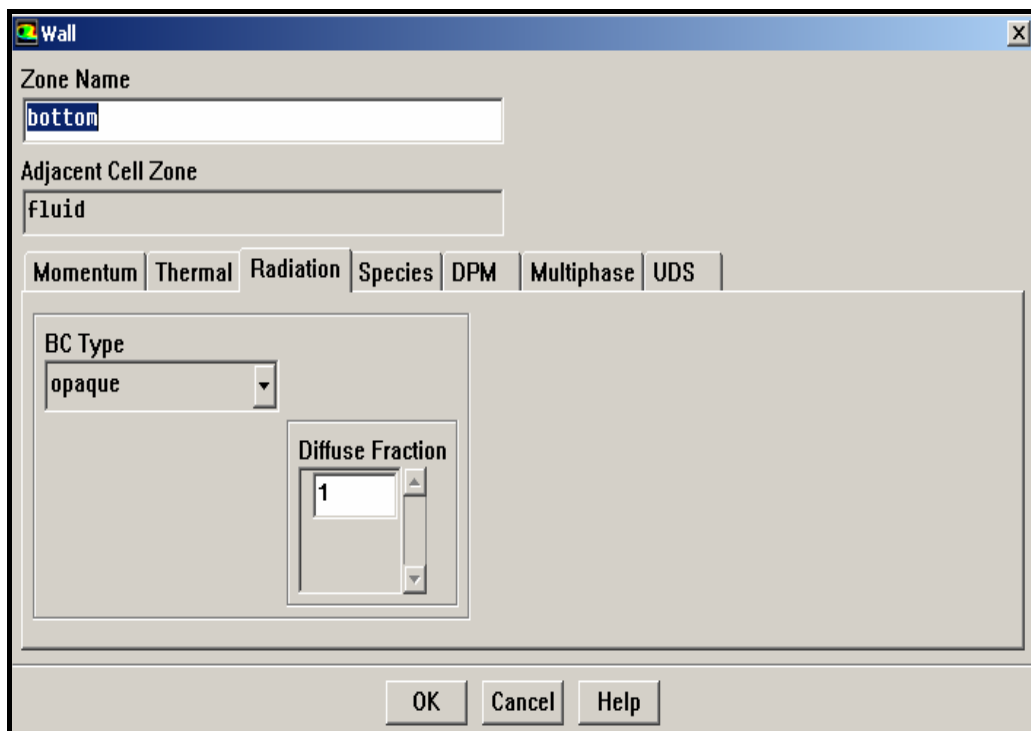
Figure B.6. *Continued,* Boundary conditions panel of fluent program
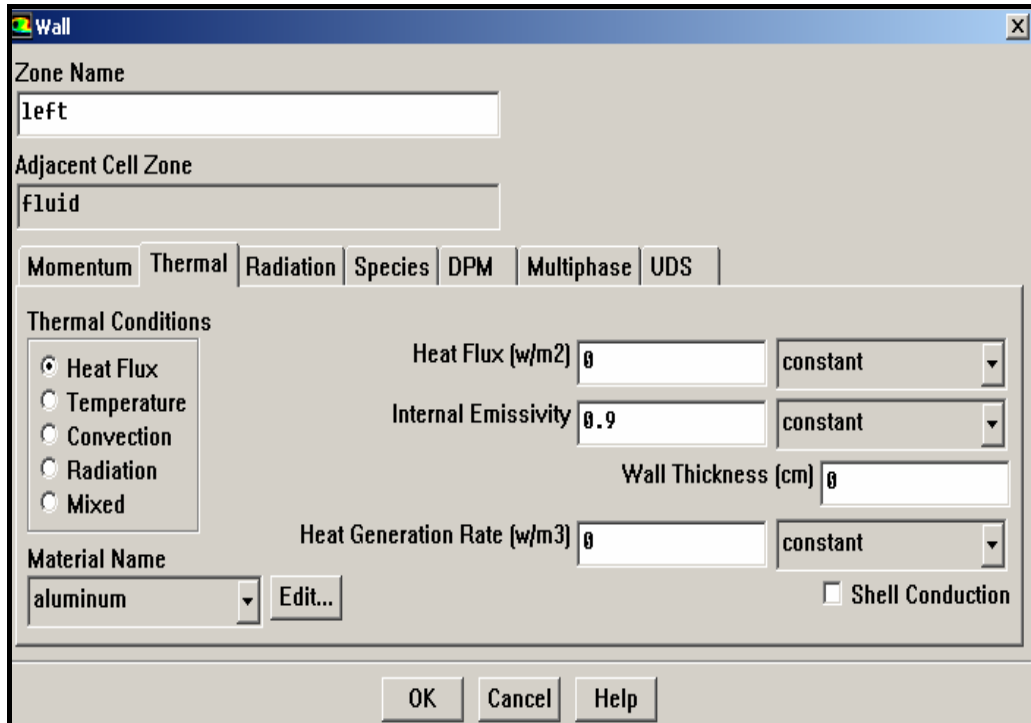
Figure B.6. *Continued,* Boundary conditions panel of fluent program
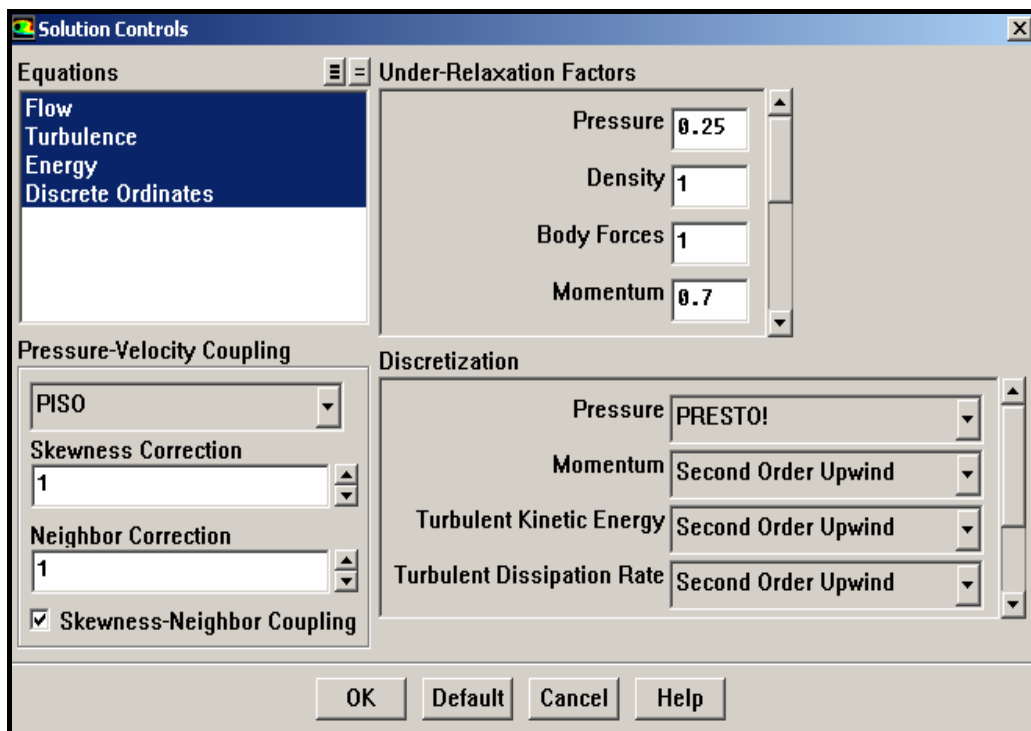
Figure B.7. Solution controls panel of fluent program
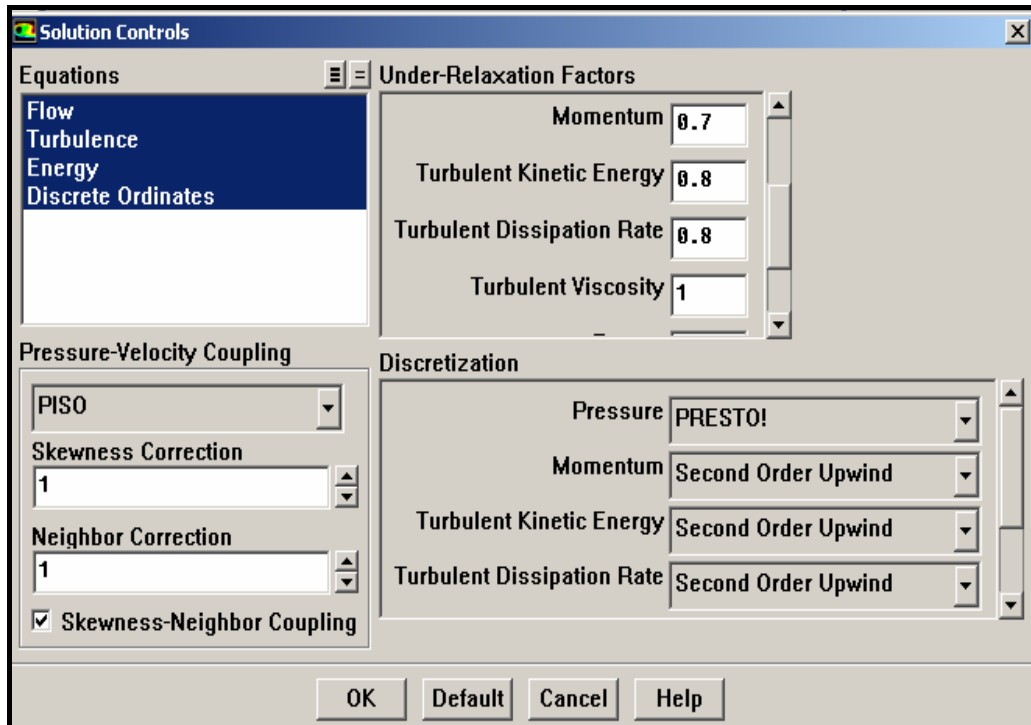
Figure B.7. Solution controls panel of fluent program
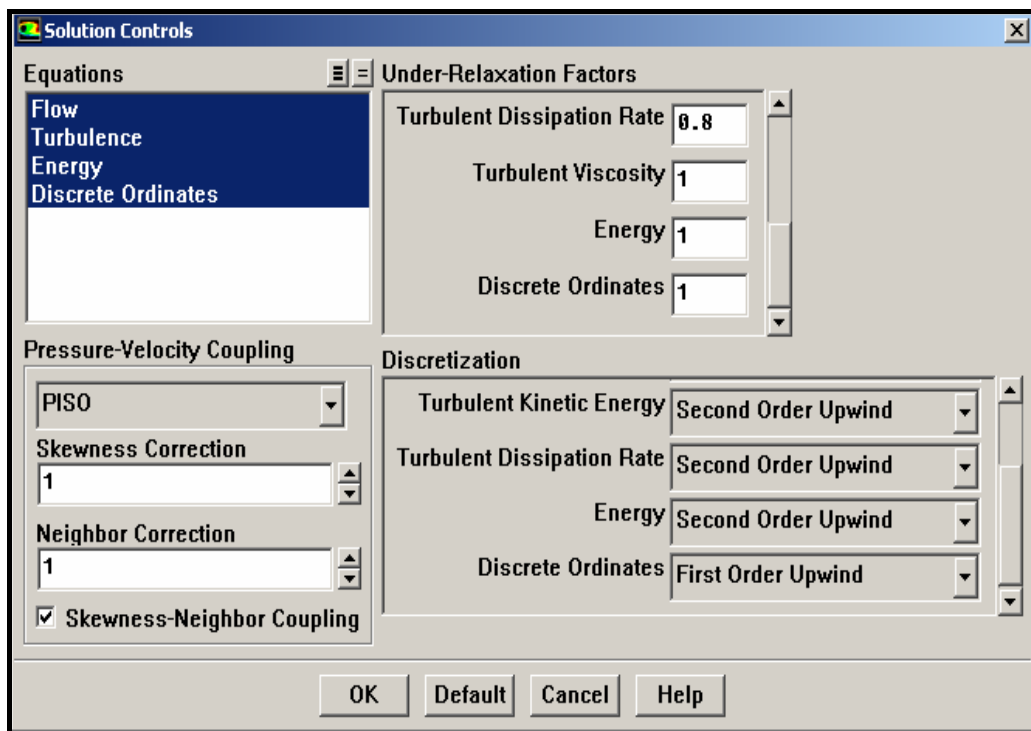
Figure B.7. *Continued,* Solution controls panel of fluent program
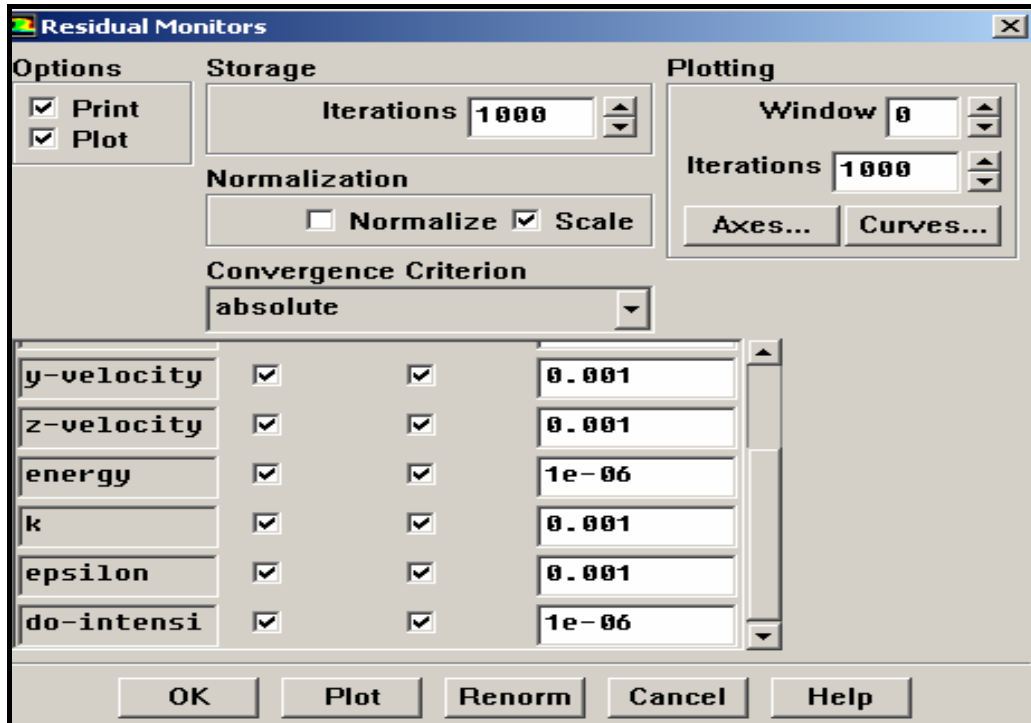
Figure B.8. Residual monitors panel of fluent program
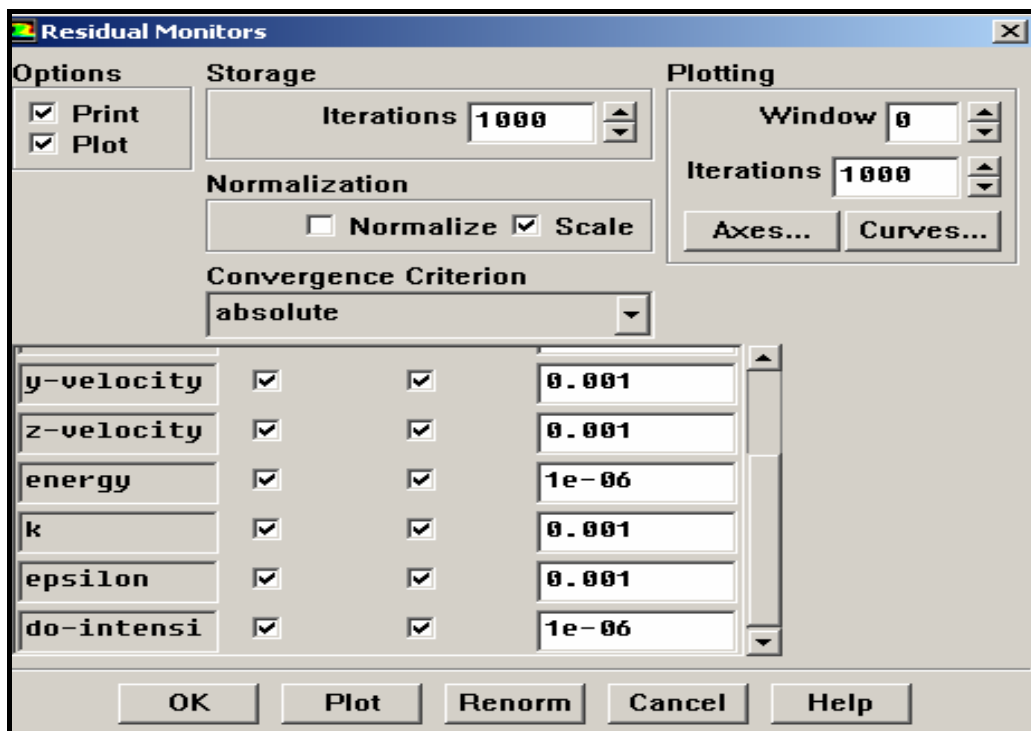
Figure B.8. *Continued,* Residual monitors panel of fluent program
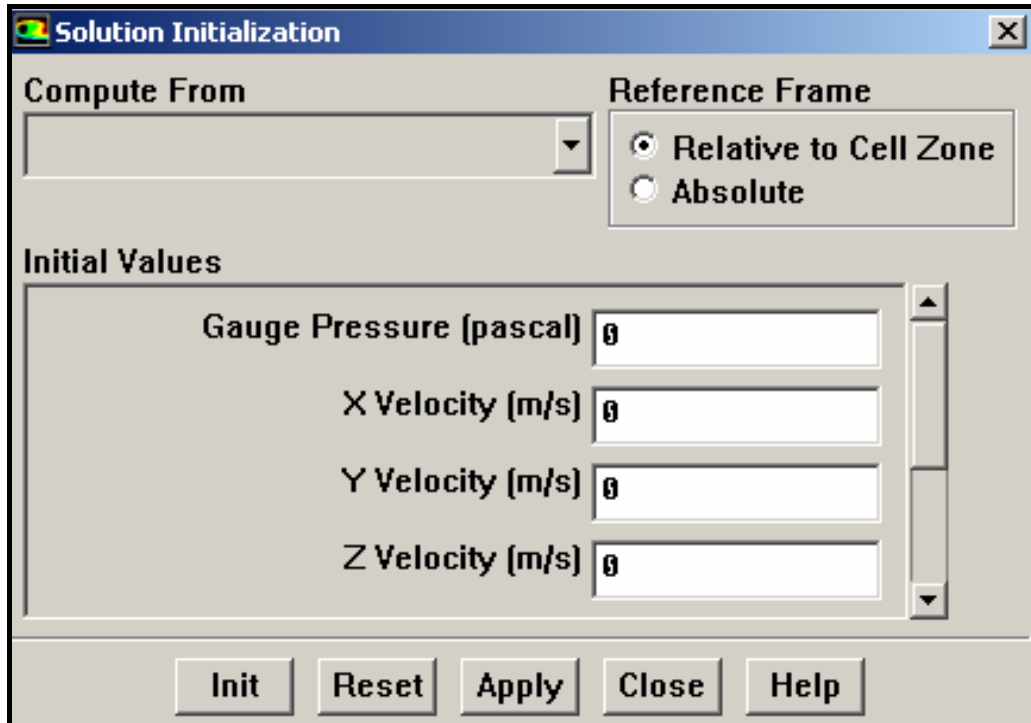
Figure B.9. Solution initialization panel of fluent program
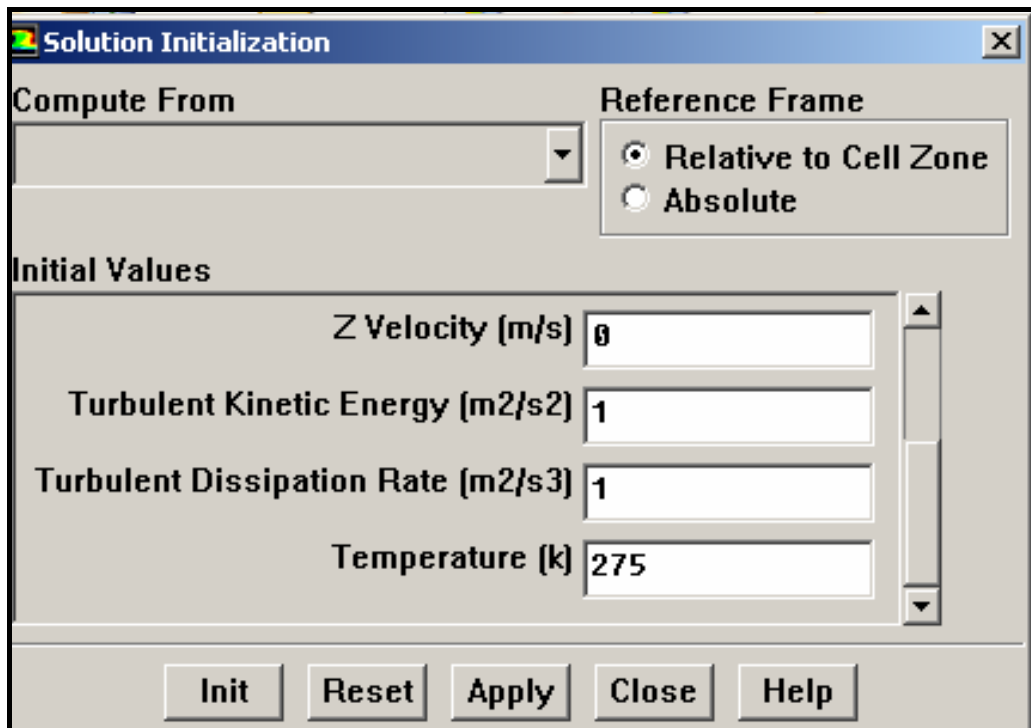
Figure B.9. *Continued,* Solution initialization panel of fluent program

APPENDIX C

EXPERIMENTAL TEMPERATURE DISTRIBUTIONS FOR SINGLE COMPARTMENT AND TOTAL REFRIGERATOR
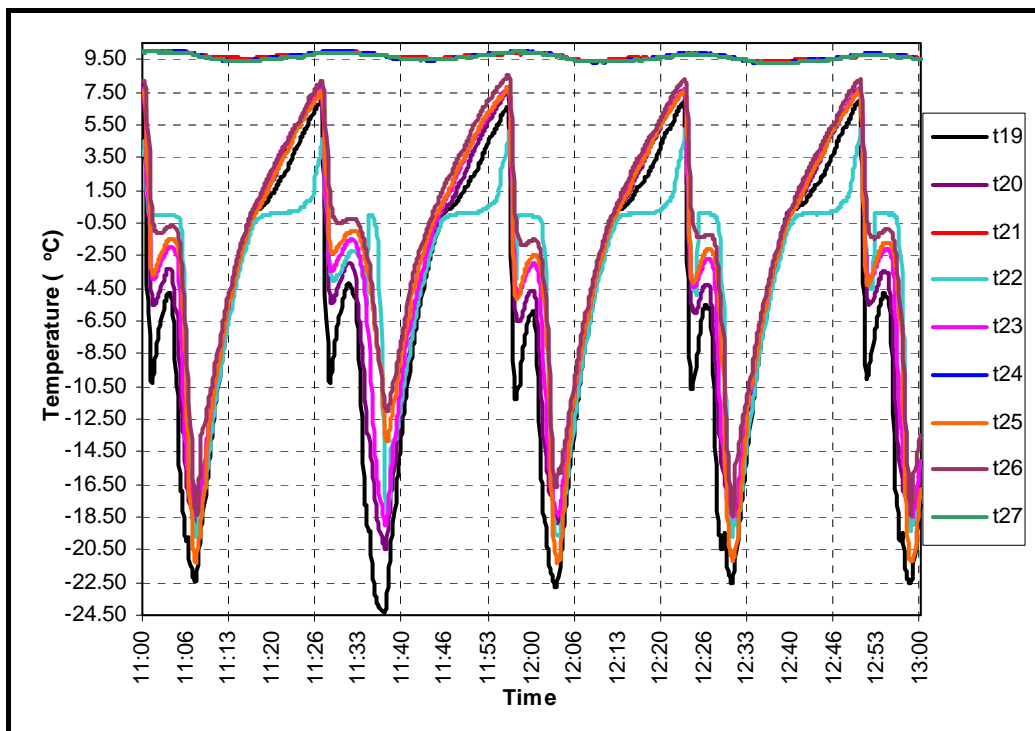
Figure C.1. Single compartment back wall temperature distribution
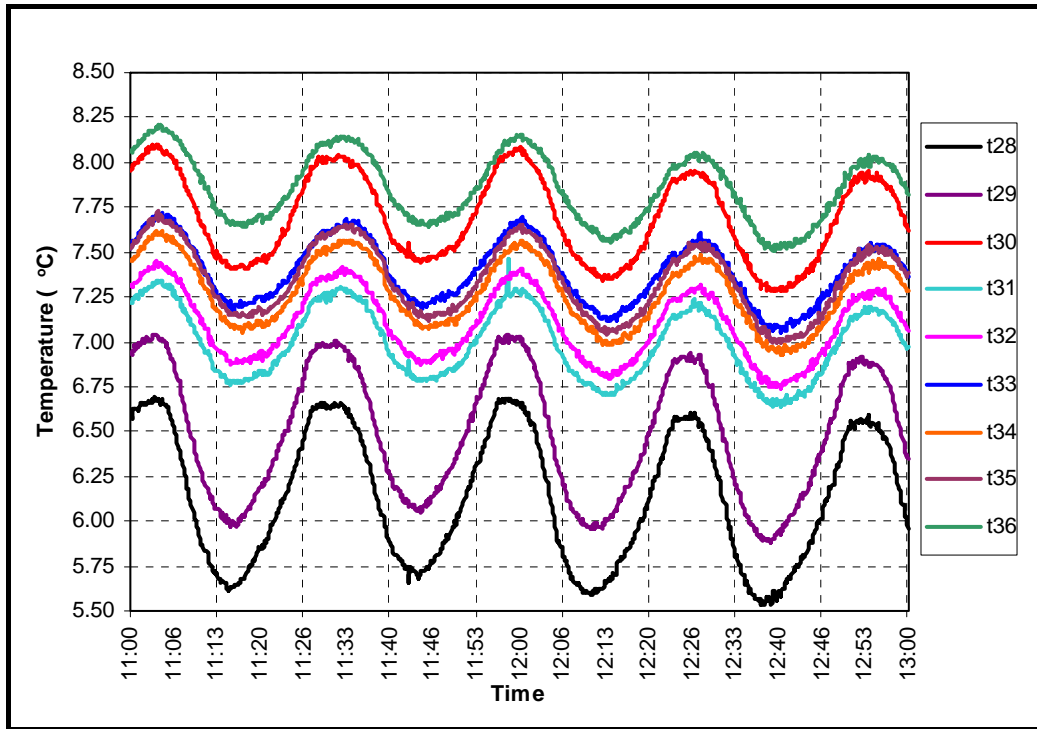
Figure C.2. Single compartment bottom wall temperature distribution
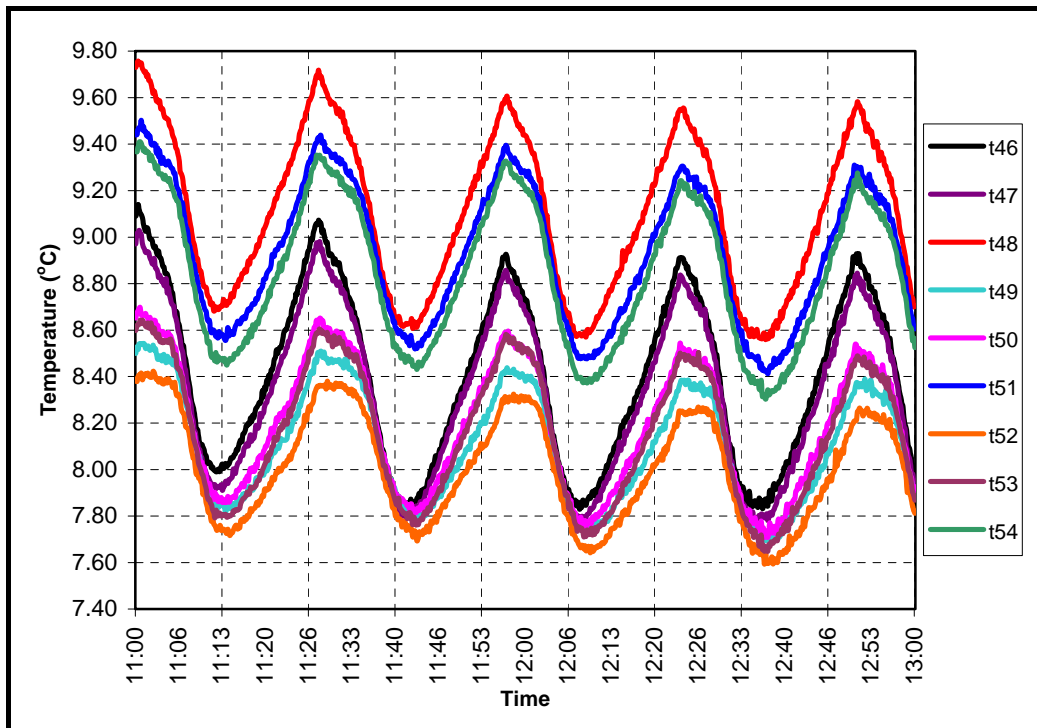
Figure C.3. Single compartment front wall temperature distribution
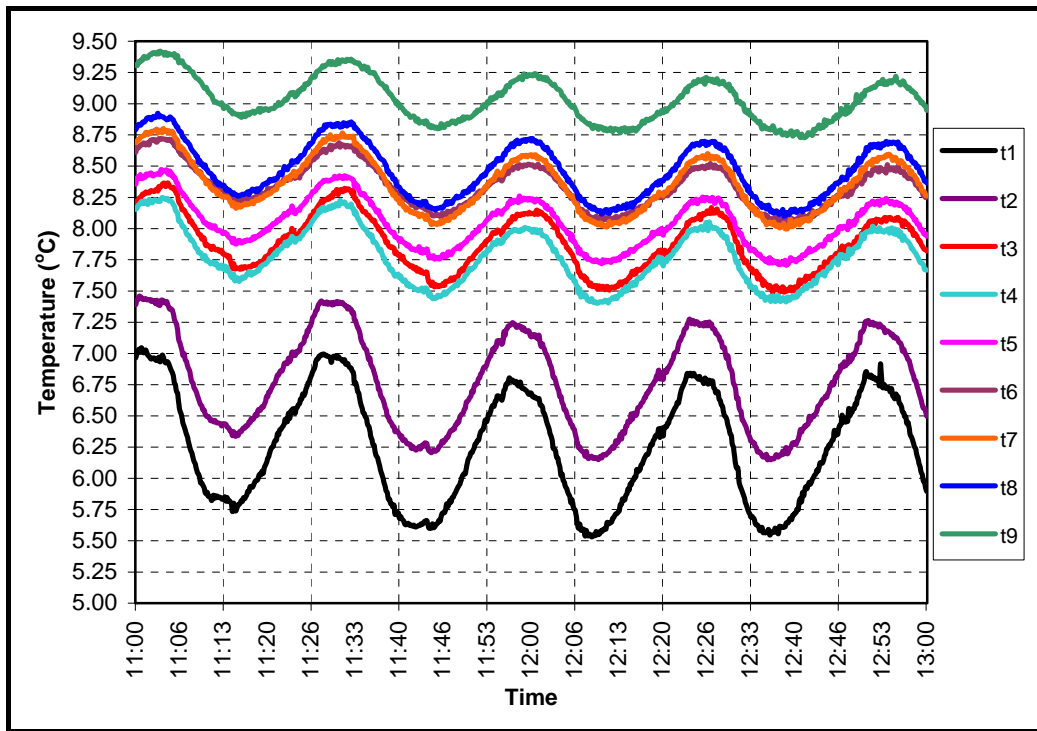
Figure C.4. Single compartment top wall temperature distribution
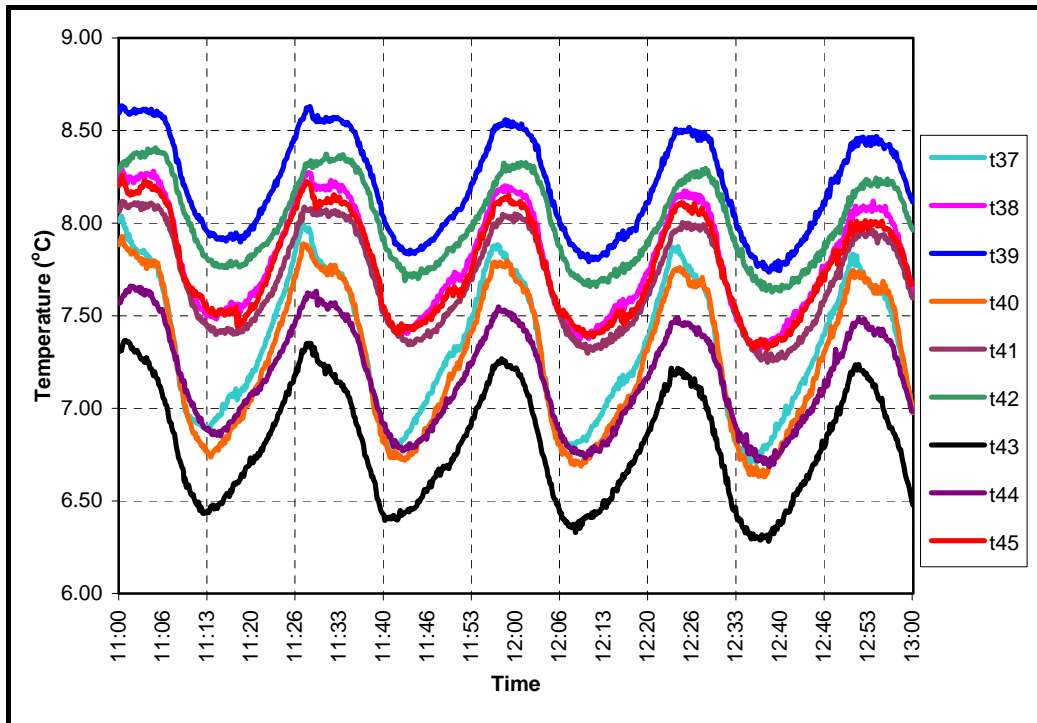
Figure C.5. Single compartment symmetry plane temperature distribution
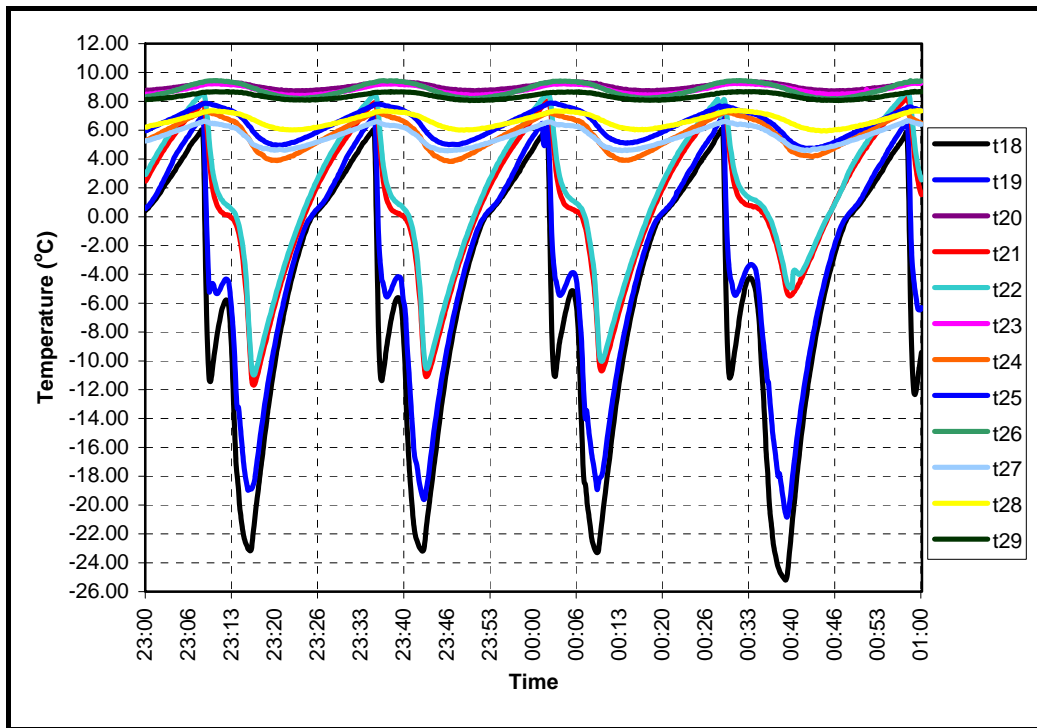
Figure C.6. Total refrigerator back wall temperature distribution
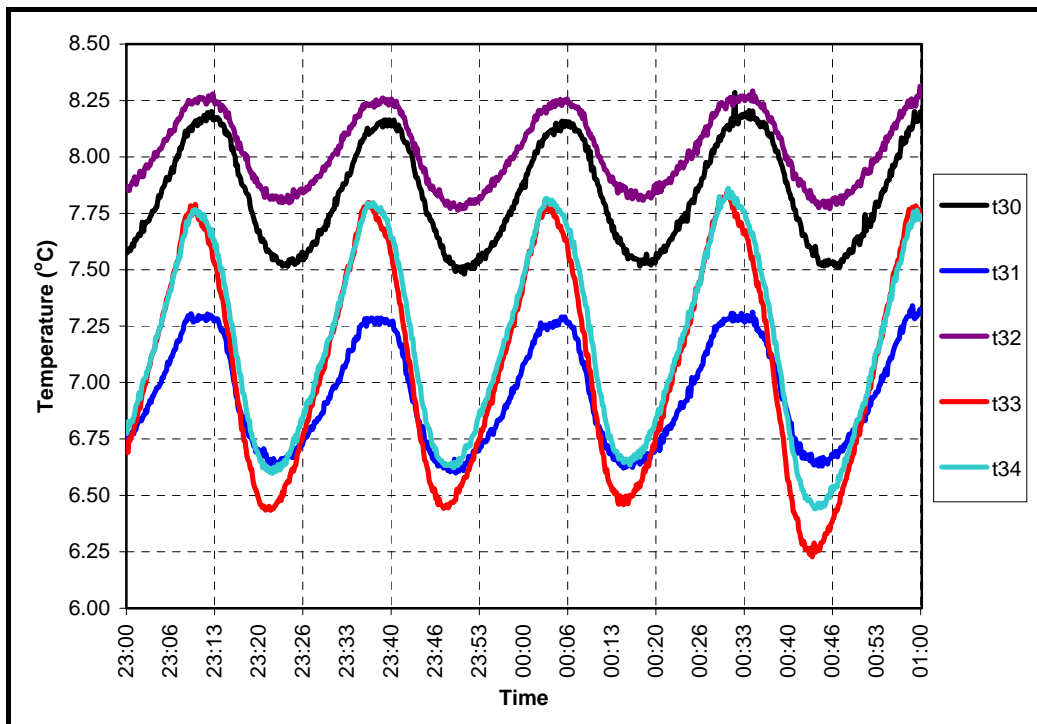

Figure C.7. Total refrigerator bottom wall temperature distribution
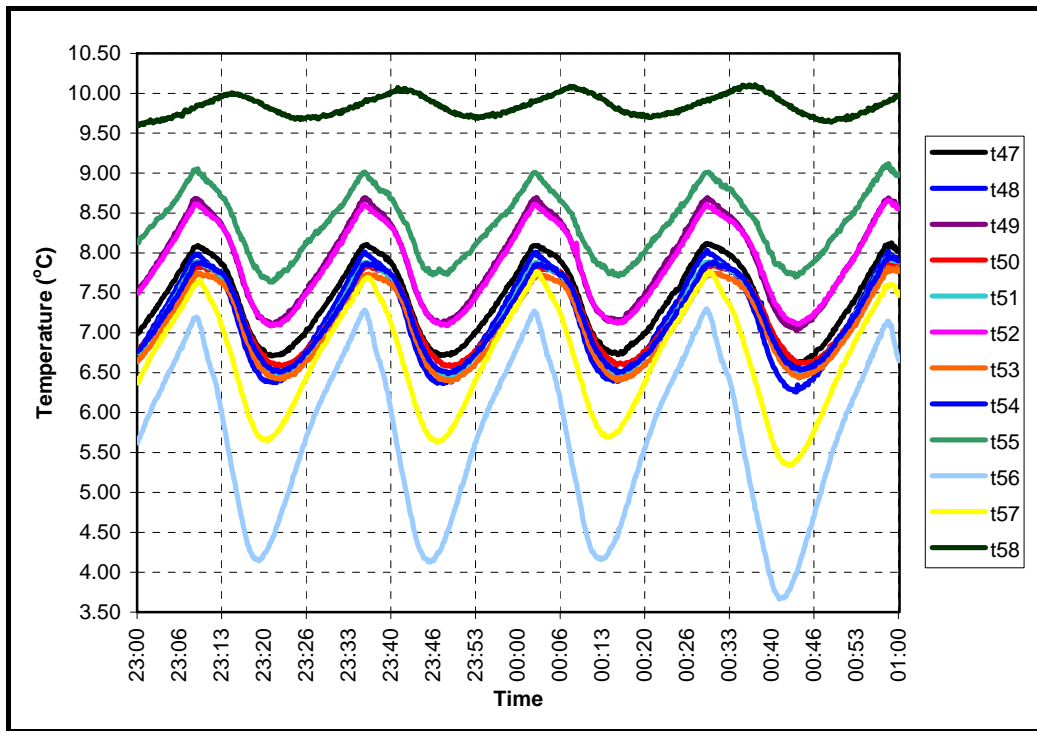
Figure C.8. Total refrigerator front wall temperature distribution
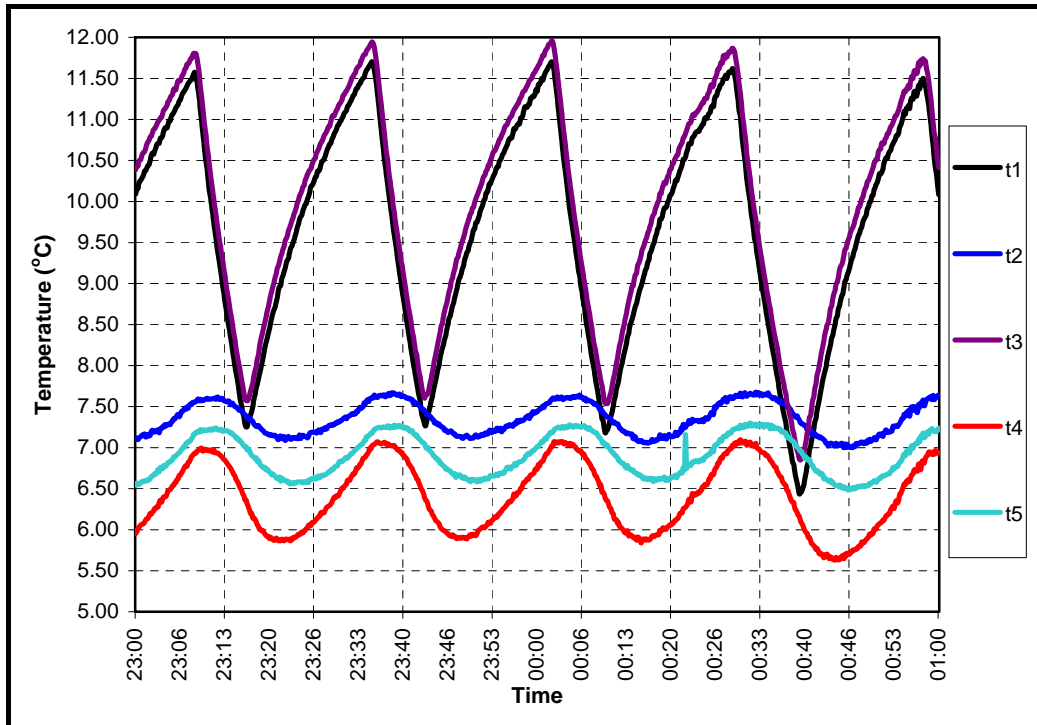
Figure C.9. Total refrigerator top wall temperature distribution
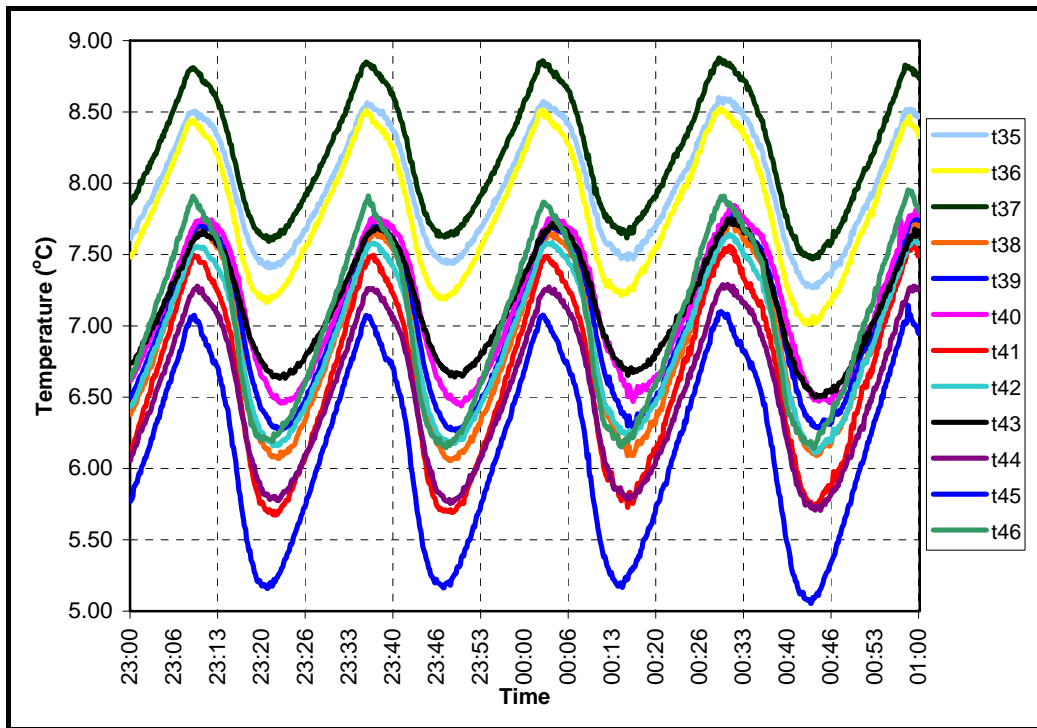
Figure C.10. Total refrigerator symmetry plane temperature distribution

CURRICULUM VITAE

PERSONAL INFORMATION

Surname, Name: Bayer, Özgür

Nationality: Turkish (TC)

Date and Place of Birth: 22 July 1977, Uşak

Marital Status: Married

Phone: +90 312 210 25 78

Fax: +90 312 210 25 36

email: bayer@metu.edu.tr

EDUCATION

Degree	Institution	Year of Graduation
MS	METU Mechanical Engineering	2002
BS	METU Mechanical Engineering	2000
High School	İzmir Science School, İzmir	1995

WORK EXPERIENCE

Year	Place	Enrollment
2006-Present	METU Dept. of Mechanical Engineering	Instructor
2000-Present	METU Dept. of Mechanical Engineering	Teaching Assistant

FOREIGN LANGUAGES

Advanced English, Beginner German, Beginner French.

PUBLICATIONS

Bayer Ö., Çetin B., Dirgin E., COP-Irreversibility Relation in Household Refrigerators, 14th National Conference on Thermal Sciences, September, 3-5, 2003 Isparta, Türkiye